1986

# Fluidization of granular media in unbounded two-dimensional domains: an experimental study, October 1986, 138p.

Edward W. Roberts

Richard N. Weisman

Gerard P. Lennon

# FLUIDIZATION OF GRANULAR MEDIA IN UNBOUNDED TWO-DIMENSIONAL DOMAINS: AN EXPERIMENTAL STUDY



BY

EDWARD W. ROBERTS
RICHARD N. WEISMAN
GERARD P. LENNON

DEPARTMENT OF CIVIL ENGINEERING
AND
CENTER FOR MARINE AND ENVIRONMENTAL STUDIES

LEHIGH UNIVERSITY
BETHLEHEM, PA 18015

OCTOBER, 1986

IMBT HYDRAULICS LAB DIVISION REPORT
IHL-109-86

# Table of Contents

# List of Tables

# List of Figures

# ABSTRACT

Fluidization is a process involving the suspension of non-cohesive particles in a fluid resulting from the submerged weight of the particle being exceeded by the drag force exerted on the particle by an upward flowing fluid. The well understood phenomenon of one-dimensional fluidization (bounded domain) is controlled and advantageously applied to a broad scope of engineering problems by a diverse group of specialists. However, in unbounded domains, the formation of an interface between the fluidized and unfluidized region is a complicated phenomenon which is poorly understood at present. This experimental study, utilizing a two-dimensional fluidization apparatus, is meant to advance the fundamental understanding of the phenomena of two- and three-dimensional fluidization, and to provide a data base for numerical models attempting to simulate the phenomena.

The results of this experimental study reveal that the hydraulic head in the fluidized region is constant in the x-direction at any elevation (y coordinate) and begins to decrease at the fluidized/unfluidized region interface regardless of initial bed depth condition tested in this study. The fluidized region width is a linear function of the fluidization flow rate regardless of initial bed depth conditions tested in this study. The width of the fluidized region at half the expanded bed depth ($W_M$) is on the average 63% of the fluidized region top width ($W_T$) and the base width of the fluidized region ($W_B$) is on the average 36% of the fluidized region top width. A one-dimensional theoretical superficial velocity needed to initiate fluidization provides a close approximation of the two-dimensional incipient fluidization conditions. The bed expansion was found to increase nonlinearly and the average sand concentration in the fluidized region

decreases nonlinearly with corresponding increases in flow rate during the post-fluidization stage. It is believed that these two processes are related.

Boundary conditions were also determined for the fluidized/unfluidized region interface consisting of hydraulic head at x and y coordinates, and the total leakage occurring across the interface from the fluidized region to the unfluidized region. It was determined that the total leakage occurring across the interface is less than 5% of the total fluidization flow rate entering the system.

# Chapter 1
# INTRODUCTION

## 1.1 Historical Background

The phenomenon of fluidization is best defined as the flow of fluid, gas or liquid, upward through a bed of non-cohesive solid particles at a sufficiently high velocity to suspend the particles in the fluid. The drag force exerted on the solids exceeds the submerged weight of the particles, which causes the particles to be lifted and separated in the fluid without continuous grain to grain contact. This solid-fluid mixture behaves as a dense fluid.

The technique of fluidizing solid particles has evolved in the fields of sanitary engineering and chemical engineering. Like many other engineering developments, the process was extensively used before it was thoroughly understood. Sanitary engineers utilize the technology in a flow process, called backwashing, to clean rapid sand filters used in water and wastewater treatment. Chemical and mechanical engineers exploit the technology of fluidization in a variety of processes including heat transfer, combustion processes, petroleum refining, petrochemical processing, coal conversion, ore roasting, coking, aluminum production, as well as the production of a variety of chemical compounds [34]. Fluidization, also known as piping or boiling, is a common cause of failure of geotechnical structures when a significant upward vertically driving head exists on one side of the structure [33].

Except for the isolated period of research during the late 1920's and early 30's, the study of backwashing granular filters in water and wastewater treatment received little attention up to the late 1960's. Most studies were empirical or semi-empirical in nature. Therefore, little effort was made to develop

sound theoretical concepts. Instead, researchers directed their energies towards developing general rules. Hulbert and Herring in the early 1900's established the rule of thumb of 50 percent expansion for effective backwashing, which laid the foundation for backwashing practice in the sanitary engineering profession in the United States for 40 years [1].

In contrast, the chemical engineering profession has performed extensive research on the process of fluidization during the period from the 1950's to the present day, resulting in the establishment of a substantial knowledge base. The Standard Oil Development Company was the pioneer in this field [10]. The application and the improved understanding of the concepts of fluidized solids arose from the desire to find a more efficient catalytic cracking process than the fixed-bed process which was introduced commercially in 1937.

The knowledge obtained during the 1950's and 1960's by chemical engineers sparked renewed interest by environmental engineers in the backwashing process beginning in the late 1960's. Amirtharajah [1], Amirtharajah and Cleasby [2], and more recently, Cleasby and Fan [8], analyzed the concepts of one-dimensional incipient fluidization and the optimization of bed expansion for a given superficial velocity in order to effectively clean the filter media and to avoid partial loss of filter media, called out-wash. The superficial velocity is simply the upward volumetric flow rate through the system divided by the cross-sectional area of the bounded domain.

In the past two decades there has been an emergence of an innovative application of fluidization technology outside the role of the traditional applications. Controlled fluidization has been demonstrated as a viable alternative to dredging for sand management in the coastal environment. Hagyard et al. [17]

conceived of fluidizing non-cohesive sediment at the mouth of an estuary via water discharging through a perforated pipe and transporting the sand to a desired location (possible beach replenishment). Their lead was followed by Kelley [20], Murray and Collins [22], Weisman and Collins [30], and by Weisman et al. [31]. All researchers conducted successful two-dimensional laboratory experiments. Murray and Collins [22] and Weisman and Collins [30] conducted successful three-dimensional laboratory experiments. However, it was the field test work of Weisman et al. [32] that firmly established fluidization as a technically feasible method for sand management in the coastal environment.

## 1.2 Fundamental Concepts of Fluidization

### 1.2.1 One-Dimensional Fluidization (Bounded Domain)

One-dimensional fluidization results from a well distributed source of upflowing fluid under a bed of confined solid particles (bounded domain of porous media). As fluid flows upward through a bed of granular material, a resistance to the flow and a corresponding head loss occurs across the bed, attributable to viscous and inertial effects. At low superficial velocities, when the flow is laminar with the Reynolds number ($R = Vd_{eq}/\upsilon$, $V$ = superficial velocity, $d_{eq}$ = grain diameter of a sphere of equal volume, $\upsilon$ = kinematic viscosity of water) less than three, the head loss, across the fixed bed will be a linear function of the flow rate [8]. Camp [7] has reported strictly laminar flow through filters up to a Reynolds number of about six [8]. If the Reynolds number enters the transitional regime ($R>6$), typical of coarser or heavier grain material, the head loss may become a power function of flow rate [8]. The increase in resistance of the particles to the subsequent increased flow rate reaches a maximum when

the submerged weight of the particles in the water is exactly balanced by the upward drag on the particles. The result is a suspension of the solids in the fluid, representing the point of the minimum flow rate or superficial velocity essential for achieving fluidization. Further increase in the flow rate causes further expansion of the bed to accomodate the additional flow while effectively maintaining the same head loss across the bed.

The behavior of a real bed departs from the characteristics of an idealized bed system, as shown in Figures 1 and 2. The slope of the line representing the linear relationship between head loss through the bed, $\Delta h$, and superficial velocity, V, prior to actual fluidization is greater for closely packed beds than for loosely packed beds. This phenomenon is due to the decrease in voids and increase in frictional resistance to flow due to the increase in compaction of the bed. It can also be seen in Figure 1 that the superficial fluid velocity required for the onset of fluidization occurs at the change in slope (pt. B) for an ideal fluidized bed of uniform size and shape particles and uniform compaction [8]. The point of incipient fluidization for real beds deviates from an ideal bed due to varying degrees of compaction, variable particle sizes and distributions, and varying degrees of sorting. The minimum fluidization velocity varies for particles of a bed composed of a gradation in particle sizes; consequently, the larger grains become fluidized at a higher superficial velocity than the smaller grains. Therefore, there is a gradual change from the fixed bed condition to the completely fluidized state with point C representing full-bed fluidization (Figure 1) [8].

The conditions of post-fluidization of a real bed asymptotically approach the characteristics of an ideal bed. For ideal post-fluidization, the porosity ap-

proaches a value of one as the particle concentration decreases with increases in the flow rate. The superficial velocity equals the free-settling velocity of a single particle (unhindered terminal settling velocity) at a porosity approaching one [8]. Figure 2 demonstrates the accommodating expansion of the bed with further increases in the superficial velocity after the point of incipient fluidization. The real graded bed departs from the idealized case in Figure 2 for the same reasons described for Figure 1.

The formation of paths of least resistance through beds tends to occur in media consisting of fine or agglomerated particles. This phenomenon is called channeling and is commonly referred to as a "self-propagating discontinuity" [1] or piping in porous media. Channeling is an important factor to consider when analyzing the physical processes of fluidization. Once this preferential flow path is formed, it begins to grow in size with increased flow rate. Channeling is an undesirable phenomenon, because it tends to hinder the establishment of uniform fluidization [1].

Spouting occurs predominantly in gas-solid bed mixtures and is a phenomenon which results from the fluidizing fluid taking a single path from the source to the bed surface. This bed condition is regarded as a special case of channeling [1].

### 1.2.2 Two- and Three-Dimensional Fluidization (Unbounded Domain)

Two- and three-dimensional fluidization can be described as flow emanating from a source pipe within an unbounded domain that fluidizes a region of the media above the source as shown in Figure 3. The flow issues as jets from small perforations located on the sides of the fluidization pipe. The result consists of an interface separating the porous media into two regions with distinctly

different physical characteristics, a fluidized region and an unfluidized region. The fluidized region behaves as a dense fluid and allows leakage, the flow of water, across the fluidized/unfluidized region interface to the unfluidized region . The unfluidized region has characteristics similar to a fixed bed. Also sand particles are eroded from the fluidized/unfluidized region interface with increase in flow rate during the fluidized region growth process. Therefore, the width of the fluidized region widens with corresponding increases in the fluidizing flow rate. This progressive change in fluidized region geometry is shown in Figure 4. The eroded sand particles form berms or remain in suspension within the fluidized region. In Figure 3 the velocity of the jet decreases as the jet extends further into the fluidized region until it reaches a negligible velocity . Therefore, the suspended sand particles settle in the center of the fluidized region and are re-entrained in the jet as shown in Figure 3.

## 1.3 Objective and Scope

One-dimensional fluidization of granular materials is a relatively well understood phenomenon. However, for unbounded domains, an interface between the fluidized and unfluidized regions results in complicated phenomena which are poorly understood at present. This experimental study is meant to advance the fundamental understanding of two- and three-dimensional fluidization, and to provide data for numerical models attempting to simulate the phenomena.

The two-dimensional apparatus used for this experimental research represents the cross-section of a hypothetical channel. The experimental research serves two specific purposes:

1. To provide experimental information to:

a. formulate the interfacial boundary conditions between the fluidized and unfluidized regions,

b. obtain physical parameters including hydraulic conductivity, porosity, and physical properties of the selected granular material,

c. assess the physical processes and flow patterns established within the fluidized region attributed to the high pressured flow being ejected from the fluidization pipe into the porous medium.

2. To provide data for verification of a numerical model, including:

a. the head distribution throughout the sand bed for the fluidized and unfluidized cases at specific flow rates from the source pipe,

b. the flow rate from the source that initiates fluidization (denoted $Q_i$),

c. the geometry of the fluidized region,

d. boundary conditions along the fluidized/unfluidized region interface, including hydraulic heads, x and y coordinates, and leakage across the interface.

The experimental research for this study was performed utilizing a two-dimensional fluidization apparatus consisting mainly of a two- dimensional fluidization tank with a data acquisition system hooked directly into the pressure tap distribution contained on one half of the back panel of the tank. The pressure tap distribution was constructed on one half of the back panel of the tank because the two-dimensional fluidization phenomenon is fairly symmetrical about the vertical center line of the fluidization pipe for both the pre-fluidization and post-fluidization cases. The research was performed for six tests at initial bed depth conditions of 25.4 cm and 42 cm, and for relatively constant sand bed properties (porosity and hydraulic conductivity of initial bed depth condition). The fluidization tank was designed with sufficient width and depth to minimize the effects of the bottom and side boundaries. The spacing

between the front and back panels, is 30.48 cm. The minor apurtenances of the two-dimensional apparatus were designed and constructed to provide a self-contained, regulated water supply. These features consisted of a settling tank adjacent to the outfall of the fluidization tank and a head tank between the settling tank and pump used for recirculating the water back into the fluidization tank via a source pipe.

The general purpose of the testing was to obtain hydraulic head distribution data via the fluidization tank and the data acquisition system. In addition to the basic tests, there were several supplementary tests performed during the experimental research. These tests consisted of probe tests, leakage tests, and tracer studies. The probe tests were performed to assess the hydraulic head distribution at any elevation (y coordinate) in the fluidized region observed for two-dimensions and to verify the two dimensionality of the system by measuring a constant head in the third dimension (z direction). The leakage tests were performed for the initial bed depths of 25.4 cm and 42 cm and for several different flow rates. The purpose of the tests was to collect a data base in order to qualitatively and quantitatively define the rate of flow across the fluidized/unfluidized region interface. The tracer studies were performed to help visualize flow processes associated with two-dimensional fluidization.

# Chapter 2
# LITERATURE REVIEW

## 2.1 Pertinent Analysis of Fluidization in Bounded Domains

At the point of incipient fluidization (one-dimensional fluidization) there is a balance of forces between the weight of a column of saturated media and the upward acting vertical pressure force in the media. The shear force contribution to the resistance in the media is assumed to be negligible. Summation of forces (Figure 5) in the vertical y direction is,

$$\sum F_y = \overline{F}_p - \overline{W} = 0 \tag{2.1}$$

where $\overline{F}_p$ = vertical pressure force acting at the base of the column, and $\overline{W}$ = weight of column of saturated media. The one-dimensional column in Figure 5 is of finite depth, L, and horizontal unit area, consisting of solid particles with water occupying the voids. The summation of the volumes of water and solids in the column multiplied by their respective unit weights, represents the total weight of the column.

$$\overline{W} = \gamma_s L(1-\epsilon) + \gamma_w L\epsilon \tag{2.2}$$

where L is the depth of column of saturated medium, $\gamma_s$ is the unit weight of solids, $\gamma_w$ is the unit weight of water, and $\epsilon$ is the porosity of the medium. Rearrangement of Eq. 2.2 to reflect the submerged weight of the solids and the weight of the water column of dimensions L $\times$ unit area, yields,

$$\overline{W} = L(1-\epsilon)(\gamma_s - \gamma_w) + \gamma_w L \tag{2.3}$$

The pressure force acting vertically upward in the media at the base of the column for a unit area is,

$$\overline{F}_p = \Delta p \times unit\ area \tag{2.4}$$

where $\Delta$p is the change in pressure between the base and the top of the column.

At incipient fluidization the summation of the forces in the vertical direction must equal zero as indicated in Eq. 2.1. Therefore, it is evident that the upward acting pressure force must equal the weight of the column. Thus, equating Eq. 2.3 and Eq. 2.4 yields,

$$\Delta p = L(1-\epsilon)(\gamma_s - \gamma_w) + \gamma_w L \tag{2.5}$$

Dividing by $\gamma_w$ the pressure head gradient is,

$$\frac{\Delta p}{\gamma_w} = L(S_s - 1)(1-\epsilon) + L \tag{2.6}$$

where $S_s$ is the specific gravity of the sand particles.

Eq. 2.6 can be presented as a head loss, $\Delta$h, a change in hydraulic head in the media with depth, by moving the second term on the right side of Eq. 2.6 to the left side and substituting position head $\Delta$y for (-L) yielding,

$$\frac{\Delta p}{\gamma_w} + \Delta y = L(S_s - 1)(1-\epsilon) \tag{2.7}$$

which is,

$$\Delta h = L(S_s - 1)(1-\epsilon) \tag{2.8}$$

Also, the head loss per unit bed depth gives the critical hydraulic head gradient necessary to fluidize the column of media and is Eq. 2.8 divided by (L) yielding,

$$\frac{\Delta h}{L} = (S_s - 1)(1-\epsilon) \tag{2.9}$$

which can be expressed as,

$$\frac{\Delta h}{L} = \frac{[\gamma_s(1-\epsilon) + \epsilon\gamma_w] - \gamma_w}{\gamma_w} \tag{2.10}$$

or dividing by g yields,

$$\frac{\Delta h}{L} = \frac{\rho_{sat} - \rho_w}{\rho_w} \tag{2.11}$$

where $\rho_{sat}$ is the mass density of the saturated media which is about 1.94 g/cm$^3$ for the 0.15 mm sand used in this experiment, and $\rho_w$ is the mass density of water (1.0 g/cm$^3$). Using these mass densities, a typical head loss is about 1.02 cm/cm of bed depth for this fine sand.

In the field of water treatment, environmental engineers design rapid sand filters with controlled fluidization for backwashing. Cleasby and Fan [8] emphasized the need to address the dependency of models for predicting bed expansion and minimum fluidization velocity on the porosity of the fixed bed and the sphericity of the grains comprising the filter media. The fluidization behavior of the media is influenced by the sphericity of the bed material when the material is irregular in shape [8]. The higher the sphericity ($\psi$), the less angular the grains and the lower the fixed bed porosity. The minimum fluidization velocity required for backwashing a filter can be calculated based upon the concept that the head loss for the fixed bed equals the constant head loss of the fluidized bed at the point of incipient fluidization.

There is significant error encountered when using the traditional Kozeny equation [13], for flow through granular filters, to calculate head loss through a fixed bed for flow other than the laminar regime (R<3) [8]. The equation developed by Ergun [12] is a more accurate solution over the entire range of flow regimes (laminar, transitional and turbulent), for a Reynolds number from 1 to 2000 [8]:

$$\frac{\Delta h}{L} = 150\left(\frac{\mu}{\rho g}\right)\frac{(1-\epsilon)^2}{\epsilon^3}\left(\frac{S_v}{6}\right)^2 V + 1.75\frac{(1-\epsilon)}{\epsilon^3}\left(\frac{S_v}{6}\right)\left(\frac{V^2}{g}\right) \tag{2.12}$$

where $\Delta h$ = head loss, L = depth of the bed, V = superficial velocity, $\mu$ = viscosity of the fluid, $\rho$ = mass density of the fluid, $\psi$ = sphericity of the grains, $S_v$ = specific surface = grain surface area per unit of grain volume = $6/d_{eq}$ for spheres and $6/\psi d_{eq}$ for irregular grains, $d_{eq}$ = grain diameter of a sphere of equal volume, $\epsilon$ = porosity of bed, g = acceleration of gravity [8]. In the Ergun equation (Eq. 2.12) the first term (Kozeny's term) represents the viscous energy loss and the second term represents the kinetic energy loss, which are proportional to V and $V^2$, respectively [8]. Therefore, the Kozeny equation only considers the head loss through the media attributed to the viscous effects, while the Ergun equation accounts for both viscous and inertial effects causing head loss through the fixed bed [8].

Hence, to determine the incipient fluidization superficial velocity ($V_i$), the head loss for flow through a fixed bed, Eq. 2.12, is equated to the head loss of a fluidized bed, Eq. 2.9, resulting in [8]:

$$150\left(\frac{\mu}{\rho g}\right)\frac{(1-\epsilon_i)^2}{\epsilon_i^3}\left(\frac{1}{\psi d_{eq}}\right)^2 V_i + 1.75\frac{(1-\epsilon_i)}{\epsilon_i^3}\left(\frac{1}{\psi d_{eq}}\right)\left(\frac{V_i^2}{g}\right) = (S_s - 1)(1-\epsilon_i) \tag{2.13}$$

Before solving for $V_i$, representative values of $\psi$ and $\epsilon$ must be chosen in order to attain accurate results. From experimental observations (Figure 6), Wen and Yu [34] were able to develop a relationship between the sphericity and the bed porosity at incipient fluidization ($\psi$,$\epsilon_i$). These relations are [8]:

$$\frac{1}{\psi \epsilon_i^3} = 14 \tag{2.14}$$

and

$$\frac{(1-\epsilon_i)}{\psi^2 \epsilon_i^3} = 11 \tag{2.15}$$

Substituting the above relations, Eq. 2.14 and Eq. 2.15, into Eq. 2.13 and simplifying gives the following results:

$$R_i = [(33.7)^2 + 0.0408Ga]^{0.5} - 33.7 \tag{2.16}$$

and

$$Ga = \frac{d_{eq}{}^3 \rho(\rho_s - \rho)g}{\mu} \tag{2.17}$$

where Ga is the Galileo number and $R_i = d_{eq}V_i\rho/\mu$ represents the particle Reynolds number at incipient fluidization velocity [8].

A practical grain diameter to use for $d_{eq}$ in Eq. 2.17 is $d_{90}$, 90% of the grains by weight are smaller, when applying this concept to real beds with non-uniform grain size distributions. This will ensure that the entire bed will be fluidized at the predicted minimum fluidization superficial velocity ($V_i$) [8].

## 2.2 Analysis and Application of Fluidization in Unbounded Domains

Hagyard et al. [17] were the first investigators to conceive of a fluidizing pipe for removal of sediment in the coastal environment. They presented a design to fluidize and transport sand from an estuary mouth sand bar by pumping water through a perforated pipe set on a slight slope toward the ocean. Their investigation of fluidization above a small point source, using a Perspex model filled with sand and fluidized from a downward directed jet [17], indicated that the leakage across the interface from the fluidized region to the unfluidized region decreases rapidly with increasing flow rate. They also concluded from their experimental observations, that the angle of the fluidized zone increases with corresponding increases in the flow rate.

Investigators such as Inman and Harris [19], Bailard and Inman [4], and

Harris et al. [18] have studied the phenomenon of duct flow, which is the transport of sand through "ducts" formed by injecting water downward at an angle beneath a sloped pipe through holes solely in the bottom of the pipe. This phenomenon is a related area of study, but differs fundamentally from the concept of fluidization. The eventual creation of a channel is attributed to the collapse of the overlying sand bed as a result of a loss of support from the lower lying layers. The difficulty encountered with this type of system is that "fluid holes" are formed, which are regions of well-fluidized sand separated by regions of unfluidized sand. The unfluidized regions behave as dams impeding the longitudinal flow of slurry. Wilson and Mudie [35] applied the fluidization technique to create an open channel and experienced delta formation which impeded flow of the slurry in a similar manner as the above investigators. This occurred in spite of the fluidizing pipe causing upward oriented discharge.

Using a small scale two-dimensional experimental apparatus, Kelley [20] studied a variety of fluidization pipe hole configurations for determining which one would produce the largest top width of the fluidized region. A fluidization pipe with 0.238 cm diameter perforations spaced 2.54 cm on center provided the source of water. The fluidization pipe was located under a bed of sand near the base and in the center of the apparatus. Water emanated from the holes in the distributor and fluidized the region of the media directly above the source. Kelley [20] observed relationships between the flow rate and the characteristics of the fluidized region. He concluded that the size and shape of the fluidized region and the point of incipient fluidization is strongly influenced by the hole configuration in the fluidization source, and by the erosive power of the jets issuing from the holes. He also concluded that for a given flow rate, the

widest fluidized zone can be achieved by orienting the fluidization holes in the horizontal direction on opposing sides of the source. The wide angle of the fluidized region results from a maximizaton of the erosive power of the jets for this hole configuration.

Kelley [20] also obtained theoretical results for the pre-fluidization condition using an analytical model initially developed by Muskat [23] and a numerical model using the finite element method. The experimental head distribution was obtained by an array of piezometer tubes tapped into the plexiglass wall at selected locations. A non-dimensional head distribution was obtained for each model, and then dimensional head values were chosen so that the theoretical head equalled the experimental head at a "match point" located at the piezometer tap below the injection pipe. Error in the theoretical data would be amplified by any errors in the experimental reading as a result of the head varying substantially over a short distance in the vicinity of the match point tap. Due to the forced match and the relatively simple pre-fluidization flow phenomenon, the theoretical and experimental flow fields showed adequate agreement. However, significant discrepancies were apparent upon the initiation of fluidization. Therefore, the actual head distribution and flux rates should be determined independently of this match point technique. An additional limitation to Kelley's [20] analytical solution is that it uses a point source to represent the injection pipe, which does not account for the influence of a finite pipe size and the orifice configuration on the size and shape of the fluidized zone.

Murray and Collins [22] investigated the qualitative aspects of three-dimensional fluidization. They performed laboratory experiments using a 3.81

cm diameter distributor with a flume filled to a sand depth of 15.25 cm above the pipe. A completely fluidized top width of 50.8 cm was achieved with no apparent problems of "fluid holes" or "damming" as experienced by previously mentioned investigators. When the pipe system was sloped toward one end of the flume, the fluidized sand migrated down slope as a result of gravity flow.

Murray and Collins [22] developed the following conclusions from their experimental observations:

- Fluidization is achievable under a variety of initial conditions such as uniform and nonuniform sand coverage and horizontal and non-horizontal distributors.
- Given similar initial conditions, the process leading to a fully fluidized channel is reproducible. Individual areas of boiling enlarge laterally and longitudinally and join until the entire channel is fluidized as the flow rate is increased through the system.
- Once full fluidization of the sediment is achieved, the slurry can be rapidly removed from the entire channel by pumping without having to reposition the pump.
- The sediment in a fully fluidized channel flows under the influence of gravity to the downstream end of the sloped distributor. There is no tendency for the pipe to self-bury under full fluidization conditions.

Since the experimental investigation by Murray and Collins [22] was of a qualitative nature, there existed very little data that could be utilized in the design of a prototype system.

Weisman and Collins [30] or Weisman, Collins, and Parks [31] performed laboratory experiments to establish a data base to aid in the design of a prototype fluidization system. The investigators used the two-dimensional apparatus of Kelley [20] and the three-dimensional system of Murray and Collins [22] to accomplish their goals. They studied the effect of varying the principal system parameters on the relationship between flow per unit length of

distributor and the characteristics of the fluidized region. They also recognized the great importance of sediment removal from the channel once it is completely fluidized in order to achieve a channel of maximum width. Three methods of removal were analyzed; gravity flow of slurry down a sloping pipe, pumping of slurry, and the scouring action of overlying ebb flows.

Several conclusions and design recommendations of significance reached by Weisman and Collins [30], and Weisman et al. [31] are as follows:

1. Conclusions

    a. A well-defined relationship between flow rate per unit length of distributor and fluidized channel width exists for known sand type, sand depth, and fluidization hole size and hole spacing.

    b. Sand depth affects the flow rate per unit length necessary for the initiation of fluidization. Greater flow rates are needed as the depth of sand cover is increased. The flow rate/fluidized zone width relationship is not greatly affected by depth of sand cover in the range of the experiment.

    c. The smaller the fluidization hole diameter, the larger the top width of the fluidized region for a constant flow rate per unit length of pipe. However, the holes must be of adequate size to minimize headloss and clogging and to maintain proper flow rate per unit length of pipe.

    d. Incipient fluidization and fluidized channel width are independent of fluidization hole spacing up to a spacing of 10.16 cm.

    e. The fluidized channel width is increased by 50% due to the channel walls slumping to the angle of repose of the sand, when the fluidized sediment is removed from the fluidized region.

2. Design Recommendations

    a. For large channels, an array of parallel fluidization pipes with the appropiate separation width (dependent on sand cover) must be incorporated into the system to maintain a reasonable navigable channel width.

    b. A fluidization hole size of 0.317 cm spaced at 5.08 cm centers

and a flow rate of 4 liter/sec-meter of fluidization pipe is recommended for complete fluidization.

c. The pump and distributor are designed soley on hydraulic considerations and are independent of the fluidization process. They are designed so that adequate pressure is maintained throughout the pipe to ensure the design flow rate per unit length of distributor.

d. Slope pipe seaward and provide additional pump(s) for removal of slurry from fluidized channel.

Based on the design and performance data gathered from the laboratory experiments, Weisman et al. [32] conducted a field test on a beach near Corsons Inlet, New Jersey, using a 15.2 cm diameter PVC fluidization pipe. The pump generated a flow rate of 48.8 l/s and delivered it through fluidization holes of diameter 0.316 cm spaced 5.08 cm on center along opposing sides of the distributor.

Several experiments were performed, including (i) 30 cm of sand cover fluidized above a single 12.2 m long horizontal pipe, (ii) fluidization and transport of 38 cm of overlying sand above a single 12.2 m long pipe placed on a (2%) slope, and (iii) the interaction between 6.1 m long parallel fluidization pipes. Based on the field test, Weisman et al. [32] concluded that fluidization is a technically feasible method for sand management in the coastal environment and that the design data obtained in the laboratory were sufficient to design a prototype, experimental system [33].

# Chapter 3
# EXPERIMENTAL TWO-DIMENSIONAL FLUIDIZATION APPARATUS

## 3.1 Design, Construction, and Essential Features of The Apparatus

The experimental system was designed to have a recirculating fluid supply system needing only one operator to maintain efficient and productive operation of all parts of the system (Figure A1).

Steel was chosen for the superstructure of the two-dimensional fluidization tank based on strength properties and price of the materials compared to plexiglass and wood (Figure A2). Tempered glass was chosen for the front panel due to its high degree of transparency (high transmission of light) which enhances visual observation and photographing of the two-dimensional fluidization phenomenon.

The hydraulic system, consisting of the manifold, fluidization pipe, feed pipes, and the leakage test drainage pipe is predominantly Schedule-80 PVC pipe (Figure A1). Schedule-80 PVC pipe was utilized for the hydraulic system of the apparatus based on its corrosion resistant quality, high strength properties, and workability. The 5.08 cm diameter fluidization pipe is 30.48 cm in length and has 0.317 cm diameter orifices spaced 5.08 cm centers and 2.54 cm from tempered glass panel and back steel plate panel. There are twelve orifices with six located on opposing sides of the pipe (Figure A3). The leakage test drainage pipeline system is used to perform fluidized/unfluidized region interface leakage tests. Details of the test procedure are discussed in Section 3.2.

An outfall weir chute transmits overflow from the fluidization tank to a

settling tank. The settling tank was designed to allow for the sedimentation of any out-wash from the fluidization tank. This process extends the life expectancy of the pump system by preventing pitting of the impeller by the sand particles and ultra-fine sediment particles from entering the seals of the pump.

The head tank is located between the settling tank and the recirculating pump. The two major purposes of the head tank are to provide the pump with an adequate positive suction head and an adequate volume of water to satisfy volume requirements in the tank system.

The pump was chosen based on flow rate and head requirements for a 6.4 cm bed expansion of a 11,148 sq. cm. sand bed consisting of a 0.15 mm sand (mean for the sand used in this study) and for possible coarser distributions in the future. One-dimensional fluidization of the entire bed was originally designed to be accomplished via the manifold located at the bottom of the fluidization tank (Figure A1). This would be performed prior to testing to wash out any ultra-fines from the system and to mix the bed medium to produce as close to a homogeneous and isotropic porous structure as possible. However, there were problems of clogging and filling of the manifold pipe which prevented it from operating efficiently.

Fine sand was chosen because it has the size, shape, and consistency of material found in the coastal environment, since this environment is the area of direct application of this technology. Refer to Appendix C for sand properties and Figure C1 for grain size distribution of the sand used in this study.

Reservoir cages, located in the fluidization tank, were designed to allow water to seep into the reservoir while preventing sand particles from entering the caged region during horizontal hydraulic conductivity tests. Attempts were

made to use the Dupuit-Forchheimer theory to determine a representative horizontal hydraulic conductivity of the fixed bed during pre-fluidization conditions, but were unsuccessful (refer to Appendix A).

The data acquisition system is designed to collect hydraulic head data for two initial bed depth conditions (25.4 cm and 42 cm) at various flow rates (Figure B1). Approximately 72 of the 143 pressure taps are monitored as a part of the data acquisition system (Figure B2). Because of the steady state manner in which the fluidization phenomenon is investigated here, one pressure transducer can be used to monitor the pressures from all 72 pressure taps. This is accomplished using several "fluid switch wafers" which sample only one pressure tap at a time; therefore, this provides for time sharing of the single transducer by all the taps in operation.

## 3.2 Test Preparations and Procedures

Initial bed depths of 25.4 cm and 42 cm were chosen to perform the experimental research because they are representative of the range of depths possible in the fluidization tank. Therefore, sand is removed from or added to the fluidization tank to satisfy bed depth requirements for a test. Preparation for testing consists of the following:

- Mix the bed by fluidizing the entire bed via the tank base manifold and assistance from jet aggitation via a hose hooked up to the laboratory's municipal water supply (under pressure). This mixing provides for a closer approximation of a homogenous and isotropic bed condition.

- Rod the bed to remove air entrapped in bed and to mix the bed to make it more uniform. This process also compacts the bed and reduces the porosity and thus the hydraulic conductivity and corresponding seepage rate.

- Mark tempered glass front panel with water soluble markers to indicate initial bed surface and fluidization pipe locations.

- Close drainage valve of leakage test drainage system.
- Install baffle into the settling tank.
- Make sure there is an adequate volume of water in all functioning divisions of the apparatus (fluidization tank, settling tank, head tank). By filling the head tank to a level of at least 60.96 cm from the bottom, the pump is automatically primed and provided with adequate suction head.
- Keep the valve installed in the line from settling tank to head tank closed at low flow rates. Open the valve when appreciable draw down is noticed in head tank at higher flow rates.
- Have 1000-ml cylinder and stopwatch accessible for making flow rate measurements and data sheets for recording all raw data.

**Test Procedures:**

1. General Test Procedures

   a. Determine hydrostatic level measurement for surplus head on outfall weir prior to turning on the pump. This head is determined by a staff gage attached to the inside of the tank adjacent to the reservoir cage.

   b. Turn on the pump and open the valve to the pump slightly to allow for the establishment of a small initial flow rate during pre-fluidization conditions.

   c. Increase flow rate in relatively small increments to allow the sand bed system to adjust and stabilize and also to allow pre-fluidization hydraulic heads to build in the porous medium. This incremental increase in flow rate procedure enables the experimenter to better estimate when incipient fluidization occurs and to observe the physical processes contributing to the change in bed condition.

   d. At each flow rate take flow rate measurements of the outfall discharge via the 1000 ml volumetric cylinder and stopwatch. Scan pressure taps (channels) and read corresponding pressures in millivolts on the multimeter. Measure the surplus head on the outfall weir.

e. Note the point of incipient fluidization and any observed physical processes. For post-fluidization, sketch and record the bed expansion depth on the data sheets and the tempered glass front panel, and also sketch the fluidized/unfluidized region interface with the corresponding flow rates, respectively. Continue to record pressure readings at each flow rate.

2. Probe Test Procedures

a. Allow the system to stabilize at post-fluidization conditions of a particular flow rate of interest. Fluidized region must be completely developed.

b. Using the probe system attached to the Scanivalves and in turn to the pressure transducer, three-dimensional hydraulic head distribution data is collected. Record pressures at defined x, y, and z coordinates.

c. Record flow rate measurements and surplus head readings. Sketch interface and bed expansion depths on tempered glass.

3. Leakage Test Procedures

a. Allow fluidized region to completely develop (reach equilibrium or stable state).

b. Install interface leakage partition into fluidization tank. Insert the partition into the top of berm and drive it in far enough to ensure isolation of unfluidized region head water, of the side opposite the outfall end, from the rest of the tank.

c. Isolation of the fixed bed head water from the fluidized bed head water allows the head to build on the fixed bed side of the partition. This is a direct result of an additional volume of water leaking across the interface from the fluidized region to the unfluidized region and flowing to the stagnation zone above the fixed bed surface.

d. The volume of leakage is determined by opening the leakage drainage valve and allowing the heads on either side of the partition to reach equilibrium (the same water elevation) and measuring the flow rate at the outfall of the leakage test drainage pipe system. Maintaining relatively equal heads on either side of the partition indicates the water is being drained out of the tank at a rate equal to the rate it is flowing across the interface. Therefore, if the filling of a volumetric cylinder

is timed, the flow rate across one side of the interface can be determined.

e. The total leakage from the fluidized region to the unfluidized region is equal to double the value attained from the measurement of one side of the interface. The value can in turn be compared to the total flow rate entering the fluidization tank via the fluidization pipe.

4. Tracer Study Test Procedures

a. Install dye reservoir with petcock valves and copper tubing feed line above fluidization tank.

b. The dye reservoir must have adequate head in order for the tracer to flow by means of gravity into the fluidized region. It encounters pressures produced by flow into this region from the fluidization pipe. Therefore, the reservoir is placed on the second floor of the laboratory and the feed line is threaded through the floor grates to the fluidization tank on the first floor of the laboratory.

c. The tracer can be regulated by a valve in the line located immediately below the reservoir on the second floor of the laboratory or by a valve in the feed line attached to the fluidization tank on the first floor of the laboratory.

d. Blue and green dye tracers were chosen because they produce the highest quality photographs (color intensity, clarity).

# Chapter 4
# EXPERIMENTAL RESULTS

The experimental data for 25.4 cm and 42 cm initial sand bed depths are presented. The initial depth of the sand bed is the depth of bed from the center of the fluidization pipe to the initial bed surface. The center line of the pipe is at (x, y) = (254.0 cm, -68.6 cm), according to the grid system devised for the pressure tap data acquisition system. The y coordinates for the sand bed depths of 25.4 cm and 42 cm are y = -43.2 cm and y = -26.6 cm, respectively.

There were six independent tests performed and in each test the hydraulic head distribution was measured for six to ten steady flow rates. Tests 1, 2, 3 and 6 were performed with a 25.4 cm initial bed condition and Tests 4 and 5 were performed with a 42 cm initial bed condition. Flow rates were varied from a very low flow rate for pre-fluidization Q = 0.007 liter/sec-meter to a reasonably high post-fluidization flow rate of Q = 3.77 liter/sec-meter.

Testing was not performed specifically at incipient fluidization conditions due to the rapid speed at which the bed responds to this somewhat transient phenomenon in unbounded domains. The transient nature makes steady state measurements of hydraulic head difficult. To determine the point of incipient fluidization, data must be obtained in the pre-fluidization and post-fluidization stages as close as possible to this point and then predict from the data where this point occurs. This predicted value can be compared to estimates obtained by theoretical techniques.

In addition to the head distribution data obtained, data was collected on the geometry of the fluidized region. These data consisted of the size and

shape of the fluidized region including: (1) the top width (berm to berm), (2) middle width (width at one half the expanded depth), (3) base width (width between points indicated by a change in slope of the interface from horizontal to vertical), (4) fluidized/unfluidized region interface location, (5) and the resulting bed expansions. Interface leakage test data were also collected.

Tracer studies were performed as part of this overall effort because flow visualization is necessary to aid in the understanding of two- and three-dimensional fluidization. The dye tracer injected along the side of the fluidization pipe in the fluidized region conforms to the flow pattern established by the jets issuing from the fluidization pipe.

Figures 3 and 4 and Plate 7 show the general physical processes at the fluidized/unfluidized boundary and within the fluidized region. The remainder of this chapter will address the results of the data collection.

## 4.1 Hydraulic Head Distribution

Hydraulic head distribution plots are developed from the data collected from the pressure tap distribution located on the back steel plate panel of the fluidization tank. This tap distribution is shown in Figure B2. The grid system is established for use in producing the head distribution plots. A numerical model will use this data for verification prior to prediction simulations. Taps were constructed on one side of the center line of the fluidization pipe since this line represents the expected line of symmetry for the two-dimensional fluidization phenomenon. The intersection of the apex of the outfall weir on the fluidization tank and the center line of the fluidization pipe is chosen as the origin of the grid system (Figure B2). The x coordinate of the origin is arbitrarily chosen as 254.0. The pipe center coordinates and the y coordinates of the in-

itial bed depths presented at the beginning of this chapter are based on this coordinate system .

The pressure transducer was calibrated via the balancing pressure column and a linear regression program was used to obtain the slope of the relationship between water pressure and transducer signal. A typical set of hydraulic head distribution plots for flow rates ranging from pre-fluidization to post-fluidization conditions is shown for Test 2 in Figure 7A through 7C. The relationship for hydraulic head in terms of tap pressure, $P_x$, in millivolts, and in terms of hydrostatic pressure, $P_o$, in millivolts yields,

$$\phi = [\frac{1}{\gamma_w}(P_x - P_o) \times \beta] 2.54 \tag{4.1}$$

where $\gamma_w$ is the specific weight of water, $lb/in^3$, $\beta$ is the slope of linear relationship of pressure to pressure transducer signal (psi/mv), and 2.54 is the conversion factor from inches to centimeters. Therefore, the hydraulic heads in the plots have units of centimeters. Test 2 was performed for an initial bed depth of 25.4 cm (y = -43.2 cm), flow rates ranging from 0.012 l/s-m to 3.22 l/s-m, and an initial compacted bed porosity ($\epsilon_o$) of 39 percent.

The lines of equal hydraulic head (equipotential lines) form an elliptical shape around the immediate vicinity of the fluidization pipe during pre-fluidization (Figure 7A). As the flow is increased, the equipotential lines grow in value as expected and the elliptical shape becomes more pronounced (Figure 7B).

In Figure 7C for the high flow rates during post-fluidization, the equipotential lines are constant in the horizontal x direction at any given elevation (y coordinate) in the fluidized region. The hydraulic head lines in the fluidized region decrease, become non-horizontally directed, at the intersection with the

fluidized/unfluidized region interface. The hydraulic head drops off dramatically in the unfluidized region from the fluidized region value for the same corresponding y coordinate. Also, Figure 7C indicates the location of the fluidized/unfluidized region interface for the post-fluidization flow rate of 2.16 l/s-m and 3.60 l/s-m, respectively.

A probe test was performed to determine if the hydraulic head is constant in the third dimension (z direction). Only raw experimental pressure data (millivolts) was collected at various x, y, and z coordinates on either side and along the center of the pipe. These data reveal that the hydraulic head is constant in the third dimension; therefore, the head is constant throughout the fluidized region at any y coordinate. The probe test was performed on two fluidization flow rates of Test 6 (Q = 2.79 l/s-m and Q = 3.77 l/s-m).

The remaining hydraulic head plots for the other five tests can be found in Appendix E. These plots show similar characteristics to the plots just discussed.

## 4.2 Incipient Fluidization

### 4.2.1 Relationship Between Hydraulic Gradient and Flow Rate

The plots of the vertical hydraulic gradient, $\Delta\phi/\Delta y$, versus flow rate, Q, Figures 8 and 9, are obtained by plotting the hydraulic head difference between two chosen taps for a given flow rate. Tap numbers 14 and 59 were chosen for this purpose because the greatest head difference occurs between these two taps. There is a high probability that the initiation of fluidization will occur in the vertical zone containing these two taps. This vertical zone is the sand bed space adjacent to and directly above the fluidization pipe (Figure B2). These

taps are indicated on the head distribution plots of Figures 7A through 7C as half solid circles.

As stated in Section 2.1, the theoretical hydraulic gradient necessary for fluidization, the critical hydraulic gradient, is typically a value of 1.02 cm/cm for the sand tested. Figures 8 and 9 show that a critical hydraulic gradient of at least 1.02 cm/cm was obtained for both initial bed depth conditions. In particular, critical hydraulic gradient values of 1.06 cm/cm and 1.25 cm/cm were obtained for the initial bed depths of 25.4 cm and 42 cm, respectively. These values are represented by the peaks of the plots (Figures 8 and 9) of initial bed depths of 25.4 cm and 42 cm at the corresponding flow rates of 0.090 liter/sec-meter and 0.135 liter/sec-meter.

The experimental incipient fluidization superficial velocity for both initial bed depths (25.4 cm and 42 cm) can be calculated using the above estimated incipient flow rates. The flow rates are used to enter Figures 15 and 16 for the top widths of the corresponding fluidized regions ($W_T$). These top widths are in turn used to calculate the cross-sectional areas of the top of the respective fluidized regions. The cross-sectional areas are equal to the product of the fluidization pipe length and the fluidized region top width ($W_T$). Therefore, the experimental incipient fluidization superficial velocity of either bed depth is the estimated incipient fluidization flow rate divided by the top cross-sectional area of the respective fluidized region. The experimental incipient fluidization superficial velocities ($V_i$) at the bed surface were calculated to be 0.043 cm/s and 0.045 cm/s for the initial bed depths 25.4 cm and 42 cm, respectively.

These values can be compared to the one-dimensional theoretical incipient fluidization superficial velocity. The Galileo number, $G_a$, is calculated using Eq.

2.17 and is substituted into the particle Reynolds number, $R_i$, Eq. 2.16. Once the particle Reynolds number, $R_i$, is determined, the incipient fluidization superficial velocity, $V_i$, can be calculated from $V_i = R_i\mu/\rho d_{eq}$, as defined in Section 2.1 [8]. The incipient fluidization superficial velocity resulting from this calculation for an equivalent grain diameter of $d_{eq} = d_{90} = 0.21$ mm is $V_i = 0.044$ cm/s. The percent deviation between the experimental and theoretical values is 2.3% and 2.3% for the 25.4 cm and 42 cm initial bed depth conditions, respectively. Although Eq. 2.16 and Eq. 2.17 were derived to predict the incipient fluidization superficial velocity for one-dimensional fluidization, the theoretical solution appears to be a very close approximation to the actual experimental two-dimensonal incipient fluidization conditions.

### 4.2.2 Relationship Between Hydraulic Head and Flow Rate

The hydraulic head, $\phi$, versus flow rate, Q, plots, Figures 10 through 14, demonstrate how the hydraulic head changes at several bed locations with corresponding increases in flow rate for both initial bed depths (25.4 cm and 42 cm). Hydraulic head at pressure taps 14, 59, 6, 67, 1, and 106 are plotted against the respective flow rates for the 25.4 cm initial bed depth conditions. The hydraulic head for pressure taps 14, 59, 1, and 106 are plotted against respective flow rates for the 42 cm initial bed depth conditions. Refer to Figure B2, and Figure 7A through 7C for tap locations with reference to the fluidization pipe.

Taps (14,59,6,67,1,106) were chosen to be representative of the head changes occurring throughout the entire bed due to the symmetry of the two-dimensional phenomenon. Taps 14, 6 and 1 are located on the horizontal line of trajectory of the jets and tap 59 is located in the space above the pipe.

These four taps proved to have the greatest increase in hydraulic head with increase in flow rate of the six taps chosen. Tap 14 experienced the most substantial head increases, followed by taps 59 and 6 which showed comparable head increases for corresponding increases in flow rate. The head increases for tap 1 are about half the value of tap 59 or 6, but are still higher than either tap 67 or 106 which are not located in the bed areas most significantly influenced by the jets.

It is shown in Figures 10 and 13 that a distinct peak in the hydraulic head formed at the point of incipient fluidization flow rate at tap 14 for both initial bed depths. This is attributed to the fact that tap 14 is directly adjacent to the fluidization pipe and is exposed to extreme increases in hydraulic head with corresponding increases in flow rate during the pre-fluidization stage. These figures also show that the pre-fluidization relationship is linear until incipient fluidization. After the initiation of fluidization, the hydraulic head drops significantly, the bed stabilizes and the hydraulic head begins to increase during post-fluidization. Eventually, the head levels off and drops at the higher flow rates, which is more pronounced in the 25.4 cm initial bed depth condition.

In Figure 13, tap 59 shows a slight peak formation at the point of incipient fluidization for the 42 cm initial bed depth condition, but a more gradual transition from the pre-fluidization state to the post-fluidization state, as shown in Figure 10, was experienced for the 25.4 cm initial bed depth condition. Tap 59 experienced post-fluidization behavior similar to that of tap 14 for both initial bed depth conditions.

Taps 6 and 67, indicated as solid circles in Figures 7A through 7C, were chosen to represent the hydraulic head changes taking place toward the center

portion of the tap distribution (see Figure B2). Tap 6 (Figure 11) experiences a linear rise in head during pre-fluidization, a slight drop at incipient fluidization. and a rise during post-fluidization as the region widens with increased flow rate. Figure 11 shows tap 67 experiencing a gradual rise in head from pre-fluidization to post-fluidization and a temporary leveling off of head until it directly encounters the influence of the fluidized region. The head begins to rise again as the fluidized region widens and includes tap 67 within its boundary of influence. These taps were only plotted for the 25.4 cm initial bed depth condition.

Taps 1 and 106, indicated as open circles (Appendix E), were chosen to represent the hydraulic head changes occurring at he extreme far end of the pressure tap distribution (Figure B2). In Figure 12, taps 1 and 106 show a linear pre-fluidization stage and a gradual rise up to and through the post-fluidization stage for an initial bed depth condition of 25.4 cm. In Figure 14, tap 106 shows similar behavior for the 42 cm initial bed depth condition as tap 106 showed for the 25.4 cm bed depth condition. However, tap 1 in Figure 14 shows a linear pre-fluidization relationship, a formation of a peak and a drop at the point of incipient fluidization, and then a nonlinear rise during post-fluidization. This peak and drop are not attributed to the portion of the bed at tap 1 being fluidized. Instead, the peak is attributed to the head build up around the fluidization pipe, during the pre-fluidization stage, extending its influence throughout the bed (predominately in the horizontal direction). The head drop in the bed at Tap 1 is attributed to the release of this pre-fluidization head build up, around the pipe, at the point of incipient fluidization.

The peak or drop is not formed at tap 1 for a 25.4 cm initial bed depth (see Figure 12); instead, a more gradual transition is made from pre-fluidization to post-fluidization. Also, the heads are substantially higher for taps 14 and 59 for the 42 cm initial bed depth condition than for the 25.4 cm initial bed depth condition. This implies that the jet issuing from the fluidization pipe has a greater influence on the bed, that is an ability to increase the heads in the bed, at the larger initial bed depth. This is attributed to the fact that there is an increase in resistance to the upward acting flow with increase in bed depth. Therefore, an increase in resistance results in an increase in hydraulic head in the bed and a corresponding extension of the zone of influence of the fluidization pipe jets issuing from the pipe orifices.

## 4.3 Geometry of the Fluidized Region

### 4.3.1 Flow Rate / Fluidized Region Width Relationships

During post-fluidization, the geometry data of the fluidized region were directly recorded onto the tempered glass face of the tank. Markers were used to indicate the location of the fluidized/unfluidized region interface, berm formation and the location of the expanded bed for corresponding increases in flow rate. These data were in turn transferred to templates providing permanent records of the various test results. Once the data were recorded onto the templates, the top width (berm to berm) of the fluidized region ($W_T$), the width of the fluidized region at one half the expansion depth ($W_M$), the base width of the fluidized region ($W_B$), and the expanded bed depth were all measured. The data appear in Table 1 with the respective flow rates. Figures 15 through 17 were constructed utilizing the data contained in Table 1. These

figures demonstrate the linear relationship that exists between base width, $W_B$, mid-width, $W_M$, top width, $W_T$, and flow rate, Q, for the range of flow rates and initial bed depths studied. Figure 15 shows the linear relationship between the fluidized region widths, $W_T$, $W_M$, $W_B$, and flow rate, Q, for the 25.4 cm initial bed depth. Figure 16 shows the linear relationships for the 42 cm initial bed depth. It is believed that if the flow rate/width relationship is linear for each individual initial bed depth condition, then it should be linear regardless of initial bed depth condition and range of flow rates studied. The data for both bed depths is compiled into one plot (Figure 17). The linear functions are indicated on each plot including slope and intercept information along with correlation coefficients. The flow rates, Q, in the functions given have the units of $cm^3/s$.

Figure 18 shows the flow rate/top width relationship for this experimental study compared to data collected by Weisman and Collins [30]. It is evident, for the same fluidization orifice diameters, similar bed depths, and fairly similar specific gravities of the sand particles of the two studies, that the finer sand distribution of this study, $d_{50}$ = 0.15 mm, has a wider fluidized region top width for any given flow rate. The Weisman and Collins study [30] used two sand distributions having two different mean diameters ($d_{50}$ = 0.23 mm and 0.51 mm) and the finer sand distribution also has a wider fluidized region top width for a given flow rate. Note that the Weisman and Collins data indicates that the width/flow rate relationship is initially linear, but appears to level off at higher flow rates.

The six tests performed in this experimental study are compiled in Table 2 in which the ratios of $W_M/W_T$ and $W_B/W_T$ are listed for given flow rates and

tests. The average fluidized region middle width is 63% of the top width and the average base width is 36% of the top width. The standard deviations are 4.9% and 8.9%, respectively. These relatively small standard deviations indicate that the geometry of the fluidized region is quite consistent regardless of initial bed depth, indicating the consistency of data collected in all six tests.

There are several factors influencing the growth of the fluidized region, but it is believed that the erosion potential of a sand particle is one of the most important factors in determining the characteristics of this growth. The flow rate/width relationship of the fluidized region is viewed to be significantly influenced by the erosion potential of a particle, once the post-fluidization condition is fully developed. Thus, for a given flow rate, this may explain why the fluidized region is much wider for a fine particle distribution than a coarser particle distribution as shown in Figure 18.

The fluid velocity of the jets decreases as a result of the bed resistance and entrainment as it extends further out from the fluidization pipe in the x and y directions. Therefore, it takes greater flow rates to achieve the critical erosive velocity of a particle at a particular x and y coordinate. In addition, the flow rate required to achieve the critical erosive velocity of a coarse sand particle is greater than that of a fine sand particle of the same specific gravity. Therefore, if a given flow rate provides a critical velocity to erode a fine particle from a given point on the interface between the fluidized region and the unfluidized region, it is probable that this velocity may be insufficient to erode the coarser particle from the same location on the interface.

### 4.3.2 Boundary Conditions of the Fluidized / Unfluidized Region Interface

Boundary conditions of the fluidized/unfluidized region interface refer to the x and y coordinates and the hydraulic head of points along the interface. These boundary conditions were determined initially by measuring the location of the arbitrarily chosen points along the interface with respect to the center of the fluidization pipe using the templates described in Section 4.3.1. These measured distances with respect to the fluidization pipe center were in turn converted to the fluidization tank's pressure tap grid system (x and y coordinate system). The plots of the interfacial boundary conditions as shown in Figure 4 for Test 2 include initial and expanded bed depths and corresponding flow rates in addition to the hydraulic head indicated at various points along the interface. The boundary conditions for the other tests can be found in Appendix D. The boundary conditions are also listed in Tables 3 through 7 to assist the reader in attaining more exact values for boundary conditions than might be obtained by reading x and y coordinates from the plots. Boundary conditions for a 25.4 cm initial bed depth condition are found in Figure 4 and Figures D1 and D2. Boundary conditions for a 42 cm initial bed depth condition are found in the Figures D3 and D4.

The figures show similarities for the size, shape, and hydraulic head values along the interfaces for the same initial bed depth conditions. This shows that the results were reproducible from test to test.

Another boundary condition of importance is leakage across the interface from the fluidized region into the unfluidized region during the two-dimensional fluidization process (Figure 3). Leakage was measured as outlined in the test

procedure of Section 3.2. The data collected are presented in Table 8 for various fluidization flow rates and initial bed depth conditions. The fluidization tests during which the leakage tests were run are indicated in the table. The total leakage across the interface and the percent of the total fluidization flow rate during which the leakage tests were run are presented in the table. It is evident from the values measured, that the leakage across the interface of a well established fluidized region is less than 5% of the total fluidization flow rate entering the system. In addition, the leakage across the interface during Tracer Study 2 was visually studied. It was observed that the velocity of the leakage across the interface decreases with decreasing driving head. In particular, as fluidized bed material or slurry was removed from the fluidized region via a siphon, a dramatic decrease in the velocity was observed as the tracer leaked from the fluidized region to the unfluidized region.

### 4.3.3 Bed Expansion and Fluidized Region Sand Concentration

Figure 19 shows that the post-fluidization relationship between flow rate and bed expansion is not a linear function as is the case with one-dimensional fluidization (Refer to Figure 2). The relationship also appears to level off with increasing flow rate. These data are also presented in Table 1.

The average sand concentration in the fluidized region, $\overline{C}$, is the mass of sand particles in the region per volume of the region. The volume of sand particles comprising the original fixed bed inside the boundary of the existing fluidized region, $V_{st}$, is calculated from the total volume of the fixed bed located within the boundary of the fluidized region, $V_T$, multiplied by $(1 - \epsilon_o)$, where $\epsilon_o$ is the porosity of the compacted fixed bed (39%). The volume of sand particles in the fluidized region, $V_l$, is calculated by subtracting the volume of sand par-

ticles in the berms, $V_B$, from $V_{st}$. To obtain the volume of sand particles in the berms, $V_B$, the volume of the berms sketched on the front glass panel of the fluidization tank is measured and multiplied by $(1-\epsilon_B)$, where $\epsilon_B$ is the porosity of the loosely compacted berms assumed to be 46%. The volume of the fluidized region, the volume occupied by the expanded bed, is measured from the geometry of the fluidized regions sketched on the front glass panel of the fluidization tank, $V_2$. The mass of sand in the fluidized region, $m_s$, is calculated by multiplying the volume of sand particles in the fluidized region, $V_1$, by the mass density of the sand particles, $\rho_s$. Therefore, the average concentration of sand in the fluidized region, (grams/liter), is equal to the mass of the sand in this region , $m_s$, divided by the volume of the fluidized region, $V_2$.

The average concentration data are listed in Table 9 and plotted in Figure 20. The data show a nonlinear decrease in average concentration with an increase in flow rate.

The leveling off of the relationship between bed expansion and flow rate, as shown in Figure 19, can be attributed to the fact that greater and greater flow rates are needed to produce significant changes in the fluidized region width. Therefore, with equal incremental increases in flow rate, there is less and less bed material to be expanded vertically and thus the bed expansion tapers off. The reduction in the suspended bed material is possibly attributed to the reduction in newly eroded material available for suspension and a loss of old and new material to the process of berm construction at the higher flow rates. As the flow rate is increased, more material is added to the berms. The decrease in the amount of suspended material available in the fluidized region is evident by the decrease in the average sand concentration in the fluidized region

with increase in flow rate as shown in Figure 20. It appears that the bed expansion/flow rate relationship and the average sand concentration in the fluidized region/flow rate relationship are related.

## 4.4 Tracer Studies of Two-Dimensional Fluidization Physical Processes

Tracer studies were performed to help visualize flow processes associated with two-dimensional fluidization. Photographs were taken to document the tracer studies, providing visual representation of various aspects of the flow. Selected photographs are presented in Plates 1 through 8 for a 42 cm initial bed depth condition and an initial bed porosity of 39%.

Plate 1 is an overall photograph of the two-dimensional fluidization tank containing a 42 cm sand cover above the fluidization pipe indicated by the circle marked on the face of the tempered glass front panel. The photograph is taken at a low flow rate during the pre-fluidization stage; therefore, there is no response of the bed to this flow rate.

Plate 2 shows the initiation of fluidization above one source hole (orifice) located on the side of the fluidization pipe. The water supplied under high pressure through the fluidization pipe packs the bed adjacent to the orifices resulting in the establishment of a cavity and pressures or hydraulic heads in this vicinity which are much higher than heads found in the rest of the bed. The head increases up to the point where the critical hydraulic gradient is equal to a value of approximately 1.25 cm/cm (for 42 cm bed depth), resulting in a corresponding eruption of a small region of the bed surface above the pipe. The small fluidized region begins to grow until the establishment of complete uniform two-dimensional fluidization. This process has also been observed by

other investigators such as Weisman and Collins [30], Weisman et al. [31], and Kelley [20].

Plate 3 shows horizontal lines marked on the glass which represent the initial bed depth and expanded depth locations. Also, the fluidized/unfluidized region interface and the berms are recorded on the glass. The figure also shows the establishment of uniform fluidization and completed berm formation at an estimated flow rate of Q = 1.61 liter/sec-meter, which is greater than the flow rate of Q = 1.35 liter/sec-meter indicated by the interface line drawn on the glass. A high concentration tracer is injected into the fluidized region along the side of the fluidization pipe via a tube attached to a reservoir of dye above the tank for a short period of time (~5 sec). The jets issuing from the fluidization pipe as displayed by the tracer represents a typical flow pattern at a relatively low flow rate.

Plate 4 shows the progressive widening and overall enlargement of the fluidized region with increases in flow rate. It also indicates that the flow pattern of the jet conforms to the boundary of the fluidized region up to a point equal to approximately half the expansion depth of the fluidized bed. At this point the jets separate into large and small eddy patterns. The flow rate is estimated to be Q = 2.18 liters/sec-meter.

The formation of a tracer front in the unfluidized region, the arc of dye located in the bottom-left of the photograph, is clearly seen in Plate 5. The tracer front marks the leakage occurring across the fluidized/unfluidized region interface of a high concentration of dye injected for a short period of time. The tracer front continues to migrate very slowly into the unfluidized region as a result of the driving head in the fluidized region.

Plate 6 shows the growth of the fluidized region for a flow rate of Q = 3.47 liter/sec-meter. The growth of this fluidized region is accomplished via the erosion of the fluidized/unfluidized region interface formed for the previous flow rate of Q = 2.18 liter/sec-meter. The jets erode the bottom of the wall, thereby causing an unstable slope condition for the wall of the unfluidized region. Downward slope movement of the unsupported sand material occurs as a result of this unstable condition. The eroded sand particles are entrained in the jets and are either used to build the berms, or the particles remain in suspension in the fluidized region as a result of the dynamics of the jets.

Plate 7 reveals the overall size, shape, and symmetry of the fluidized regions formed by the various flow rates. The flow pattern of the jets is shown for a higher flow rate of Q = 3.47 liter/sec-meter.

The settling of the fluidized bed after the flow to the source pipe is turned off is demonstrated in Plate 8. As the bed settles the dynamic and hydrostatic forces of the dense fluid (water and sand mixture) are eliminated above the line of settlement. Therefore, the upper portion of the interface slumps to the angle of repose of the sand (30°) in response to the removal of the dynamic and hydrostatic forces that maintain the interface at a steep angle during post-fluidization.

If the suspended material is siphoned out of the fluidized region, the berms would respond by slumping due to a loss of support along the interface. Eventually all the berm material is lost to the fluidized region and all the suspended material is removed from the region resulting in a substantial increase in the width of the fluidized region. Although a photograph is not presented, this phenomenon was observed in another tracer study during this experimental in-

vestigation. This phenomenon was also observed by Weisman and Collins [30], and is important in the application of this technology.

# Chapter 5
# SUMMARY, CONCLUSIONS AND RECOMMENDATIONS

## 5.1 Summary

The experimental research for this study was performed utilizing a two-dimensional fluidization apparatus consisting mainly of a two- dimensional fluidization tank with a data acquisition system hooked directly into the pressure tap distribution contained on the back panel of the tank. The pressure tap distribution was constructed on one half of the panel because the two-dimensional fluidization phenomenon is fairly symmetrical about the vertical center line of the fluidization pipe. Six tests were conducted at initial bed depth conditions of 25.4 cm and 42 cm, and for relatively constant sand bed properties ( porosity and hydraulic conductivity of the initial bed).

Hydraulic head distributions were obtained for six to ten steady flow rates, including both pre-fluidization and post-fluidization stages, for each of the six tests conducted. Relationships between hydraulic gradient and flow rate and between hydraulic head and flow rate were developed from the head distributions and showed consistency with the work of previous investigators.

The geometry of the fluidized region was obtained directly from the glass front panel of the fluidization tank. The widths of the fluidized region (top width, middle width, base width) were found to increase with an increase in flow rate. Thus, these data delineate the growth of the fluidized region with increasing flow rate. Boundary conditions were also determined for the fluidized/unfluidized region interface, consisting of hydraulic heads at various x and y coordinates on the interface and the leakage of water across the interface from the fluidized region to the unfluidized region.

Relationships were also obtained from the data for the vertical expansion of the fluidized region and the average sand concentration in the fluidized region as they vary with increases in flow rate. Tracer studies were performed to help visualize the flow processes associated with two-dimensional fluidization.

## 5.2 Conclusions

Based on the results of this study, the following can be concluded:

1. The data acquisition system, consisting mainly of Scanivalves, one differential pressure transducer, and the control system provides automation, sensitivity, and accuracy to the experimental data collection.

2. For pre-fluidization, the increases in hydraulic head throughout the bed with corresponding increases in flow rate are substantially higher for the 42 cm initial bed depth. There is an increase in resistance, or head build up, to the upward flow with increase in bed depth, causing an increase in the extent of the zone of influence of the fluidization pipe jets issuing from the source pipe holes. This influence on changes of head in the bed is predominantly felt in the horizontal x direction and the space directly above the pipe.

3. A theoretical one-dimensional incipient fluidization superficial velocity of $V_i$ = 0.044 cm/s for the size particle distribution used in this research is calculated from the method of Wen and Yu [8, 34]. The experimental incipient fluidization superficial velocities ($V_i$) are 0.043 cm/s and 0.045 cm/s for the initial bed depths of 25.4 cm and 42 cm, respectively. The corresponding experimental incipient fluidization flow rates are $Q_i$ = 0.09 l/s-m for a 25.4 cm bed depth and $Q_i$ = 0.14 l/s-m for a 42 cm bed depth.

4. The hydraulic head in the fluidized region is constant in the x direction at any elevation (y coordinate) and begins to decrease, become non-horizontally oriented, at the fluidized/unfluidized region interface. This phenomenon occurs regardless of the initial bed depth tested in this study.

5. The fluidized region widths ($W_T$, $W_M$, $W_B$) are a linear function of fluidization flow rate for the range of flow rates tested in this study. The average width of the fluidized region at one-half the expansion depth ($W_M$) is 63% of the fluidized region top width ($W_T$) and the average base width ($W_B$) is 36% of the fluidized region top width.

6. During post-fluidization conditions the vertical bed expansion increases nonlinearly with an increase in flow rate and the average sand concentration decreases nonlinearly with an increase in flow rate. These two processes are believed to be related.

7. The leakage across the fluidized/unfluidized interface is less than 5% of the total flow rate entering the system via the fluidization pipe. This low percentage of the overall flow rate leaking out of the fluidized region into the unfluidized region may prove to be negligible when numerically modeling the two-dimensional fluidization phenomenon.

## 5.3 Recommendations For Future Work

For further experimental work, the data acquisition system should be modified to make data collection more automated by integrating the entire present system with a data logger or a microcomputer via an analog to digital and digital to analog conversion circuit board. This would enable the experimenter to compile a data file of the hydraulic head distribution at a steady jet flow rate and have a plotting program plot the hydraulic head contour map on a graphics terminal at the site. Software can be written to provide interactive capabilities within the present system. A program can be designed to send digital signals that would be converted to electrical analog signals via the circuit board and used to address the Scanivalves to monitor a particular pressure tap of interest.

The next phase of experimental research on two-dimensional fluidization might focus on the physical processes of removing the suspended material from the fluidized region during the post-fluidization stage. Removal of the material causes the fluidized region to expand as result of the berms slumping into the fluidized region and the interface sloping to the angle of repose of the sand in response to an elimination of support of the interface by the suspended material.

This is what is meant to occur in the prototype application of this technology for sand management in the coastal environment. Photographs should be taken of the physical processes to provide documentation.

Most importantly the existing experimental data base can be used to calibrate a numerical model. Once the model is calibrated it will be used to interpolate results between data obtained in this study and make an attempt to extrapolate beyond the existing data base especially to the case of sand beds of two to five meters over the fluidization pipe. If the numerical model proves successful at simulating the two-dimensional fluidization phenomenon, then it can be used as a tool for the design of prototype fluidization systems.

# TABLES

**Table 1:** Geometry of Fluidized Region in Relation to Flow Rate

| TEST NO. | Q (cc/s) | Q (ℓ/s-m) | $L_o$ (cm) | $L_e$ (cm) | $W_T$ (cm) | $W_M$ (cm) | $W_B$ (cm) |
|---|---|---|---|---|---|---|---|
| 1 | 450 | 1.48 | 25.4 | 35.8 | 81.6 | 57.4 | 34.2 |
| 1 | 983 | 3.23 | 25.4 | 39.8 | 152 | 96.2 | 64.4 |
| 2 | 660 | 2.17 | 25.4 | 36.8 | 99.4 | 65.6 | 42.4 |
| 2 | 1098 | 3.60 | 25.4 | 40.8 | 173 | 107 | 71.0 |
| 3 | 69 | 0.23 | 25.4 | 28.6 | 27.0 | 14.5 | 6.0 |
| 3 | 72 | 0.23 | 25.4 | 29.0 | 35.5 | 20.0 | 8.0 |
| 3 | 362 | 1.19 | 25.4 | 33.0 | 66.2 | 47.4 | 27.0 |
| 3 | 703 | 2.31 | 25.4 | 38.7 | 104 | 68.2 | 48.0 |
| 3 | 977 | 3.21 | 25.4 | 39.4 | 142 | 91.2 | 60.6 |
| 4 | 56 | 0.18 | 42 | 45.4 | 28.0 | 16.0 | 6.0 |
| 4 | 397 | 1.30 | 42 | 53.3 | 77.0 | 46.4 | 24.0 |
| 4 | 671 | 2.20 | 42 | 55.9 | 110 | 71.2 | 44.4 |
| 5 | 83 | 0.27 | 42 | 45.2 | 36.6 | 21.4 | 8.0 |
| 5 | 603 | 1.98 | 42 | 54.9 | 107 | 66.2 | 40.0 |
| 6 | 853 | 2.80 | 25.4 | 36.2 | 135 | 81.2 | 50.2 |
| 6 | 1150 | 3.77 | 25.4 | 39.4 | 171 | 104 | 68.6 |

**Table 2:** Geometry of Fluidized Region in Relation to Q. Relation Between Top, Middle and Bottom Widths

| TEST NO. | Q (cc/s) | Q (ℓ/s-m) | $L_o$ (cm) | $L_e$ (cm) | $W_T/W_T$ (%) | $W_M/W_T$ (%) | $W_B/W_T$ (%) |
|---|---|---|---|---|---|---|---|
| 1 | 450 | 1.4 | 25.4 | 35.8 | 100 | 70 | 41.9 |
| 1 | 983 | 3.2 | 25.4 | 39.8 | 100 | 63 | 42.3 |
| 2 | 660 | 2.17 | 25.4 | 36.8 | 100 | 66 | 42.6 |
| 2 | 1098 | 3.60 | 25.4 | 40.8 | 100 | 62 | 41.1 |
| 3 | 69 | 0.23 | 25.4 | 28.6 | 100 | 54 | 22.2 |
| 3 | 72 | 0.23 | 25.4 | 29.0 | 100 | 56 | 22.5 |
| 3 | 362 | 1.19 | 25.4 | 33.0 | 100 | 72 | 40.8 |
| 3 | 703 | 2.31 | 25.4 | 37.2 | 100 | 66 | 46.3 |
| 3 | 977 | 3.21 | 25.4 | 39.4 | 100 | 64 | 42.6 |
| 4 | 56 | 0.18 | 42 | 45.4 | 100 | 57 | 21.4 |
| 4 | 397 | 1.30 | 42 | 52.9 | 100 | 60 | 31.2 |
| 4 | 671 | 2.20 | 42 | 55.9 | 100 | 65 | 40.5 |
| 5 | 83 | 0.27 | 42 | 45.2 | 100 | 59 | 21.9 |
| 5 | 603 | 1.98 | 42 | 54.9 | 100 | 66 | 41.1 |
| 6 | 853 | 2.80 | 25.4 | 36.2 | 100 | 60 | 37.1 |
| 6 | 1150 | 3.77 | 25.4 | 39.4 | 100 | 60 | 40.1 |

**Table 3:** Test 1. Boundary Conditions (x, y Coordinates and Hydraulic Head) Along Fluidized/Unfluidized Region Interface

| No. of Point On Interface | Q = 450 cc/s = 1.48 ℓ/s-m | | | Q = 983 cc/s = 3.23 ℓ/s-m | | |
|---|---|---|---|---|---|---|
| | x (cm) | y (cm) | $\phi$ (cm) | x (cm) | y (cm) | $\phi$ (cm) |
| 1 | 271 | -68.6 | 16.3 | 275 | -71.3 | 15.6 |
| 2 | 274 | -67.4 | 15.5 | 285 | -69.1 | 15.0 |
| 3 | 278 | -63.1 | 13.2 | 293 | -63.1 | 11.9 |
| 4 | 281 | -54.8 | 9.8 | 298 | -54.8 | 9.0 |
| 5 | 287 | -43.2 | 4.3 | 306 | -43.2 | 5.0 |
| 6 | 293 | -32.8 | - | 314 | -34.4 | 0.5 |
| 7 | 295 | -32.0 | - | 322 | -28.8 | - |
| 8 | 307 | -37.4 | - | 330 | -24.9 | - |
| 9 | 341 | -43.2 | - | 346 | -34.4 | - |
| 10 | - | - | - | 394 | -43.2 | - |

**Table 4:** Test 2. Boundary Conditions (x, y Coordinates and Hydraulic Head) Along Fluidized/Unfluidized Region Interface

| No. of Point On Interface | Q = 660 cc/s = 2.17 ℓ/s-m | | | Q = 1098 cc/s = 3.60 ℓ/s-m | | |
|---|---|---|---|---|---|---|
| | x (cm) | y (cm) | $\phi$ (cm) | x (cm) | y (cm) | $\phi$ (cm) |
| 1 | 271 | -69.2 | 17.0 | 275 | -72.4 | 14.2 |
| 2 | 277 | -67.4 | 16.0 | 288 | -69.1 | 13.1 |
| 3 | 281 | -63.1 | 14.0 | 295 | -63.1 | 11.1 |
| 4 | 285 | -54.8 | 10.8 | 302 | -54.8 | 8.2 |
| 5 | 291 | -43.2 | 5.0 | 311 | -43.2 | 4.0 |
| 6 | 300 | -31.8 | - | 323 | -34.4 | 2.0 |
| 7 | 304 | -28.8 | - | 331 | -27.8 | - |
| 8 | 326 | -37.4 | - | 340 | -23.3 | - |
| 9 | 375 | -43.2 | - | 361 | -34.4 | - |
| 10 | - | - | - | 404 | -43.2 | - |

**Table 5:** Test 3. Boundary Conditions (x, y Coordinates and Hydraulic Head) Along Fluidized/Unfluidized Region Interface

| No. of Point on Inter-face | Q=362 cc/s =1.19 ℓ/s-m | | | Q=703 cc/s =2.31 ℓ/s-m | | | Q=977 cc/s =3.21 ℓ/s-m | | |
|---|---|---|---|---|---|---|---|---|---|
| | x (cm) | y (cm) | $\phi$ (cm) | x (cm) | y (cm) | $\phi$ (cm) | x (cm) | y (cm) | $\phi$ (cm) |
| 1 | 265 | -68.6 | 17.2 | 272 | -70.1 | 17.0 | 275 | -71. | 16.0 |
| 2 | 271 | -67.4 | 16.0 | 279 | -67.4 | 15.5 | 283 | -69.1 | 14.4 |
| 3 | 274 | -63.1 | 13.8 | 283 | -63.1 | 13.2 | 290 | -63.1 | 12.2 |
| 4 | 277 | -54.8 | 9.9 | 287 | -54.8 | 10.1 | 295 | -54.8 | 8.8 |
| 5 | 281 | -43.2 | 4.3 | 293 | -43.2 | 5.1 | 304 | -43.2 | 5.1 |
| 6 | 286 | -35.6 | 1.5 | 302 | -31.4 | 1.5 | 312 | -34.4 | 2.3 |
| 7 | 287 | -34.9 | - | 306 | -29.9 | - | 320 | -29.2 | 1.2 |
| 8 | 305 | -43.2 | - | 322 | -37.4 | - | 325 | -26.2 | - |
| 9 | - | - | - | 349 | -43.2 | - | 339 | -34.4 | - |
| 10 | - | - | - | - | - | - | 379 | -43.2 | - |

**Table 6:** Test 4. Boundary Conditions (x, y Coordinates and Hydraulic Head) Along Fluidized/Unfluidized Region Interface

| No. of Point on Inter-face | Q=55.7 cc/s =0.18 ℓ/s-m | | | Q=397 cc/s =1.30 ℓ/s-m | | | Q=671 cc/s =2.20 ℓ/s-m | | |
|---|---|---|---|---|---|---|---|---|---|
| | x (cm) | y (cm) | ϕ (cm) | x (cm) | y (cm) | ϕ (cm) | x (cm) | y (cm) | ϕ (cm) |
| 1 | 257 | -68.6 | 24.0 | 261 | -68.6 | 30.0 | 274 | -69.1 | 28.4 |
| 2 | 258 | -66.8 | 23.8 | 271 | -66.2 | 27.0 | 279 | -66.8 | 26.8 |
| 3 | 260 | -64.1 | 23.4 | 273 | -61.7 | 25.3 | 281 | -61.7 | 24.7 |
| 4 | 261 | -58.8 | 21.2 | 273 | -55.1 | 22.2 | 283 | -55.1 | 21.7 |
| 5 | 261 | -51.6 | 18.9 | 275 | -49.0 | 18.1 | 285 | -49.0 | 19.0 |
| 6 | 263 | -41.6 | 13.0 | 278 | -41.4 | 13.7 | 289 | -41.4 | 14.3 |
| 7 | 264 | -32.1 | 6.0 | 281 | -33.8 | 11.3 | 292 | -33.8 | 11.5 |
| 8 | 265 | -26.4 | 2.5 | 284 | -23.7 | 5.0 | 298 | -23.7 | 6.1 |
| 9 | 267 | -23.2 | - | 289 | -17.8 | 2.5 | 302 | -16.1 | 3.0 |
| 10 | 278 | -26.7 | - | 291 | -15.7 | - | 305 | -12.7 | - |
| 11 | - | - | - | 293 | -15.3 | - | 309 | -11.8 | - |
| 12 | - | - | - | 299 | -17.3 | - | 322 | -17.3 | - |
| 13 | - | - | - | 309 | -20.9 | - | 347 | -26.7 | - |
| 14 | - | - | - | 324 | -26.7 | - | - | - | - |

**Table 7:** Test 5. Boundary Conditions (x, y Coordinates and Hydraulic Head) Along Fluidized/Unfluidized Zone Interface

| No. of Point On Interface | Q = 83.3 cc/s = 0.27 ℓ/s-m | | | Q = 603 cc/s = 1.98 ℓ/s-m | | |
|---|---|---|---|---|---|---|
| | x (cm) | y (cm) | $\phi$ (cm) | x (cm) | y (cm) | $\phi$ (cm) |
| 1 | 258 | -68.6 | 24.5 | 261 | -68.6 | 28.2 |
| 2 | 259 | -66.8 | 24.0 | 271 | -69.1 | 26.0 |
| 3 | 261 | -64.1 | 22.2 | 277 | -66.8 | 24.4 |
| 4 | 263 | -58.8 | 21.0 | 280 | -61.7 | 21.2 |
| 5 | 263 | -51.6 | 16.5 | 281 | -55.1 | 18.0 |
| 6 | 264 | -41.6 | 11.0 | 283 | -49.0 | 14.5 |
| 7 | 267 | -32.1 | 5.5 | 287 | -41.4 | 10.5 |
| 8 | 268 | -26.4 | 2.5 | 291 | -33.8 | 5.5 |
| 9 | 269 | -23.4 | - | 296 | -23.7 | 2.4 |
| 10 | 272 | -22.7 | - | 301 | -16.1 | 1.7 |
| 11 | 285 | -26.7 | - | 306 | -13.8 | - |
| 12 | - | - | - | 308 | -13.0 | - |
| 13 | - | - | - | 317 | -17.3 | - |
| 14 | - | - | - | 337 | -26.7 | - |

**Table 8:** Relationship Between Flow Rate and Leakage Across the Fluidized/Unfluidized Region Interface

| TEST NO. | Q (cc/s) | Q (ℓ/s-m) | $L_o$ (cm) | $\varepsilon_o$ (%) | Leakage q (cc/s) | Percent of Flow Rate (%) |
|---|---|---|---|---|---|---|
| 3 | 703 | 2.31 | 25.4 | 39 | 14 | 2 |
| 3 | 977 | 3.21 | 25.4 | 39 | 17 | 2 |
| 4 | 671 | 2.20 | 42 | 39 | 22 | 3 |
| 5 | 603 | 1.98 | 42 | 39 | 18 | 3 |
| 6 | 1150 | 3.77 | 25.4 | 39 | 9 | 1 |

**Table 9:** Relationship Between Flow Rate and Average Calculated Concentration of Sand in the Fluidized Region

| TEST NO. | Q (cc/s) | Q (ℓ/s-m) | $L_o$ (cm) | $\bar{C}$ (g/ℓ) |
|---|---|---|---|---|
| 4 | 55.7 | 0.18 | 42 | 1365 |
| 3 | 362 | 1.19 | 25.4 | 985 |
| 4 | 397 | 1.30 | 42 | 918 |
| 4 | 671 | 2.20 | 42 | 813 |
| 3 | 703 | 2.31 | 25.4 | 756 |
| 3 | 977 | 3.21 | 25.4 | 633 |
| 2 | 1098 | 3.60 | 25.4 | 604 |

# FIGURES

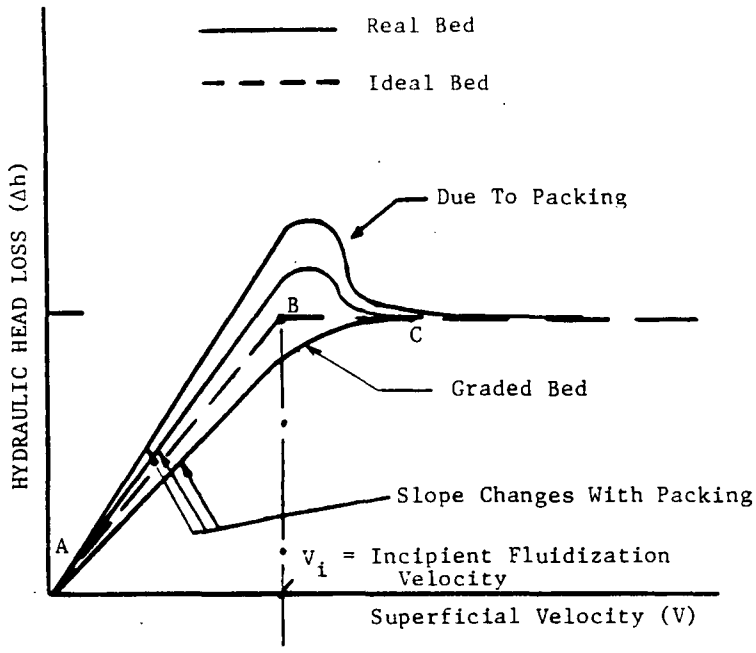


**Figure 1:** Characteristics of One-Dimensional Fluidization (Bounded Domain) [1]

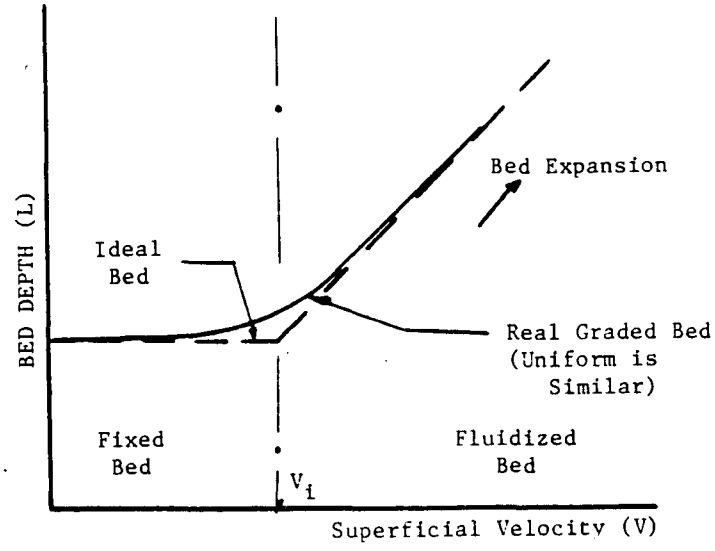


**Figure 2:** Response of Bed to One-Dimensional Fluidization [1]

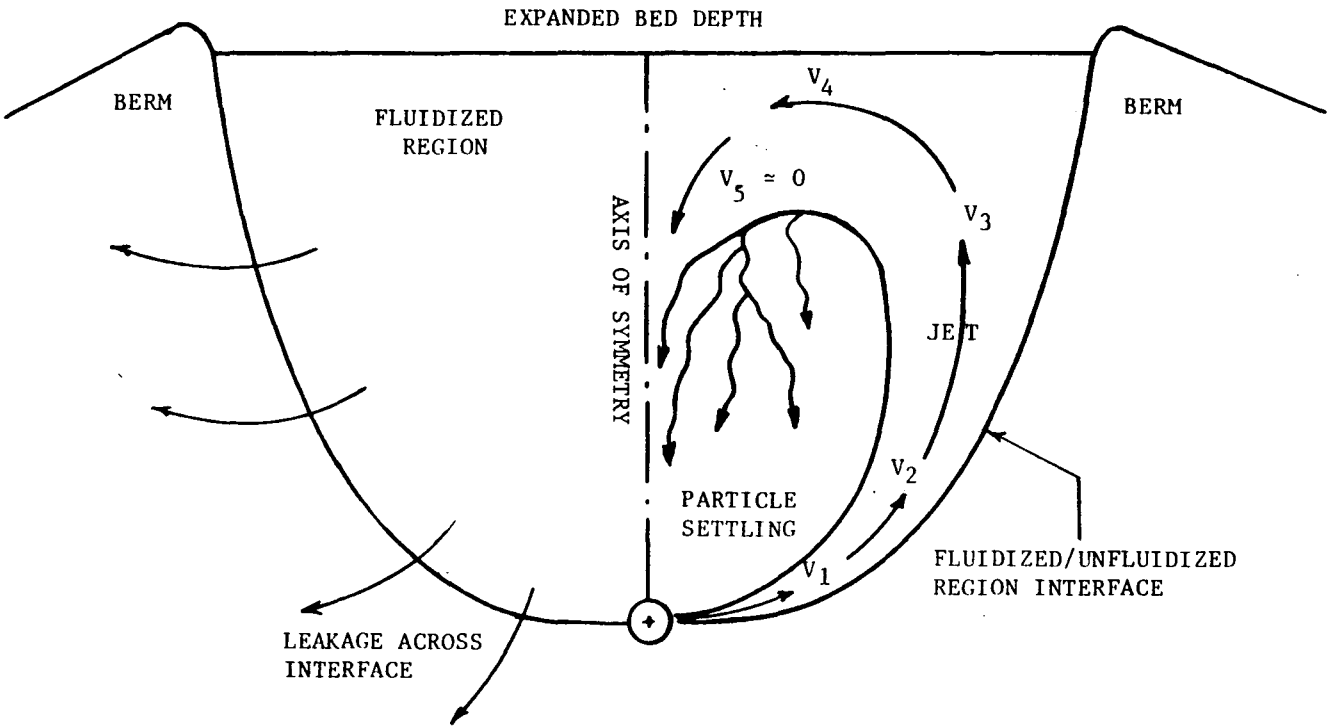


**Figure 3:** Two-Dimensional Fluidization (Unbounded Domain)

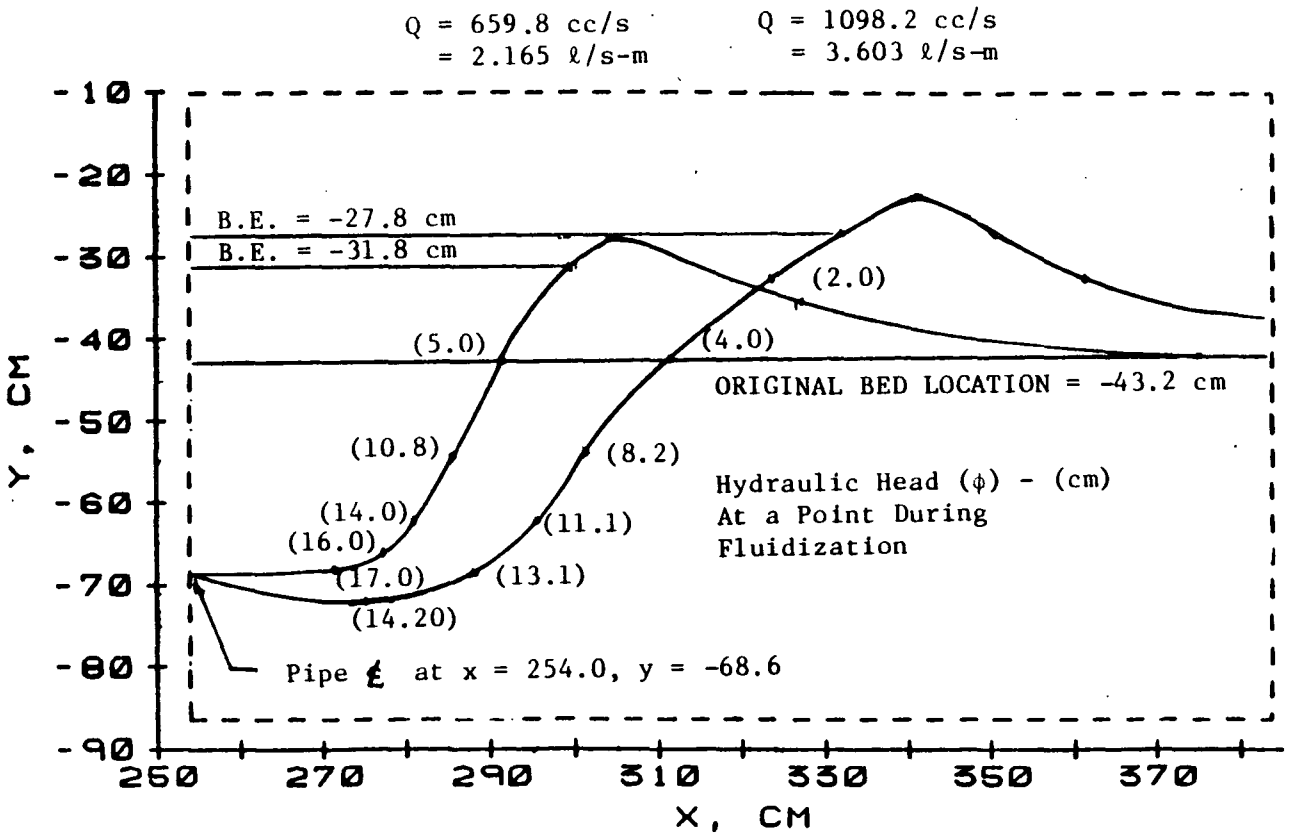


**Figure 4:** Test 2. Growth of Fluidized Region for Various Flow Rates. Initial Bed Depth = 25.4 cm at y = -43.2 cm. Initial Bed Porosity ($\epsilon_o$) = 39%

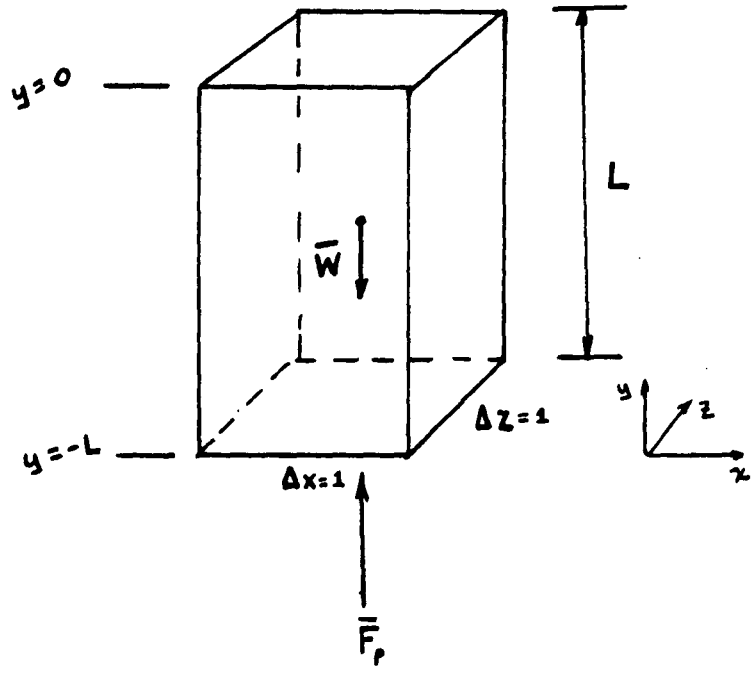


**Figure 5:** Force Balance to Determine Fluidizing Pressure

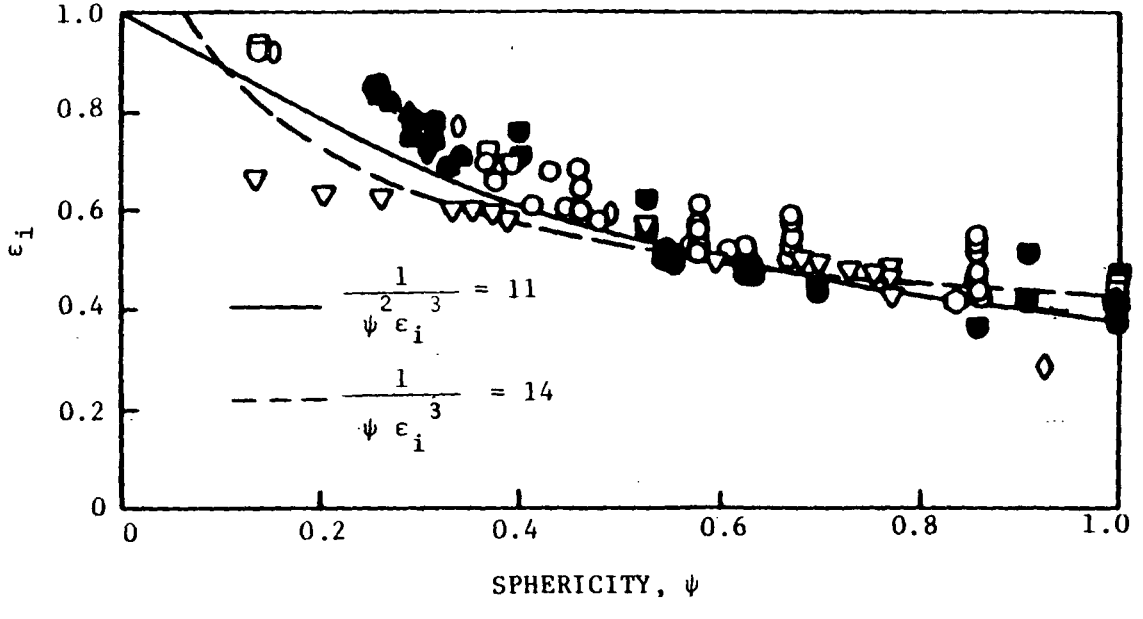


**Figure 6:** Relation Between Porosity at Incipient Fluidization, $\epsilon_i$, and Sphericity of Grains ($\psi$): Taken From Fig. 8 of Ref. 34; Different Symbols Reflect Different Initial Sources

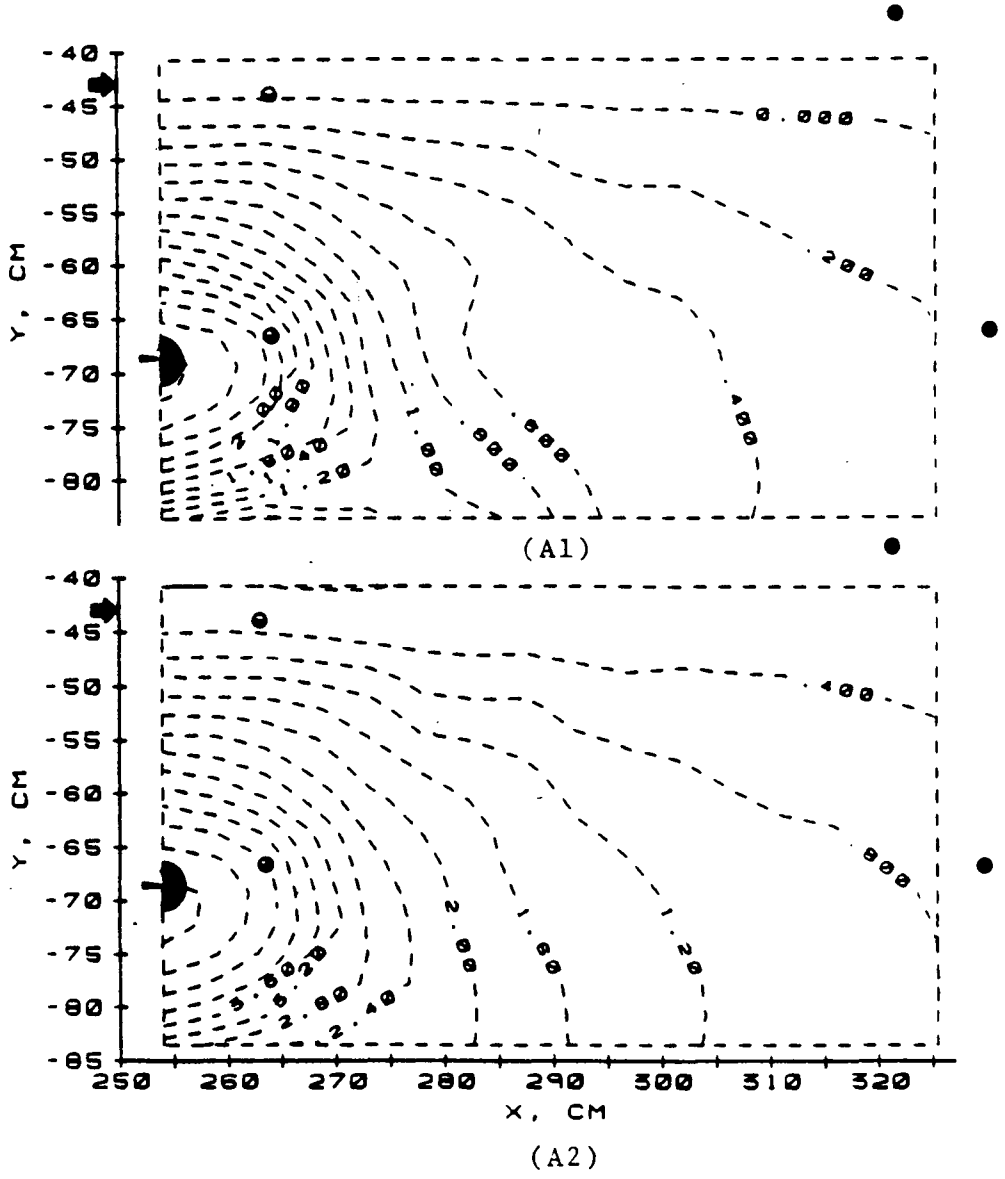


**Figure 7A:** Test 2. Hydraulic Head ($\phi$) Distribution in Two-Dimensional Unbounded Domain. Initial Bed Depth = 25.4 cm, y = -43.2 cm. Initial Bed Porosity ($\epsilon_o$) = 39%
Flow Rate (l/s-m): (A1) Q = 0.009, (A2) Q = 0.019

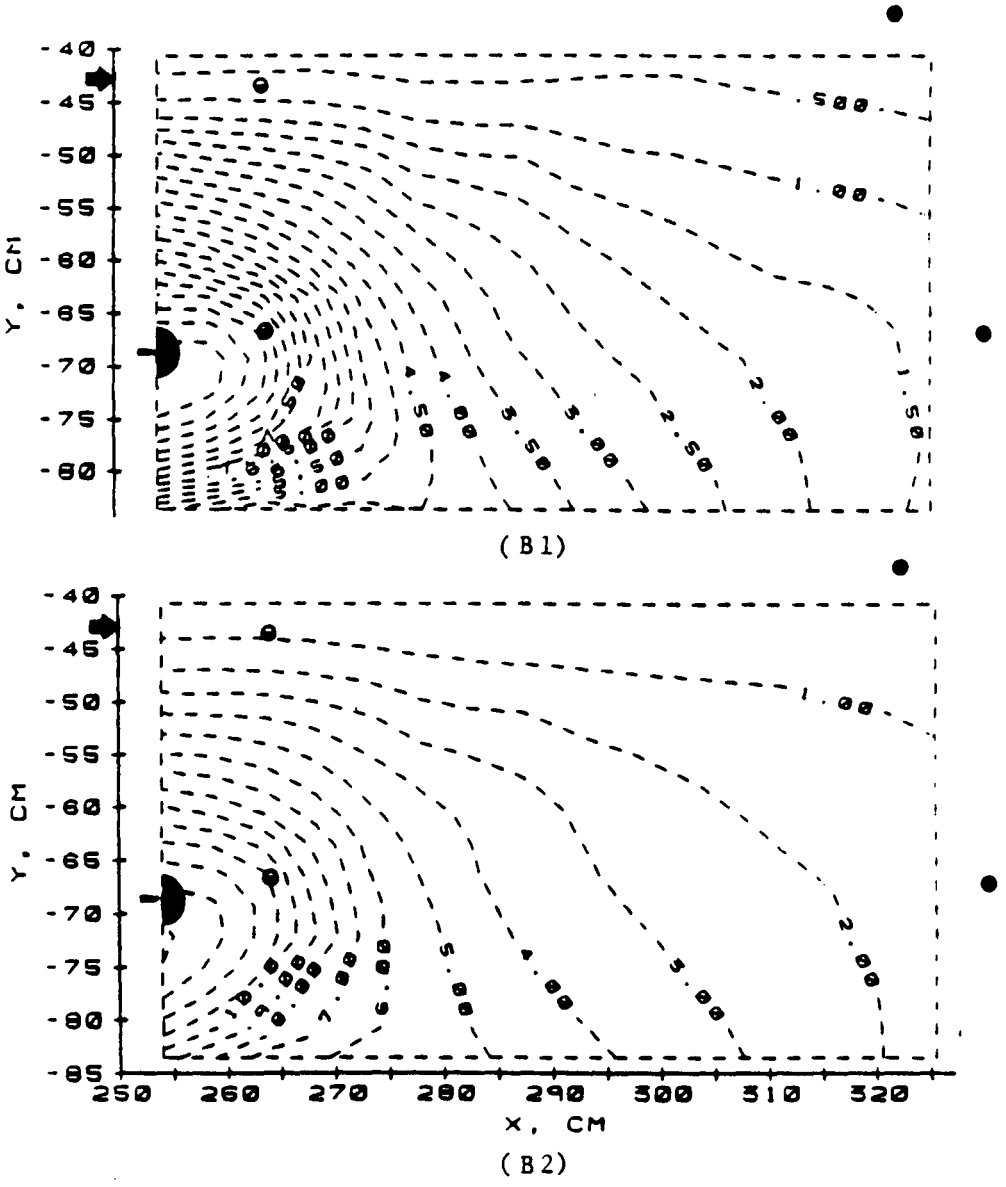


Figure 7B: Test 2. Hydraulic Head ($\phi$) Distribution in Two-Dimensional Unbounded Domain. Initial Bed Depth = 25.4 cm, y = -43.2 cm. Initial Bed Porosity ($\epsilon_o$) = 39%
Flow Rate (l/s-m): (B1) Q = 0.034, (B2) Q = 0.041

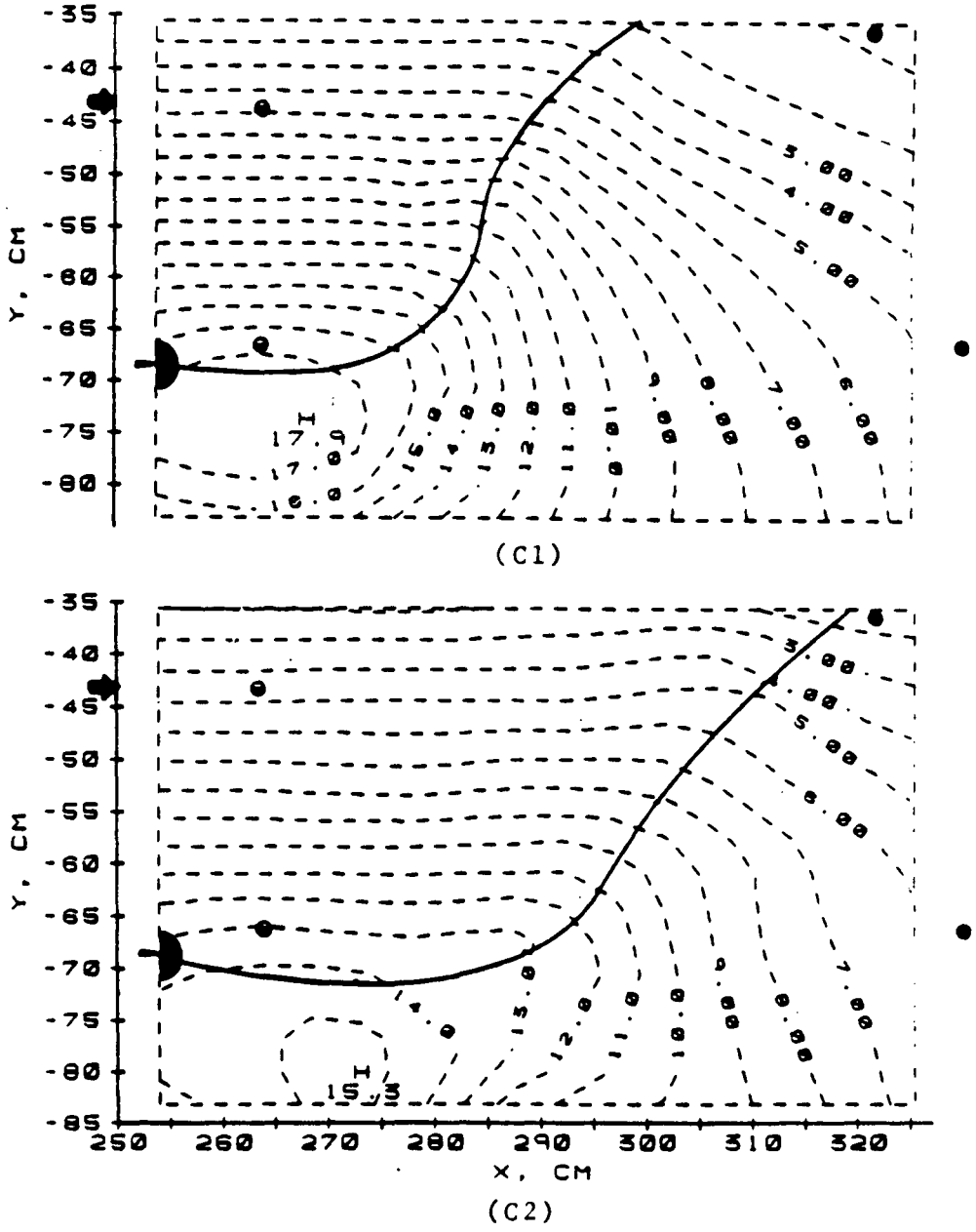


**Figure 7C:** Test 2. Hydraulic Head ($\phi$) Distribution in Two-Dimensional Unbounded Domain. Initial Bed Depth = 25.4 cm, y = -43.2 cm. Initial Bed Porosity ($\epsilon_o$) = 39%
Flow Rate (l/s-m): (C1) Q = 2.16, (C2) Q = 3.60

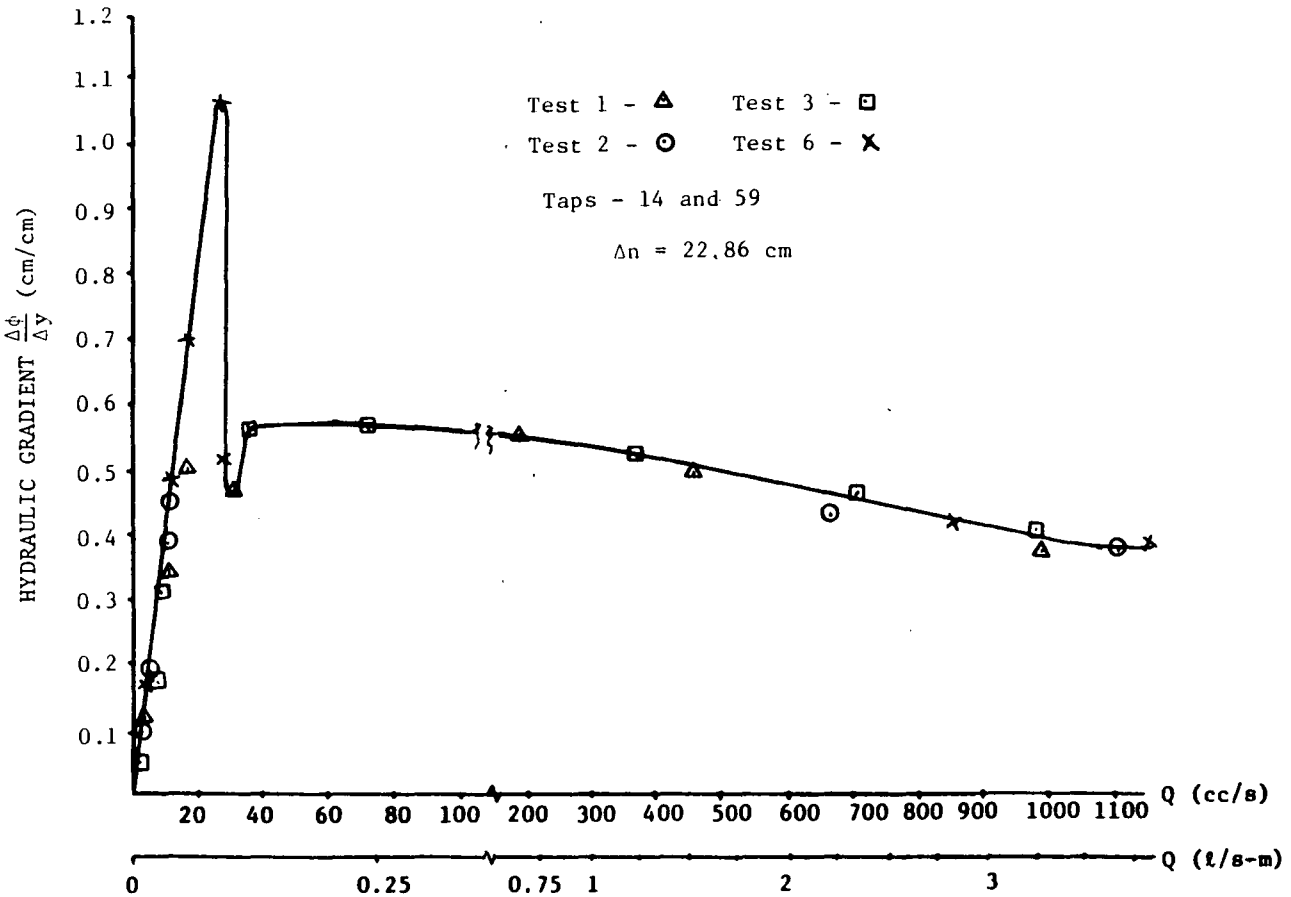


**Figure 8:** Test 1,2,3,6. Relationship Between the Hydraulic Head Gradient and Flow Rate at Taps 14 and 59. Initial Bed Depth = 25.4 cm. Initial Bed Porosity ($\epsilon_o$) = 39%

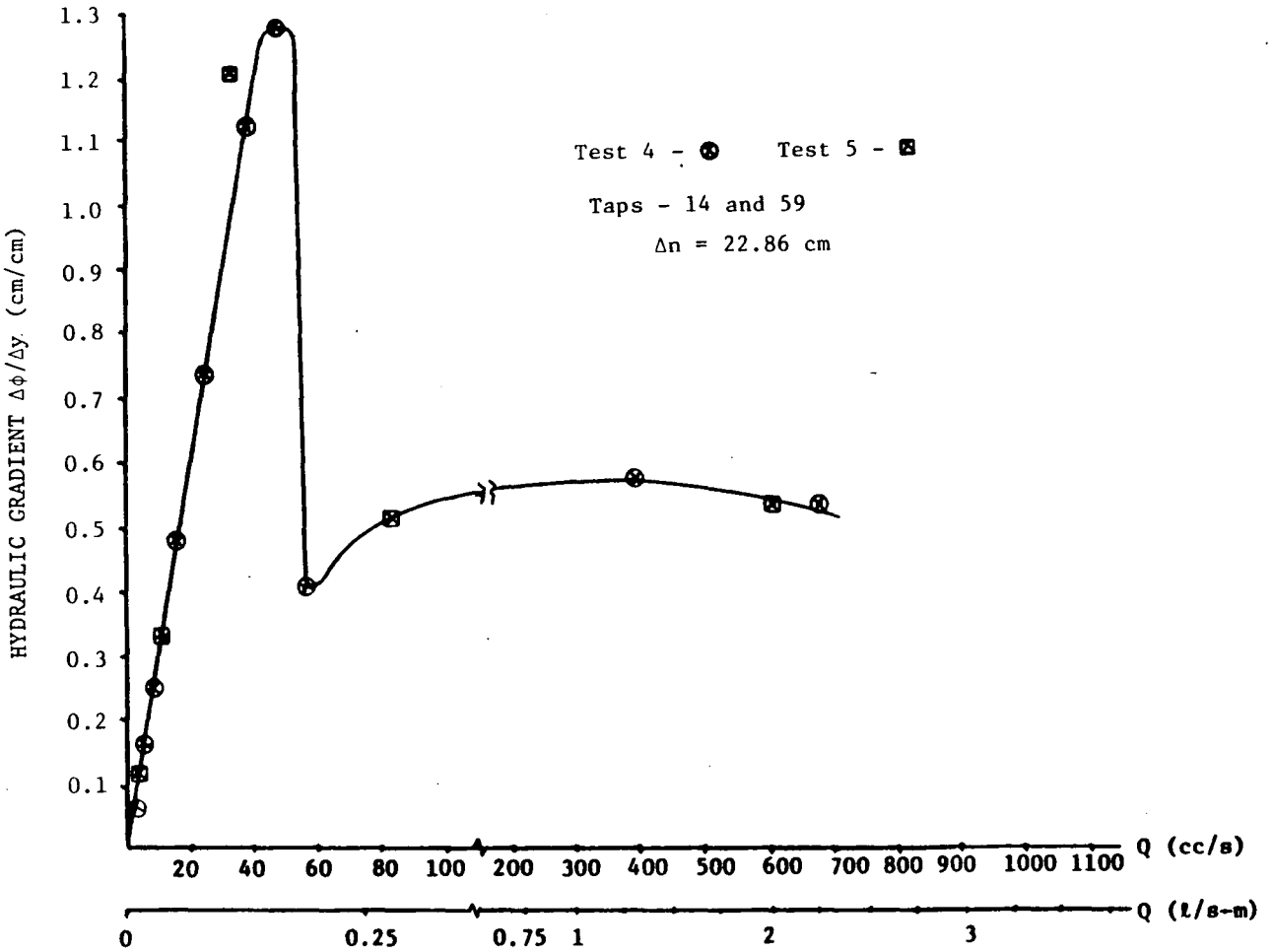


**Figure 9:** Tests 4 and 5. Relationship Between the Hydraulic Head Gradient and Flow Rate at Taps 14 and 59. Initial Bed Depth = 42 cm. Initial Bed Porosity ($\epsilon_o$) = 39%

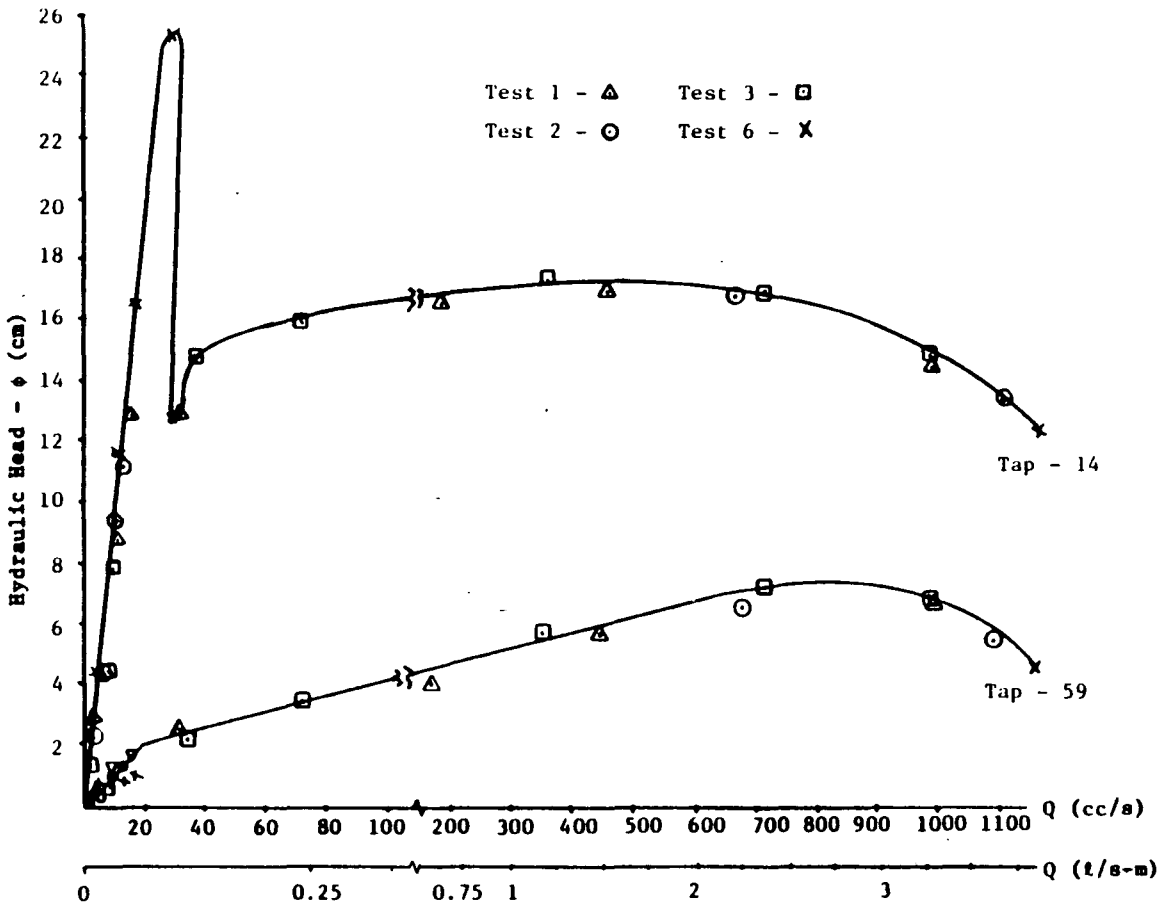


**Figure 10:** Tests 1,2,3,6. Relationship Between the Hydraulic Head and Flow Rate at Taps 14 and 59. Initial Bed Depth = 25.4 cm. Initial Bed Porosity ($\epsilon_o$) = 39%

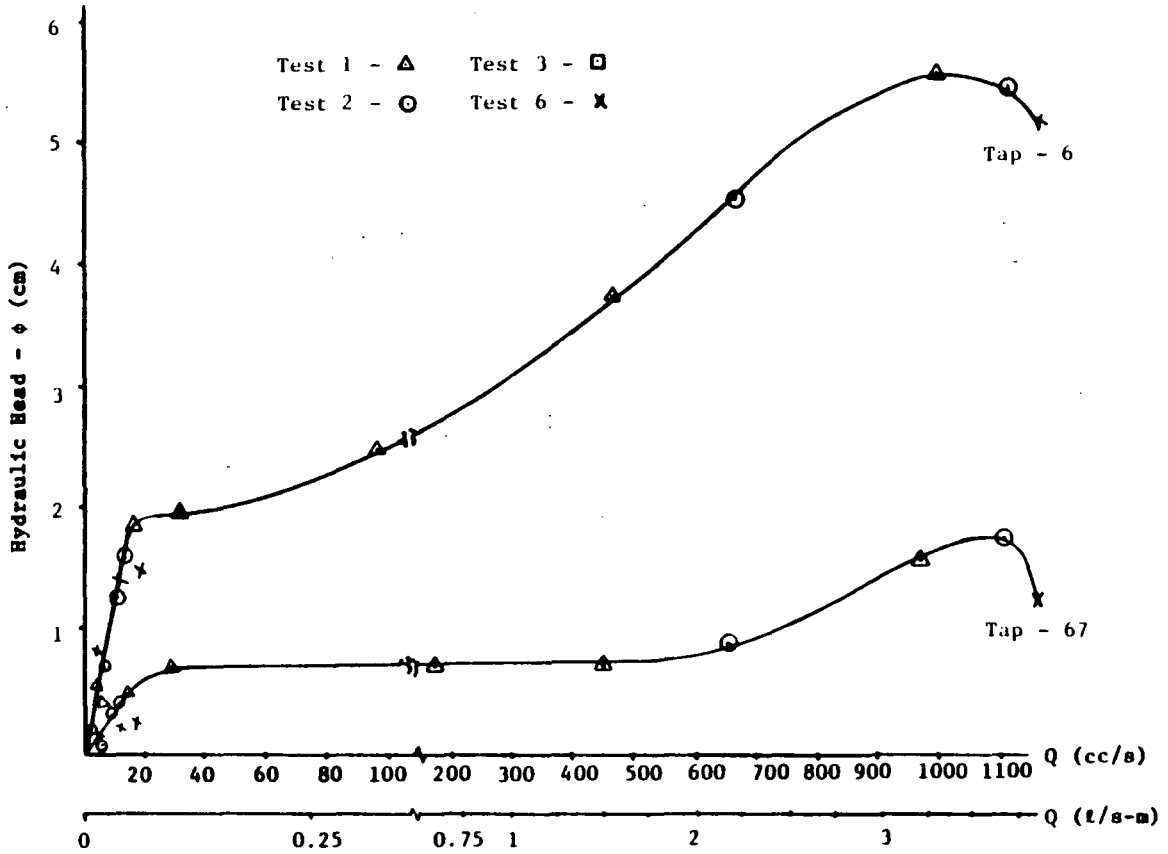


**Figure 11:** Tests 1,2,6. Relationship Between the Hydraulic Head and Flow Rate at Taps 6 and 67. Initial Bed Depth = 25.4 cm. Initial Bed Porosity ($\epsilon_o$) = 39%

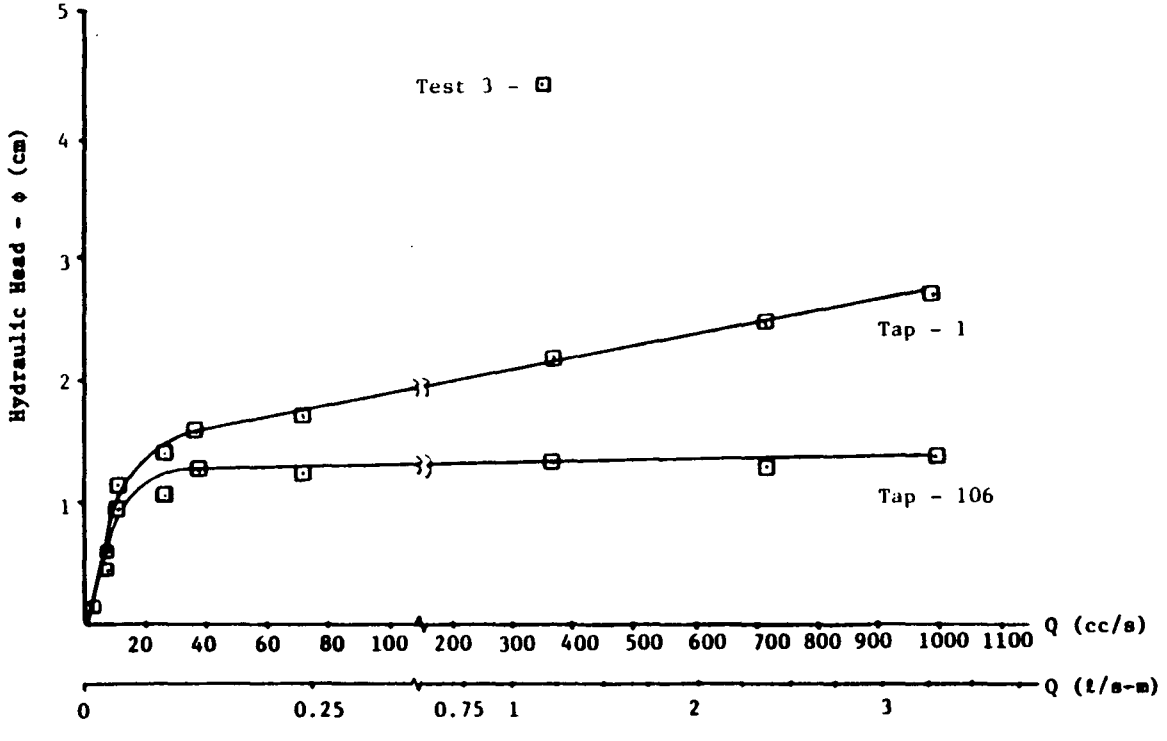


**Figure 12:** Test 3. Relationship Between the Hydraulic Head and Flow Rate at Taps 1 and 106. Initial Bed Depth = 25.4 cm. Initial Bed Porosity ($\epsilon_o$) = 39%

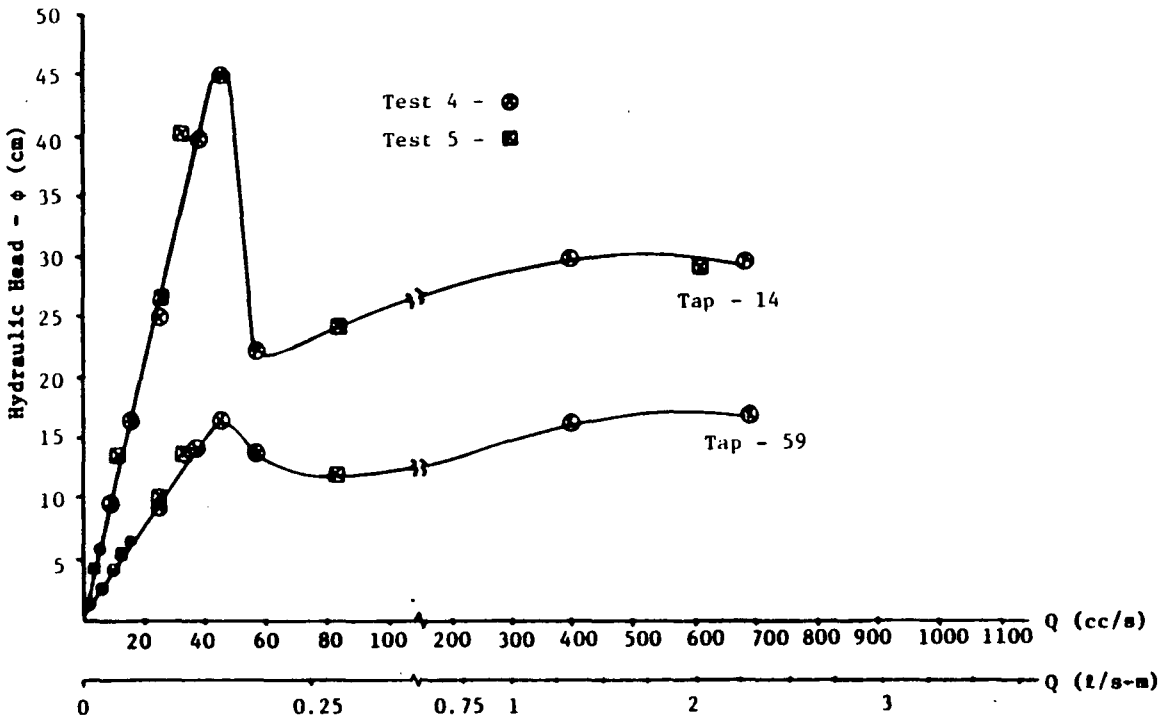


**Figure 13:** Tests 4 and 5. Relationship Between the Hydraulic Head and Flow Rate at Taps 14 and 59. Initial Bed Depth = 42 cm. Initial Bed Porosity ($\epsilon_o$) = 39%

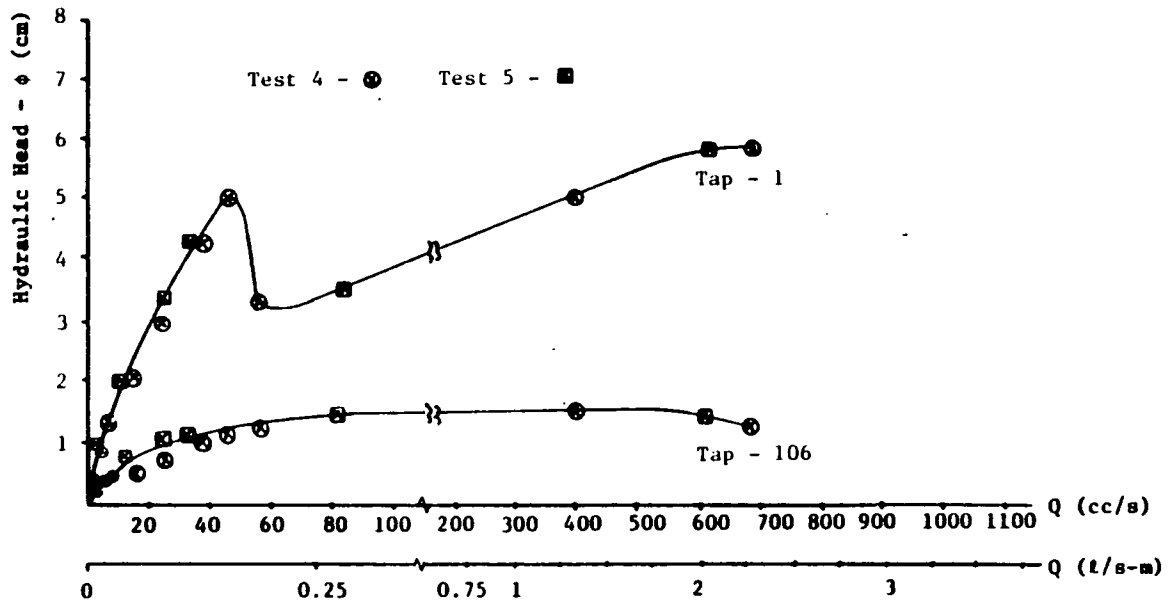


**Figure 14:** Tests 4 and 5. Relationship Between the Hydraulic Head and Flow Rate at Taps 1 and 106. Initial Bed Depth = 42 cm. Initial Bed Porosity ($\epsilon_o$) = 39%

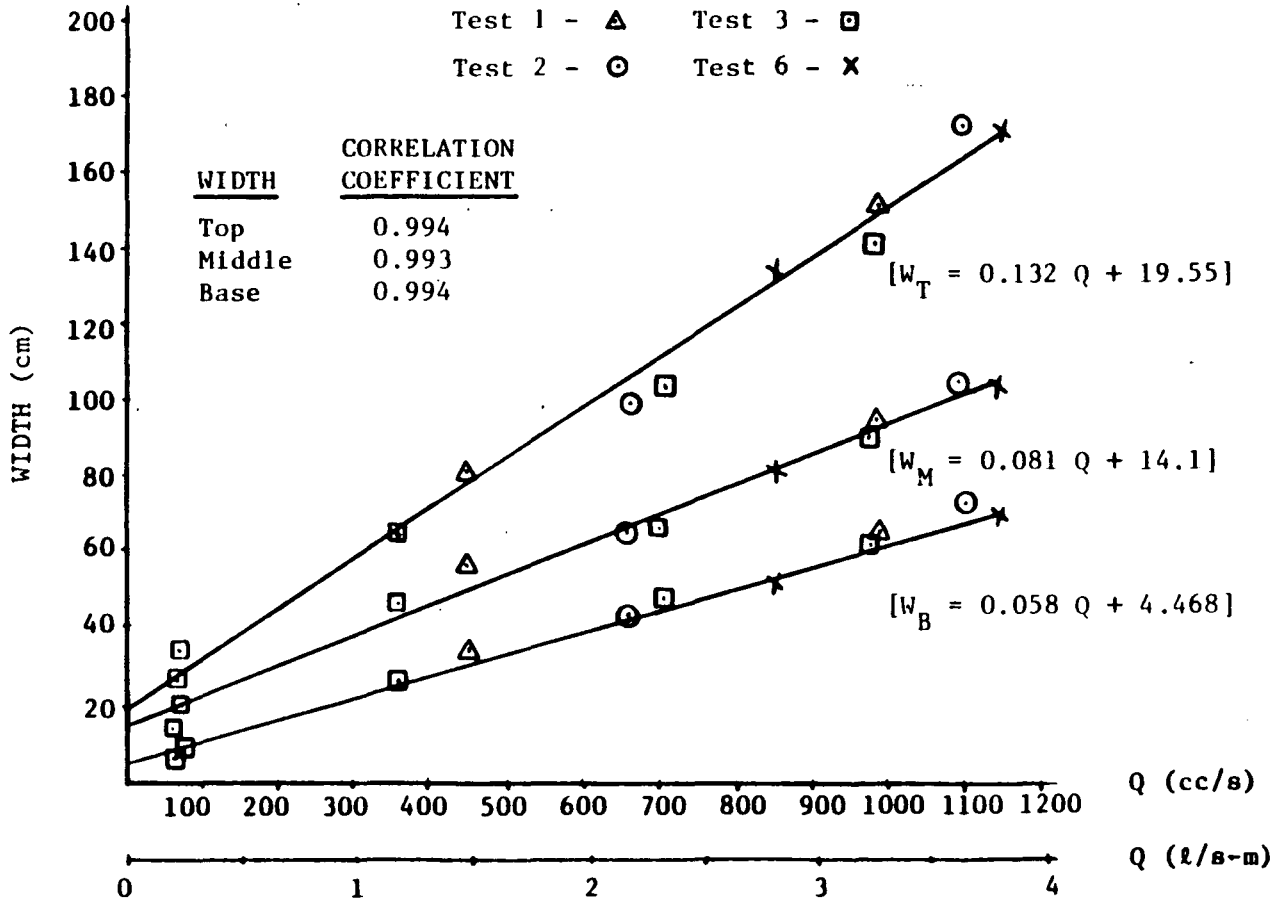


**Figure 15:** Tests 1,2,3,6. Flow Rate/Width of Fluidized Region Relationship. Initial Bed Depth = 25.4 cm. Initial Bed Porosity ($\epsilon_o$) = 39%

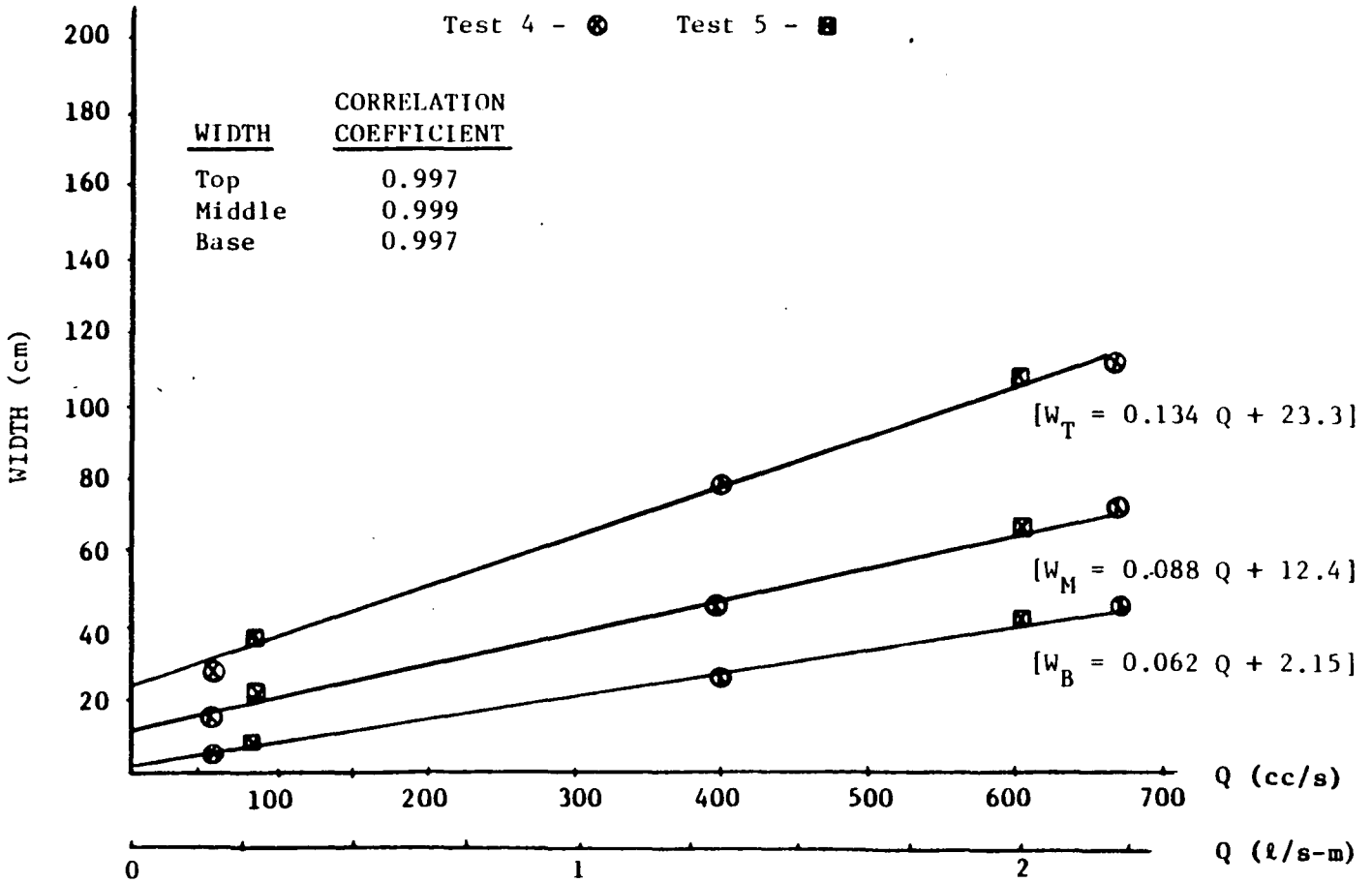


**Figure 16:** Tests 4 and 5. Flow Rate/Width of Fluidized Region Relationship. Initial Bed Depth = 42 cm. Initial Bed Porosity ($\epsilon_o$) = 39%

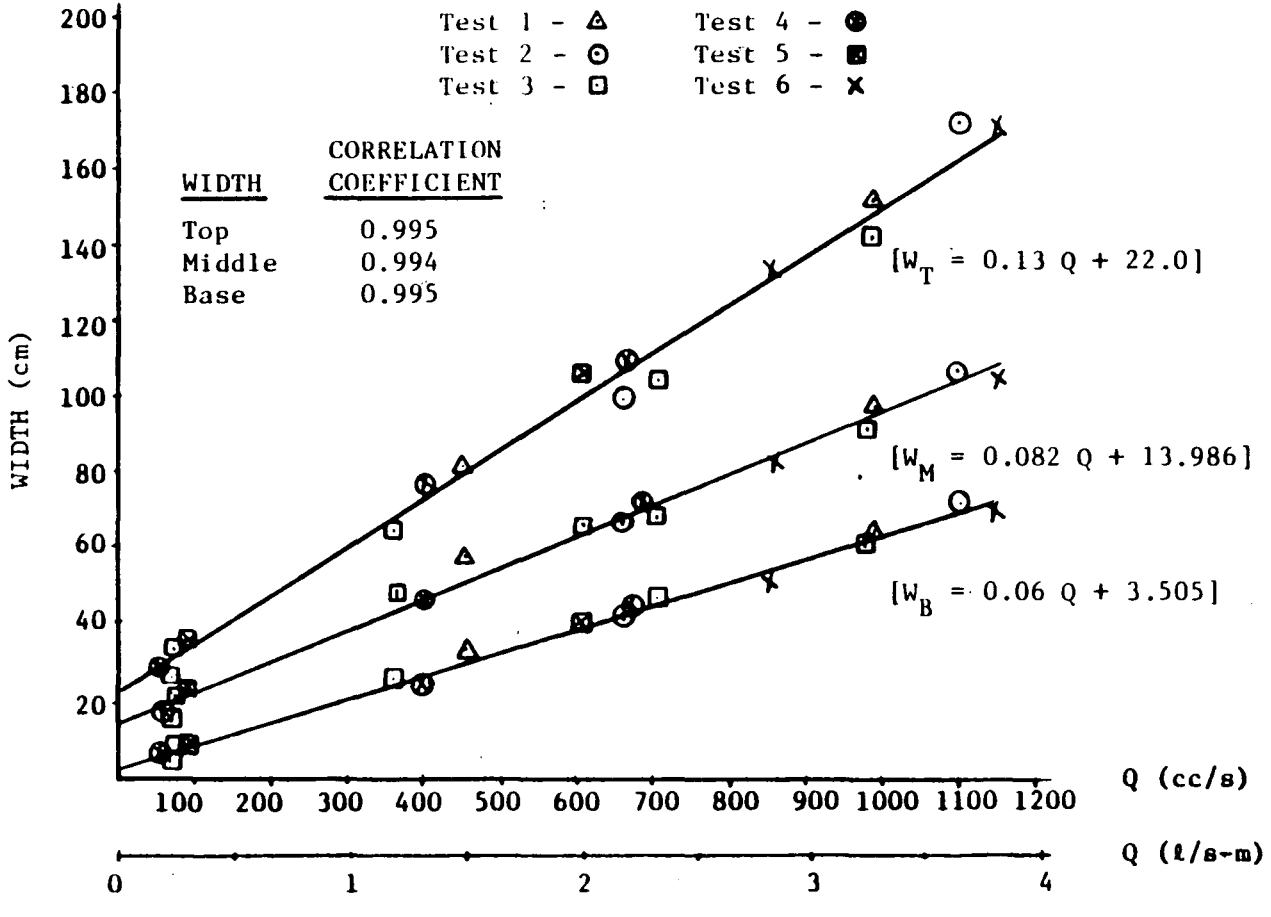


**Figure 17:** Tests 1,2,3,4,5,6. Flow Rate/Width of Fluidized Region Relationship. Initial Bed Depth = 25.4 cm and 42 cm. Initial Bed Porosity ($\epsilon_o$) = 39%

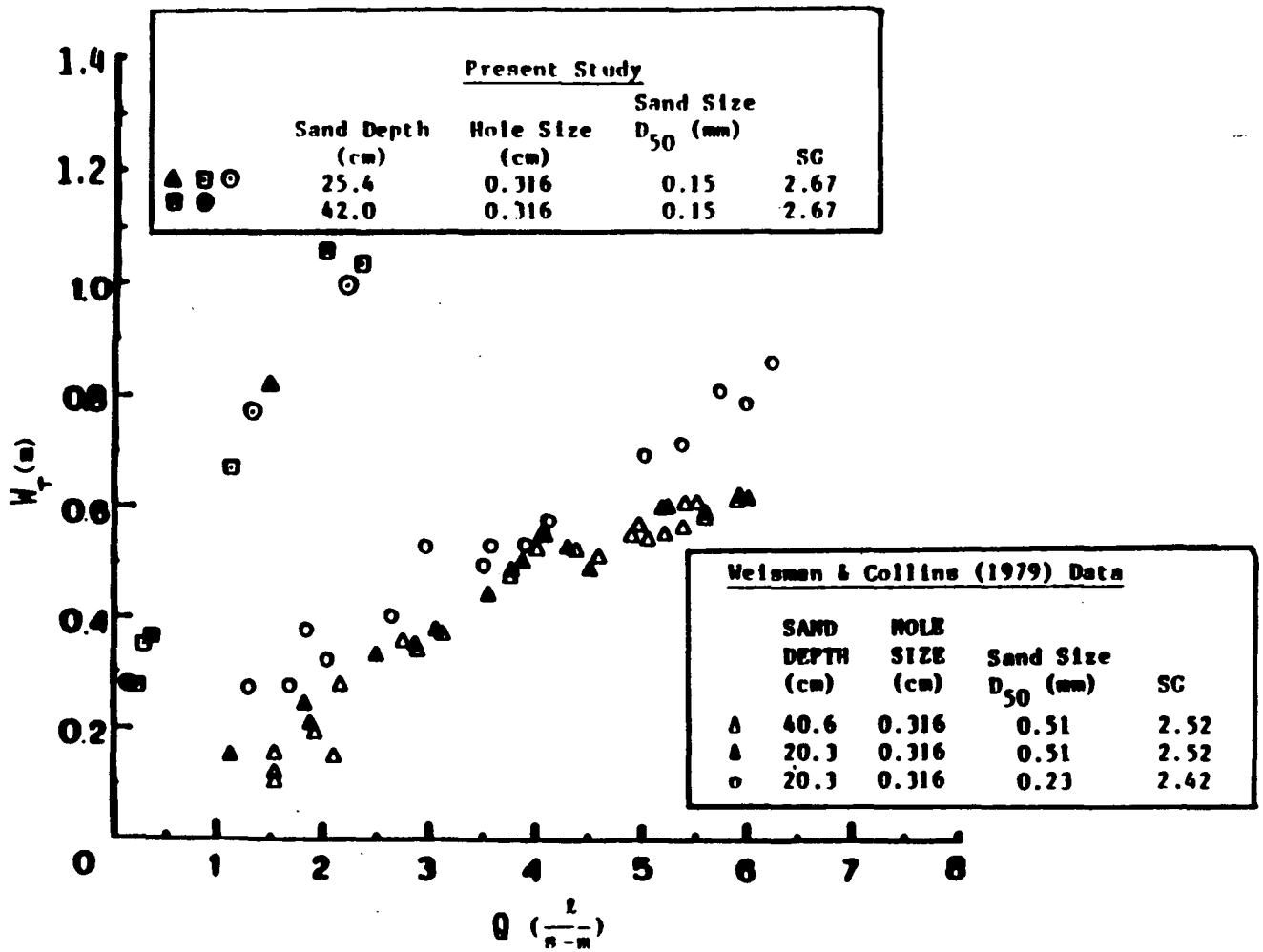


**Figure 18:** Comparison of Flow Rate/Top Width of Fluidized Region Relationship for Three Different Sand Sizes. Weisman and Collins Data Included [30]. Figure taken from Ref. [30]

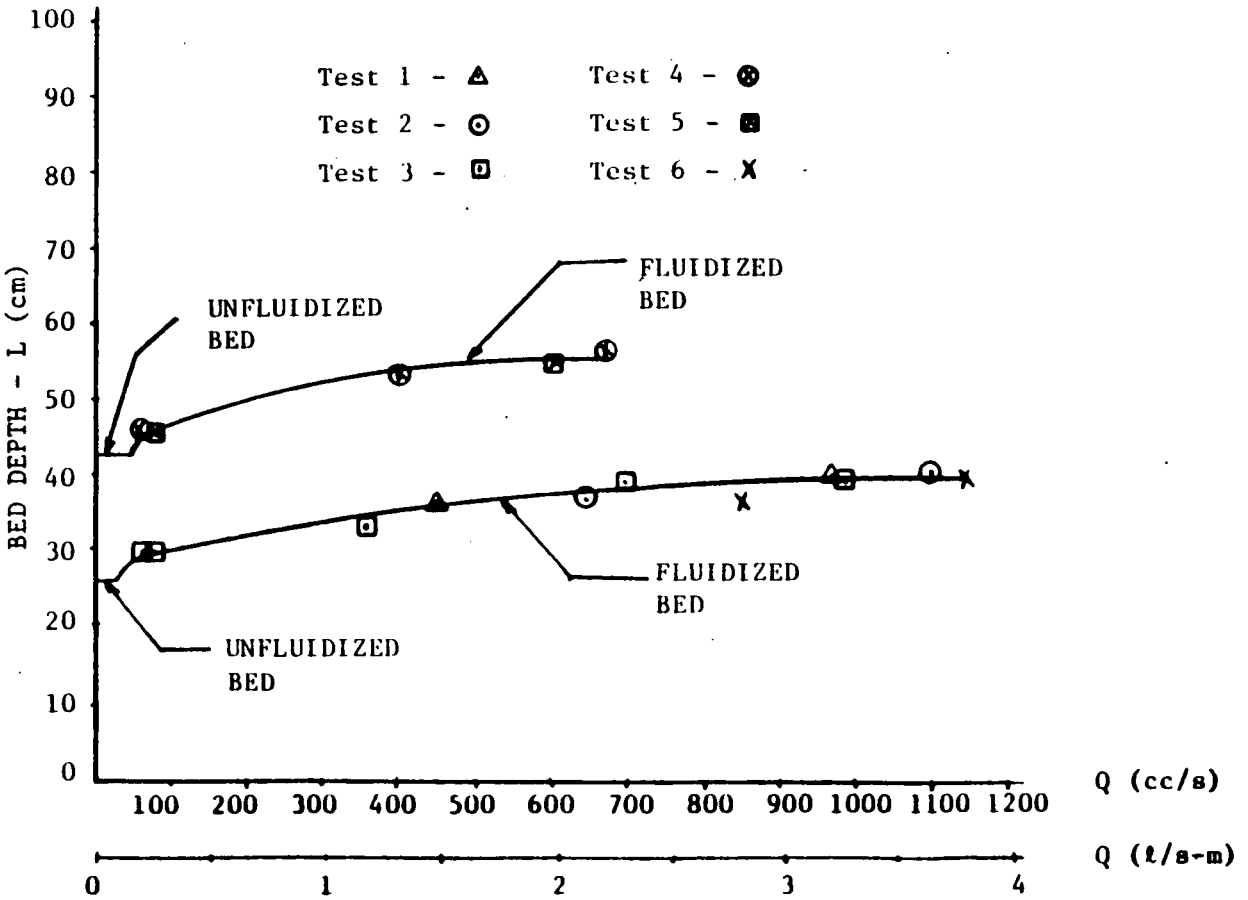


**Figure 19:** Tests 1,2,3,4,5,6. Relationship Between Bed Expansion and Flow Rate. Initial Bed Depths = 25.4 cm and 42 cm. Initial Bed Porosity ($\epsilon_o$) = 39%

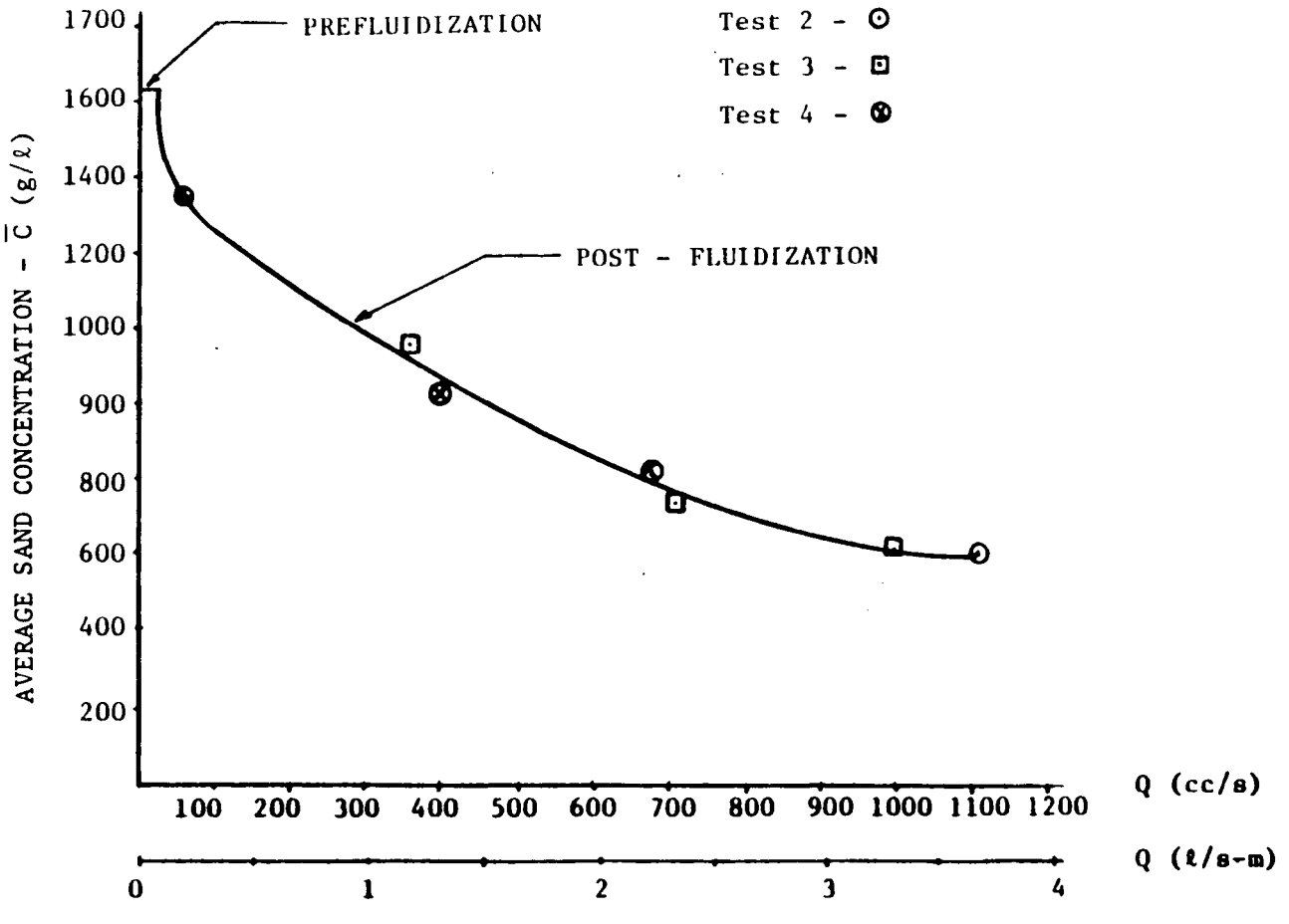


**Figure 20:** Tests 2,3,4. Relationship Between Flow Rate and Average Concentration of Sand in the Fluidized Region. Initial Bed Depths = 25.4 cm and 42 cm. Initial Bed Porosity ($\epsilon_o$) = 39%

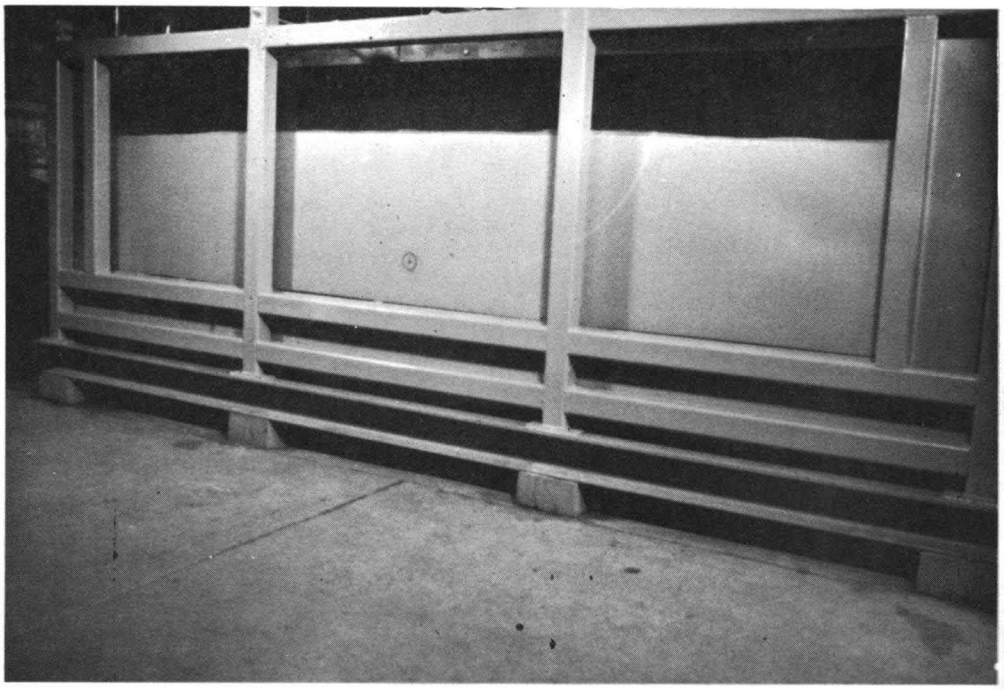

Plate 1: Overall View of the Fluidization Tank. Original Bed Depth = 42-cm. Original Bed Porosity = 39%.

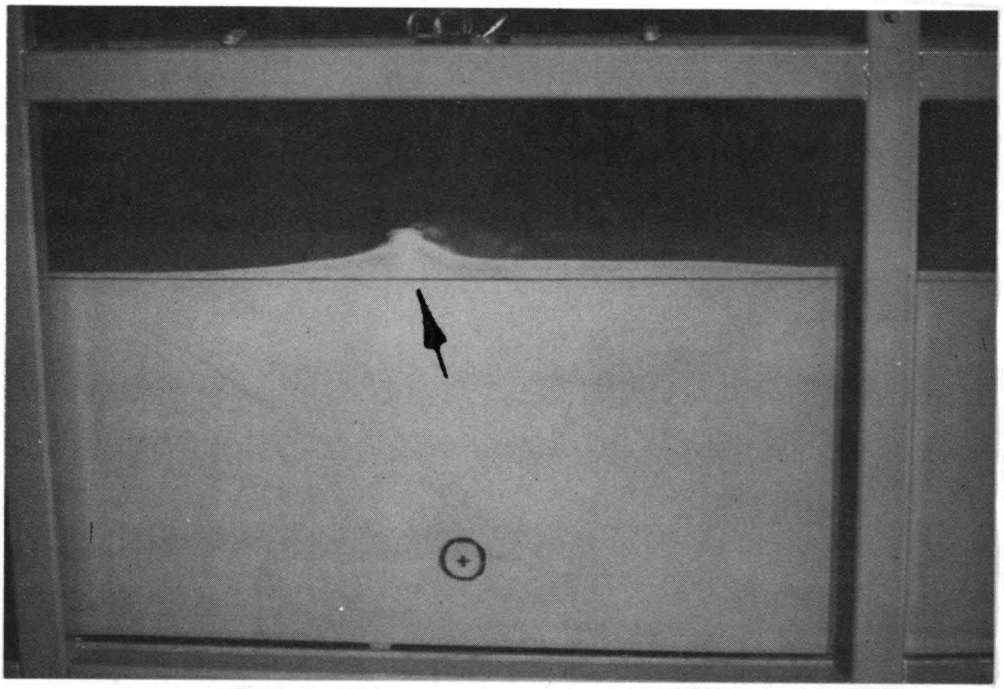

Plate 2: Initiation of Fluidization Along with Corresponding Bed Surface Eruption.

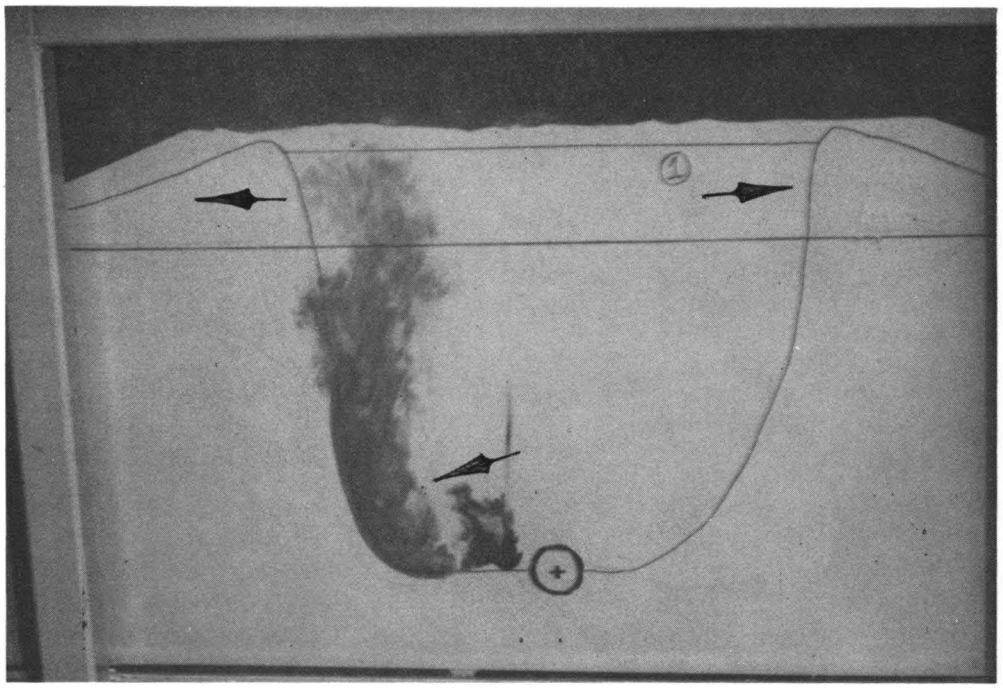

Plate 3: Complete Uniform Fluidization and Berm Formation at an Estimated Q = 1.35 l/s-m. Flow Pattern of Jet Represented by Tracer.

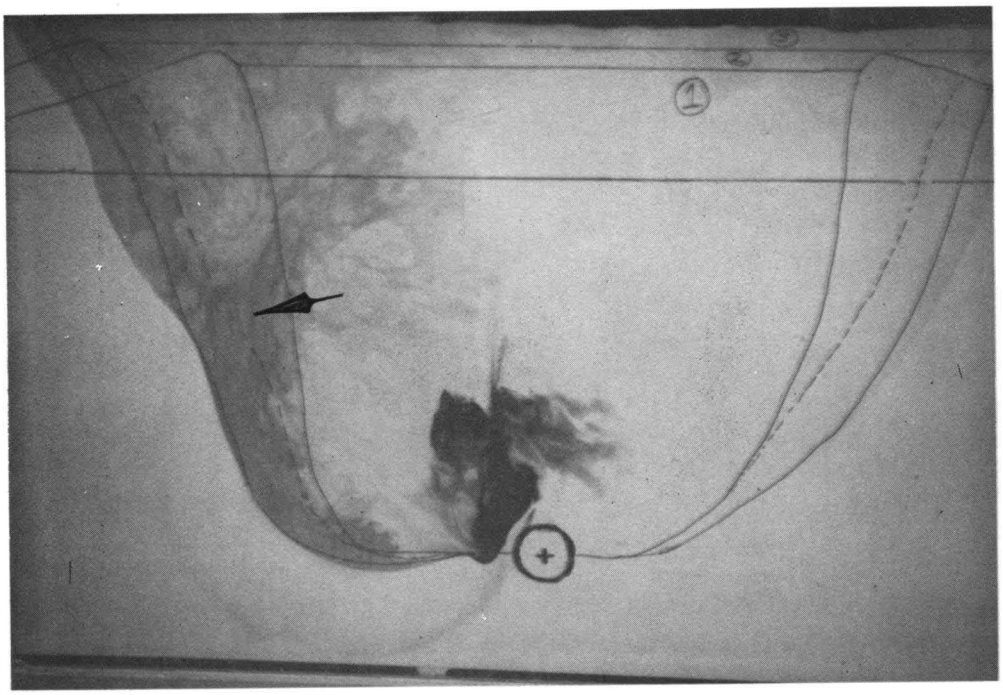

Plate 4: Jet Conforms to Fluidized Region Boundary and Separation Occurs at Half the Expanded Depth. Q = 2.18 l/s-m. Widening of the Fluidized Region is Observed With Subsequent Increases in Flow Rate.

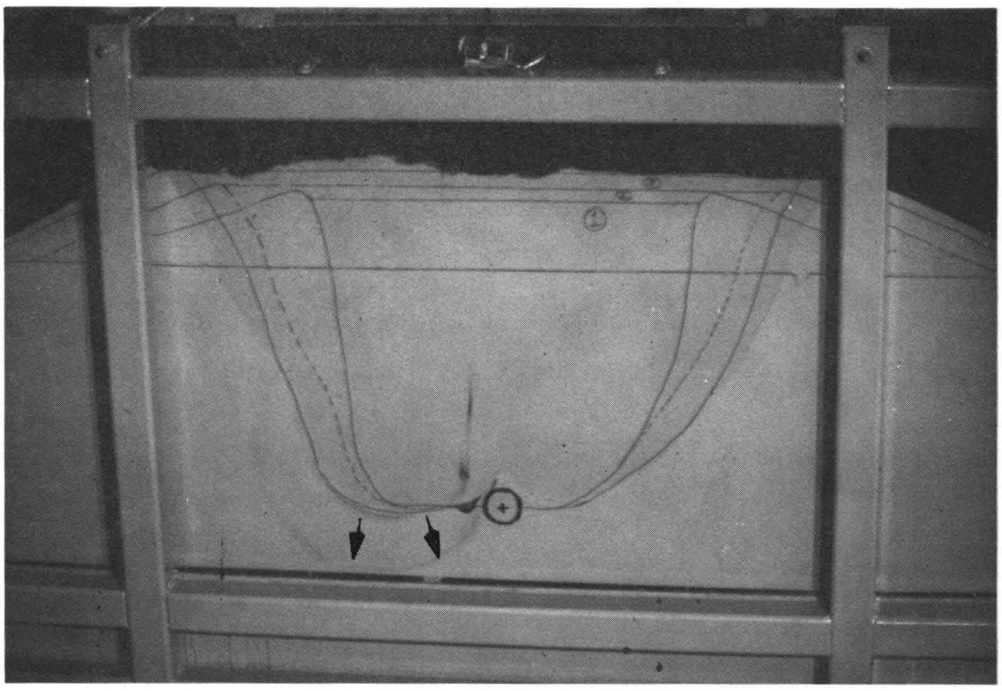

Plate 5: Formation of Tracer Front Which is Attributed to Leakage Across Fluidized/Unfluidized Region Interface. Tracer Front Migrates in the Unfluidized Region.

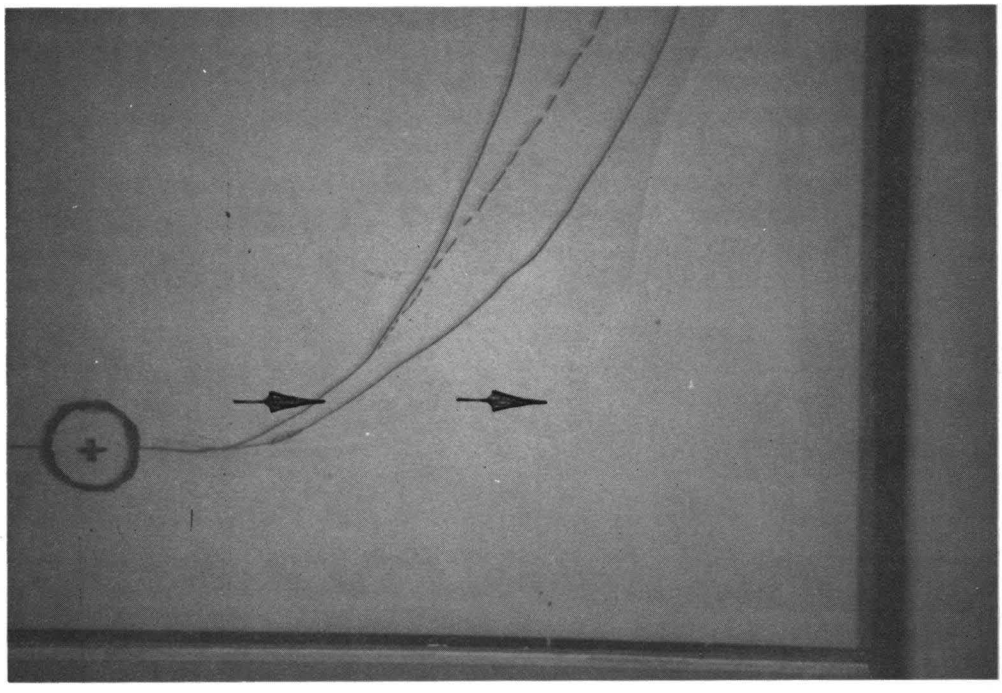

Plate 6: Growth of the Fluidized Region at Q = 3.47 l/s-m Resulting From the Erosion of the Fluidized/Unfluidized Region Interface Formed for the Previous Flow Rate of Q = 2.18 l/s-m.

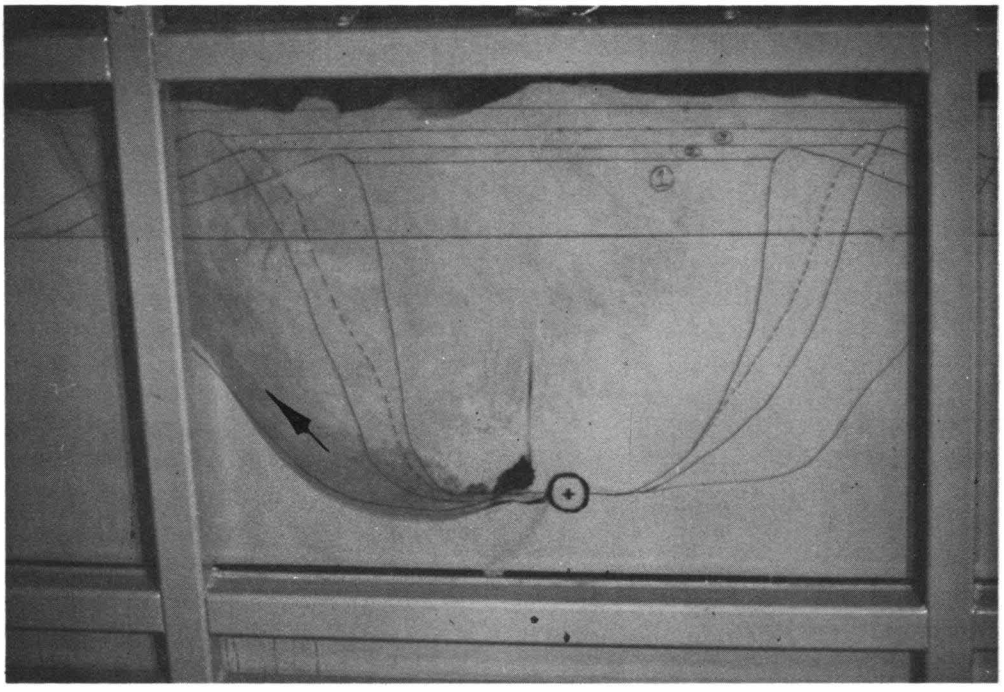

Plate 7: Overall Size, Shape and Symmetry of Fluidized Regions. Jet Pattern at Higher Flow Rate, Q = 3.47 l/s-m.

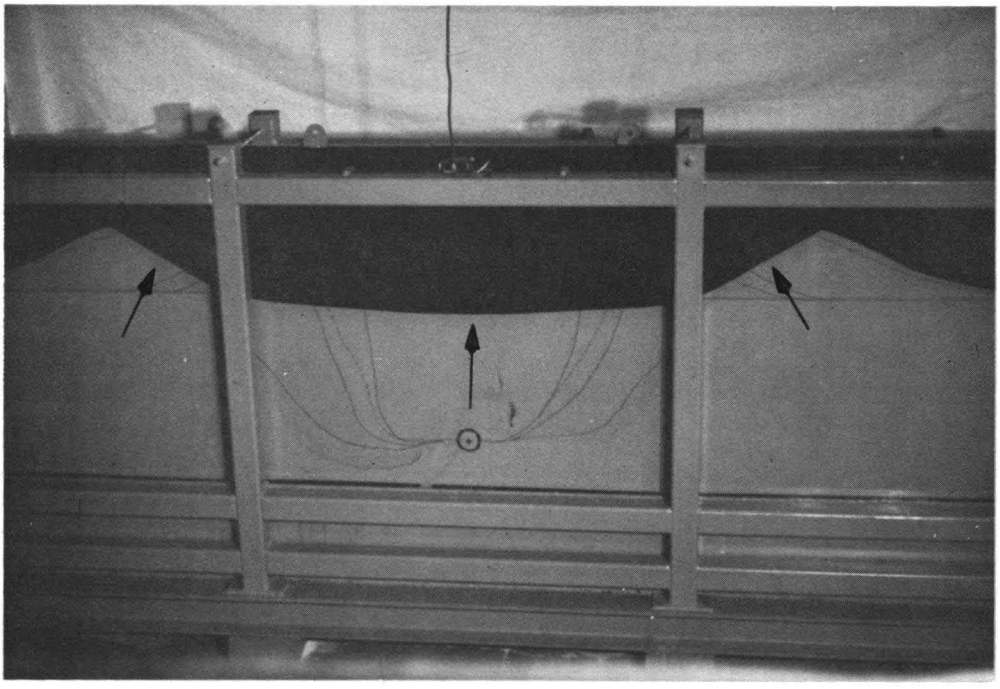

Plate 8: Settling of the Fluidized Bed After Flow is Turned Off. Fluidized Region Widens Near the Top and the Interface Slopes to the Angle of Repose of the Sand (30°).

# NOMENCLATURE

| | | |
|---|---|---|
| $\overline{C}$ | = | Average Concentration of Solids in Fluidized Region |
| Q | = | Flow Rate From Source, Fluidization Pipe |
| L | = | Bed Depth of Sand |
| $L_e$ | = | Expansion Depth of Bed at Q |
| $L_o$ | = | Original Bed Depth |
| $W_T$ | = | Top Width of Fluidized Region (Berm Peak to Berm Peak) |
| $W_M$ | = | Width of Fludized Region at 1/2 the Expansion Depth |
| $W_B$ | = | Base Width of Fluidized Zone |
| X | = | Coordinate in X - Direction |
| Y | = | Coordinate in Y - Direction |
| Z | = | Coordinate in Z - Direction |
| $\Delta\phi$ | = | Change in Hydraulic Head |
| $\Delta n$ | = | Distance Between Pressure Taps |

$Q_i$ = Incipient Fluidization Flow Rate

$V_i$ = Incipient Fluidization Superficial Velocity

$V$ = Superficial Velocity

$v_s$ = Terminal Settling Velocity of a Particle

$\phi$ = Hydraulic Head

$\psi$ = Sphericity of Sand Grains

$\epsilon_o$ = Original Bed Porosity

$\epsilon_e$ = Expanded Bed Porosity

$\epsilon_i$ = Bed Porosity at Incipient Fluidization

# REFERENCES


1. Amirtharajah, A. Expansion of Graded Sand Filters During Backwashing. Master Th., Iowa State University,1970.

2. Amirtharajah, A. and Cleasby, J.L. "Predicting Expansion of Filters During Backwash". *Journal of American Water Works Association Vol. 64* (1972), 49-52.

3. Anderson, T.B. and Jackson, R. "The Nature of Aggregative and Particulate Fluidization". *Chemical Engineering Science 19* (1964), 509-511.

4. Bailard, J.A., and Inman, D.L. "Analytical Model of Duct-Flow Fluidization". *Proceedings of the Symposium on Modeling Techniques, ASCE 1975* (1975), 1402-1421.

5. Bear, J.. *Dynamics of Fluids in Porous Media.* American Elsevier, New York, 1972.

6. Briggs, L.I., McCulloch, D.S., and Moser, F. "The Hydraulic Shape of Sand Particles". *Journal of Sedimentary Petrology Vol. 90* (1962), 645-657.

7. Camp, T.R. "Theory of Water Filtration". *Journal of the Sanitary Engineering Division ASCE, Vol.48* , No. SA4, Proc. Paper (1964), 1-30.

8. Cleasby, J.L. and Fan, K.S. "Predicting Fluidization and Expansion of Filter Media". *Journal of Environmental Engineering Division, ASCE 107(EE3)* (1981), 455-471.

9. Daily, J.W., Harleman, D.R.F.. *Fluid Dynamics.* Addison-Wesley Publishing Company, Inc., Reading, Massachusetts, 1966.

10. Davidson, J.F.. *Fluidized Particles.* The Syndics of the Cambridge University Press, New York, N.Y., 1963.

11. Davies, J.T.. *Turbulence Phenomena.* , Academic Press, New York and London, 1972.

12. Ergun, S. "Fluid Flow Through Packed Columns". *Chemical Engineering Progress New York, N.Y., Vol. 48* (1952), 89-94.

13. Fair, G.M., Geyer, J.C., and Okun, D.A.. *Water and Waste Water Engineering.* John Wiley & Sons, Inc., New York, N.Y., 1968.

14. Fan, K-s. Sphericity and Fluidization of Granular Filter Media. Master Th., Iowa State University, Ames, Iowa,1978.

15. Graf, W.H.. *Hydraulics of Sediment Transport.* McGraw-Hill Book Co., Inc., New York, N.Y., 1971.

**16.** Hagyard, T. Sand Fluidization Experiments at Westport.

**17.** Hagyard, T., Gilmour, I.A., and Mottram, W.D. "A Proposal to Remove Sand Bars by Fluidization". *New Zealand Journal of Science Vol. 12* (1969), 851-864.

**18.** Harris et al. "Study and Evaluation of Remedial Sand Bypassing Procedures". *U.S. Army Engineers Waterways Experiment Station Reprint H-76-1* (1976), .

**19.** Inman, D.L, Harris, R.W. "Cratersink Sand Transfer System". *Proceedings of the 12th Coastal Engineering Conference, ASCE* (1970), 919-933.

**20.** Kelley, J.T. Fluidization Applied to Sediment Transport. Master Th., Lehigh University, Bethlehem, PA,1977.

**21.** Mathur, K.B. and Epstein, N.. *Spouted Beds.* Academic Press, New York , 1974.

**22.** Murray, W.A., Collins, A.G. Fluidization Applied to Sediment Transport--II. Fritz Engineering Laboratory Report 710.2, Lehigh University, 1978. Fritz Engineering Laboratory Report 710.2.

**23.** Muskat, M.. *The Flow of Homogeneous Fluids through Porous Media.* McGraw-Hill Books Co., New York, 1937.

**24.** Othmer, D.F. . *Fluidization.* Rheinhold Publishing Corporation, New York, N.Y., 1956.

**25.** Rajaratnam, N.. *Turbulent Jets.* Elsevier Scientific Publishing Company, Amsterdam, The Netherlands, 1976.

**26.** Raudkivi, A.J., Callander, R.A.. *Advanced Fluid Mechanics - An Introduction.* Edward Arnold, London, 1975.

**27.** Richardson, J.F. and Zaki, W.N. "Sedimentation and Fluidization". *Trans. Institute Chemical Engineers 32*, Part I. (1954), 35-53.

**28.** Rowe, P.N. and Henwood, G.A. "Drag Forces in a Hydraulic Model of a Fluidized Bed". *Trans. Institute Chemical Engineers 39*, Part I. (1961), 43-54.

**29.** Volpicelli, G. et al. "Nonhomogenieties on Solid-Liquid Fluidization". *Fluidized Bed Technology, American Institute of Chemical Engineering* (1966), 42-50.

**30.** Weisman, R.N. and Collins, A.G. Stabilization of Tidal Inlet Channels--Design Recommendations. Fritz Engineering Lab Report No. 710.3, Lehigh University, Bethlehem, PA, 1979.

**31.** Weisman, R.N., Collins, A.G. and Parks, J.M. "Stabilization of Tidal Inlet Channels by Fluidization". *Paper presented at World Dredging Conference, WODCON IX, Vancouver, B.C.* (1980), .

**32.** Weisman, R.N., Collins, A.G. and Parks, J.M. "Maintaining Tidal Inlet Channels by Fluidization". *Journal of the Waterway Port, Coastal, and Ocean Division, ASCE Vol. 108* , No. WW4 (1982), 526-538.

**33.** Weisman, R.N. and Lennon, G.P. Fluidization in Unbounded Two-Dimensional Domains. NSF Proposal, 1984.

**34.** Wen, C.Y. and Yu, Y.H. "Mechanics of Fluidization". *Chemical Engineering Prog. Symp. Series 62 no*, No. 62 (1966), 100-111.

**35.** Wilson, C.R. and Mudie, J.D. Some Experiments on Fluidization as a Means of Sand Transport. Unpublished

36. Wisniewski, Gary M. The Application of Upconing To Improve Recovery of A Dense Fluid In An Unconfined Aquifer. Master Th., Lehigh University. Bethlehem, PA, 1984.

37. Zabrodsky, S.S. . *Hydrodynamics and Heat Transfer in Fluidized Beds.* The M.I.T. Press, Cambridge, Massachusetts, 1966.

38. Zenz, F.A. and Othmer, D.F.. *Fluidization and Fluid Particle Systems.* Rheinhold Publishing Corporation, New York, N.Y., 1960.

# APPENDIX A: Details of the Essential Features of the Experimental Two-Dimensional Apparatus

## A1. Two-Dimensional Fluidization Tank

The fluidization tank superstructure consists of a steel plate box design supported vertically, longitudinally, and laterally along the front and back and along the top and base of the tank.

The box design structure has dimensions 365.76 cm x 34.29 x 121.92 cm (Figure A2). The back and front faces are 365.76 cm x 121.92 cm x 0.952 cm steel plate with 304.8 cm x 91.44 cm x 0.952 cm sections flame cut out of the centers, resulting in plates shaped like u-sections. This design simplifies the installment of the 106.7 cm x 335.3 cm x 1.191 cm tempered glass panel, the welding of interior tank joints and various supports, tarring of tank interior to prevent corrosion and the final closing and sealing of the tank with the back face steel plate panel of dimensions 304.8 cm x 91.44 cm x 0.952 cm.

The tempered glass front panel is supported by angles and clips which are welded to the internal face of the steel plate. Sealant was applied to the contact faces of the glass and steel plate and provides an impermeable seal to contain the water and sand particles to the fluidization tank. There was leakage along the seal initially, but successful remedial action corrected the problem. Wood spacers (2.54 cm x 0.952 cm) are used to fill gaps between glass and vertical steel braces, allowing the glass to be supported without concern over the possibility of steel scratching the glass. The tempered glass was chosen as the front panel material due to its higher transparency quality and lower probability of scratching than that of plexiglass.

The 304.8 cm x 91.44 cm back steel plate panel is supported in the 304.8 cm x 91.44 cm cut section of the back face steel plate by 7.62 cm x 0.952 cm steel lap plate supports which are welded to the internal face of the back face steel plate and bolted to the back steel plate panel. The steel lap support overlaps both the back face plate and panel by 3.81 cm; therefore, providing adequate support. A gasket and sealant provide an excellent seal between the back face plate and panel.

The tank is supported vertically and longitudinally by 7.62 cm x 7.62 cm x 0.625 cm steel tube braces. The front tube support framework is prefabricated and installed by welding to a 439.4.2 cm x 54.61 cm x 1.27 cm steel base plate, which provides a base and additional longitudinal support for the tank and the support frameworks. The back tube support framework is also prefabricated, but is installed by bolting to the steel base plate. This allows for the partial disassembling of the fluidization tank at a future time. The tank can be partially disassembled by removing the back support framework, unbolting and removal of back plate panel, thus providing access to any of the internal structural or hydraulic features of the tank. The steel base plate is in turn welded to 12.7 cm I-beams which span the entire length of the tank providing excellent longitudinal support. The I-beams and the entire tank are situated on 54.61 cm x 19.05 cm x 10.16 cm wood block supports for the purpose of elevating the tank off the laboratory floor to avoid any possibility of corrosion due to floor moisture.

## A2. Hydraulic Systems

The pump used in this study must satisfy the head and flow rate requirements for providing 6.35 cm bed expansion of a 11148 sq. cm sand bed, 57.15 cm sand bed depth and maintaining 5.08 cm of clearance under the outfall weir to avoid out-wash. The flow rate requirement for the one-dimensional fluidization of this 0.15 mm sand bed was calculated using the simplified bed expansion versus superficial velocity relationship established by Fair et al, [13] ($V = v_s \epsilon_e^{4.5}$). It was determined that the fluidization flow rate for this bed expansion is 1764 $cm^3/s$. It was also determined that the pipe head losses are small relative to the fluidization pipe and manifold orifice head losses. Therefore the head requirement for the pump is based on the 0.317 cm diameter orifice head loss of 3170 cm estimated from the orifice equation. The pump chosen to adequately satisfy the above requirements is the Ingersoll-Rand High Head Centrifugal Pump (Model 1-1/2 x 1 x 5SPM-3).

**Table A2.1: IR Pump Specifications**

| | | |
|---|---|---|
| Power Input | - | 3-phase, 230v |
| Power Output | - | 3-horsepower |
| Operation Speed | - | 3600 RPM |
| Max Efficiency | - | 71% |
| Performance | - | Provides a driving head of 3536 cm at a flow rate of 1764 cc/s and an and an operation efficiency of 55% |

1. It is obvious that the pump easily satisfies the head requirements, providing 10% additional head.

2. The hydraulic pipeline system for the manifold, fluidization pipe, feed pipes, and the leakage test drainage pipe is predominantly Schedule-80 PVC pipe (Figure A1).

3. Three of the system's valves are PVC ball valves with the other being a cast iron butterfly valve. The PVC ball valves are located in the feed pipes to the manifold and fluidization pipe, respectively, and also in the leakage test drainage pipeline. The cast iron butterfly valve is situated in the pipeline linking the settling tank and the head tank.

4. The outfall weir chute transmits overflow from the fluidization tank to the settling tank. The trapezoidal outfall weir has the capacity to transmit 3237 cc/s with 5.08 cm head on the weir and a 2.54 cm free board (clearance from the top of the fluidization tank). With this capability, coarser sand grain particles can be tested without making any modifications to the outfall weir geometry.

5. Reservoir cages were designed and located in the fluidization tank to act as reservoirs during horizontal hydraulic conductivity tests using free surface concepts. This feature contributes to the versatility of this apparatus, for it allows the fluidization tank to be used for large scale two-dimensional free surface groundwater modeling. The cages are constructed of welded steel reinforcing bars to form the frame of the cage, which is in turn wrapped with No. 200 stainless steel mesh. The steel reinforcing bars provide the rigidity of the reservoirs and the No. 200 mesh allows water to seep into the reservoir while preventing sand particles from entering the caged region. Attempts were made to use the Dupuit-Forchheimer theory to determine a representative horizontal hydraulic conductivity of the fixed bed during pre-fluidization conditions, but were unsuccessful because of short circuiting through the manifold by the water from one reservoir to the other reservoir. The hydraulic conductivity determination can be found in Appendix C.

The leakage test drainage pipeline system is used to perform fluidized/unfluidized region interface leakage tests. Details of the test procedure are discussed in Section 3.2.

The 5.08 cm Schedule-80 PVC fluidization pipe is 30.48 cm in length and contains 0.317 cm orifices spaced 5.08 cm centers and 2.54 cm from tempered glass panel and back steel plate panel, respectively. There is a total of twelve orifices with six located on each side in the horizontal direction 180° opposed (directly opposite).

## A3. Settling Tank

The purpose of the settling tank is to settle out any sand particles that may have become suspended and washed out over the fluidization tank outfall weir into the basin during the fluidization process. To allow these suspended particles to remain in suspension would be detrimental to the hydraulic system. The coarser particles of the fine sand distribution will cause pitting of the pump impeller and scouring of the orifice holes of the fluidization pipe and manifold. Also, if ultra fines are allowed to remain in the system they may enter the seals of the pump and substantially reduce its life expectancy. Pitting of the impeller blades will age the blades and reduce the efficiency of the pump. Scouring of the orifice holes will change the hydraulics of the system, thus altering experimental data for the fluidization process. Therefore, this process of settling out the suspended sand particles becomes an extremely important factor to be considered when designing this type of system.

The superstructure of the settling tank is constructed with 1.91 cm (3.4-in) plywood and is longitudinally and laterally supported by 2 x 4 bracing located at 35.56 cm and 83.82 cm vertical up from the base of the basin. The basin consists of two major cells, the turbid water cell and the clean water cell. The turbid water cell is where the actual sedimentation occurs, and it is located adjacent to the outfall end of the fluidization tank. The turbid water cell is separated from the clean water cell by a 121.92 cm x 60.96 cm x 121.92 cm partition that includes a 60° V-Notch weir. The suspended particles are forced to settle out by means of a baffle made of 2 x 4's and 1.91 cm plywood with a screen (No. 200 stainless steel mesh) constructed at the bottom of the baffle. The suspended particle is forced to take a path vertically down and through the

screen in order to reach the opposing side of the baffle. By doing so, it encounters the resistance of the screen because the No. 200 mesh is finer than 99.8% of the particles. Consequently, the particles settle out if they are large enough or remain in suspension on the same side of the baffle due to turbulence. However, the particles are harmless to the pump and hydraulic systems if they remain in this location. Therefore, the water that enters the 121.92 cm x 60.96 cm x 30.49 cm clean water cell via the V-Notch weir should be quite clean. This water is in turn drained into the head tank by gravity flow via the 5.08 cm PVC pipeline regulated by a cast iron butterfly valve located in the line.

### A4. Head Tank

The head tank is located between the settling tank and the centrifugal pump. The settling tank provides the head tank with a new and clean water supply to replenish the volume of water being removed from the head tank and discharged out through the fluidization pipe into the fluidization tank by the pump. Therefore, this is a recirculating system: pump to fluidization tank to settling tank to head tank and back into the pump.

The two major purposes of the head tank are to provide the pump with an adequate positive suction head and an adequate volume of water to satisfy volume of flow requirements for the fluidization process. To ensure an adequate positive suction head, a foam float is installed in the tank. The foam float prevents any possibility of a vortex forming at the surface of the water in the tank and migrating down to the pump intake resulting in a zero positive suction head and the pump sucking air. If the vortex were allowed to form and the pump allowed to suck air, this would cause a loss of prime on the pump.

The head tank stands 71.12 cm high and is 60.96 cm wide with the invert of the outlet to the pump located at 10.16 cm from the base of the tank.

## A5. Data Acquisition System

Approximately 72 of the 143 pressure taps are monitored as a part of the physical model data acquisition system. A completely unnecessary method of monitoring would have been to use a pressure transducer for each pressure tap. Because of the near steady state manner in which the fluidization phenomenon is investigated, one pressure transducer can be used to monitor the pressures from all 72 pressure taps. This is accomplished using several "fluid switch wafers" to transduce multiple pressures by time sharing the single transducer. A recommended configuration was provided to the investigators by the Scanivalve Corporation. Three of five wafers (Model WO602/1P-24T) with 24 pressure ports (inputs) are used in this study. Each of these three wafers are connected in parallel via collector tubes to one wafer (Model W0601/1P-12T) with 3 of 12 pressure ports (inputs) being utilized. The Model W0601/1P-12T wafer in turn is connected to the differential pressure transducer via a collector tube and a zero volume pressure transducer adaptor. The pressure transducer in turn produces an electrical analog signal which is transmitted to a digital device, Valhalla multimeter, where a voltage reading, millivolts, is made and manually recorded onto a data sheet.

Fluid pressures are transmitted through Swagelok tube fittings threaded into the pressure taps located in the back plate of the steel fluidization tank. The type of fitting is a male connector - metric tube to male NPT thread. The tube receptacle opening is a 3 mm outside diameter. The thread is a 1/8 inch P-NPT male pipe size. Tygon flexible plastic tubing (Norton Performance

Plastics Co.) is used to transmit fluid pressures from tube fittings to the Scanivalves and in turn to the pressure transducer. The tubing has dimensions of 1.5 mm inside diameter, 3.0 mm outside diameter, and 0.75 mm wall thickness. Care was taken to prevent sand from entering the tubing by inserting filter screens made of fine 304-stainless mesh (No. 200) into the Swagelok tube fittings.

The Scanivalve wafer (Model W0601/1P-12T) is mounted on a single WS5-12 solenoid drive and the three Scanivalve wafers (Model W0602/1P-24T) are mounted on a single WS5-24 solenoid drive. The solenoid drives are used to rotate a rotor inside the stator of each wafer and open the stator port (input port) to any particular pressure tap on the fluidization tank being analyzed. Two 12-volt batteries are connected in series to supply the power needed for the operation of the solenoid drives. The solenoid drives each draw 3 amps and 24 volts during operation. These Scanivalve wafer models employ a pneumatic rotor thrust bearing system, which requires that an external fluid pressure ($P_x$) connected to the wafer must be counter balanced by a pressure applied diametrically across from $P_x$. This balance pressure is applied to the back of the rotor via the balance pressure port located on the cover of the wafer and prevents the $P_x$ pressures in the stator ports from separating the rotor from the stator. The pressure applied at the balance pressure tubulation should be equivalent to $P_x$ average or above, but should not exceed 20 psi above the average. These wafers are made of hard coated aluminum and epoxied with 1.5 mm diameter stainless steel tubulations (stator ports). The operational pressure range is 0-50 psi. The above specifications are in accordance with the Scanivalve Corporation Specifications (Copyright, 1971).

A 10.62 cm diameter balancing pressure column (3 in. PVC pipe Schedule-80) was designed to serve two purposes; to provide balancing fluid pressures to the Scanivalve wafers, and to provide a means of calibrating the pressure transducer. A set of holes were tapped at the bottom portion of the column. These holes served as ports to transmit balancing pressures via the Swagelok tube fittings and tygon tubing to the Scanivalves. They also served as the origin and location of the pressure transducer during the calibration test. Additional holes were tapped at 2.31 ft. (70.4 cm) vertical intervals along the pipe which correspond to intervals of 1.0 psi (6895 $N/M^2$). The pressure transducer was installed at the origin (a hole of the base set) and the column was filled with water in increments of 1 psi (6895 $N/m^2$). The pressure transducer was connected to the Valhalla multimeter and readings (millivolts) were taken at every 1 psi interval. It was determined that the pressure transducer readings are linear with fluid pressure. The column was filled to an arbitrary pressure of 5 psi (a value between $P_x$ average and 20 psi above average) to provide the balancing pressure for the Scanivalves during testing.

The pressure transducer used in the experimental research is a differential type (Model PDCR23D) made by Scanivalve Corporation. The transducer has the following specifications:

**Table A5.1: Pressure Transducer Specifications**

| | |
|---|---|
| Pressure Range: | +/- 5.0 psi |
| Sensitivity: | 50 +/- 3 mv |
| Excitation Voltage | 12 volts |
| Non-Linearity and Hysteresis: | +/- 0.05 B.S.L. |
| Temperature Operating Range: | -40 to +100 Deg C |
| Temperature Compensation Range | 0 to +50 Deg C |
| Thermal Zero Shift | +/- 0.02%/Deg C |
| Thermal Sensitivity Shift | +/- 0.02%/Deg C |

The transducer should be allowed to warm up for 30 minutes to achieve the listed specifications. Included with the differential pressure transducer is a zero volume pressure transducer adaptor equipped with a purge valve feature designed to be used with Scanivalves when scanning liquid pressures. This device allows the easy removal of all the air bubbles from the Scanivalve internal ducts and the associated pressure lines (tygon tubing) attached to the Scanivalves. If air bubbles are present in any of these ducts, the scanning speed of the Scanivalve will be greatly reduced. In addition, the presence of air in the ducts or pressure lines will cause erroneously high or low pressure readings depending on the nature of the air pocket. Small air bubbles tend to cause low readings, but long air pockets located in the pressure lines which conform to the diameter of the line tend to cause high readings. The zero volume pressure transducer adaptor with purge valve is installed with the "purge drain tubulation" (drainage port), 1.5 mm outside diameter, projecting straight up so

that no air bubbles can be trapped internally during the purging operation. If all of the pressures transmitted to the Scanivalves are above ambient pressure, it is a simple matter to simply open the purge valve to let the fluid under pressure be expelled from the "purge drain tubulation". The Scanivalve can be stepped through all of its port positions and by allocating enough time, all of the air bubbles or pockets can be purged from all of the Scanivalve ducts and pressure lines. The differential pressure transducer has one side of a small diaphragm exposed to the active pressure of the system. When the pressure changes, the diaphragm flexes and a sensing element connected to the other side of the diaphragm produces an electrical analog signal that is linear with the change in pressure in the system. The sensing element used is a resistance-wire strain gage Wheatstone Bridge type, attached to the flexible diaphragm. As the diaphragm flexes, the wires of the strain gage change length, thereby changing the resistance of the wire. It is this resistance change that is utilized electronically to produce a voltage change that is then read on the digital device, Valhalla multimeter.

The power supply used to drive the pressure transducer with an excitation voltage of 12 volts is a Kepco PAT modular power supply (Model PAT15-1.5). The pressure transducer draws a maximum of 1.5 milliamps of power from the power supply. The Kepco PAT series of programmable power supplies includes a short-circuit proof design by means of an extremely sharp current limit circuit, provisions for full-range programming and all silicon design with conservatively rated components for added reliability. The NPN output transistors are driven by a monolithic, linear IC amplifier. Kepco PAT modules may be readily adapted to provide stabilized output current by adding external sensing and control resistors.

**Table A5.2: Kepco PAT Power Supply Specifications**

| | | |
|---|---|---|
| D-C Output Range | - | 0-15 V, 0-1.5 amps |
| Max Power Input | - | 125 V A-C, 0.65 amps |
| Operating Temperature | - | -20°C to 70°C |
| Storage Temperature | - | -400°C to 85°C |
| Cooling System | - | Natural convection |
| Voltage Control | - | PAT modules are ordinarily supplied without a voltage control. A wirewound potentiometer (rheostate) is used as the voltage control resistance |
| Current Limit Control | - | A single-turn control provides current limiting from 10% to 105% of rated full load (labeled $I_b$). |
| Time Voltage Drift (8 hour drift) | - | <0.01% or 1 mv |
| Ripple or Noise | - | <0.1 mv |

The current is adjusted to provide an excitation voltage of 12 volts to the pressure transducer. The load is applied across the negative (ground) and positive terminals via butterfly clips and, in turn secured to the negative and postive jacks of the pressure transducer.

The digital device used to convert the electrical analog signal from the pressure transducer to a digital readout is the Valhalla Digital Multimeter-Counter.

**Table A5.3: Valhalla Multimeter DC Voltage Specifications**

4.5 digit LED display

| | | |
|---|---|---|
| DC Voltage Range | - | 200mv, 2, 30, 200, 1000v |
| Accuracy | - | +0.05% F.S. |
| Resolution | - | 0.005% F.S.; measurements to 10 microvolts on lowest range |
| Max Input | - | 1000v |

The Valhalla Model 4440 is a fully loaded battery powered or outlet powered (AC voltage) digital multimeter with 5 ranges of AC and DC voltage, 5 ranges of AC and DC current, 6 ranges of hi-lo ohms and a built-in 5 range 20$MH_z$ frequency counter. The electrical analog signal is transmitted via butterfly clip leads secured across the negative (ground) and positive jacks of the multimeter and the transducer, respectively.

The control panel located on the front face of the control box is used to integrate the entire data acquisition system. It includes the following: a high security round lock switch used to turn on or shut down the entire system; a "soft-feel" momentary switch used to step through the 24 channels (24 stator ports) located on each of the 3 banks (W0602/1P-24T wafers) during testing; a "soft-feel" momentary switch used to step through the three individual banks (stator ports) located on the Model W0601/1P-12T wafer; negative and positive receptacles (jacks) for the leads from the 24 volt battery supply (12 volt batteries in series) used to run both solenoid drives; pressure transducer output signal jacks; pressure transducer input power supply jacks; a homing switch used to home in on any desired channel.

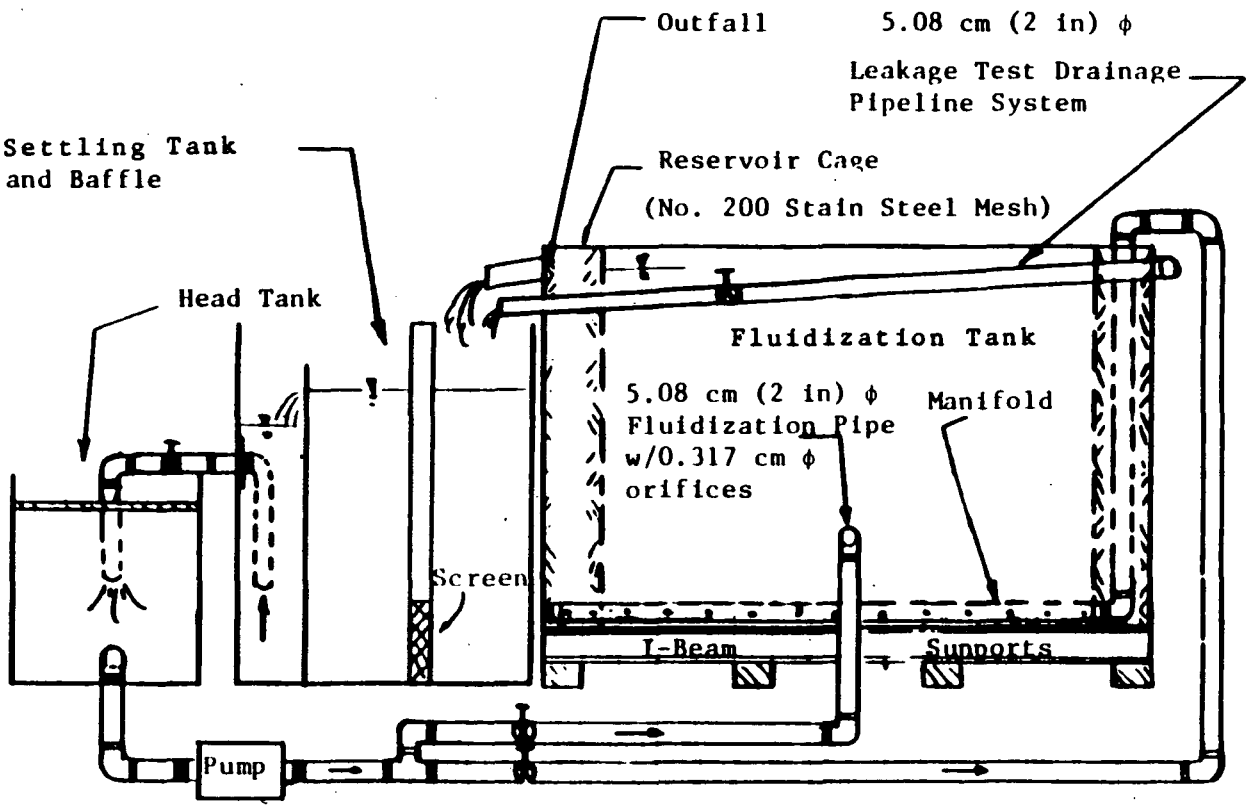


**Figure A1:** Schematic of the Experimental Two-Dimensional Fluidization Apparatus (Not to Scale)

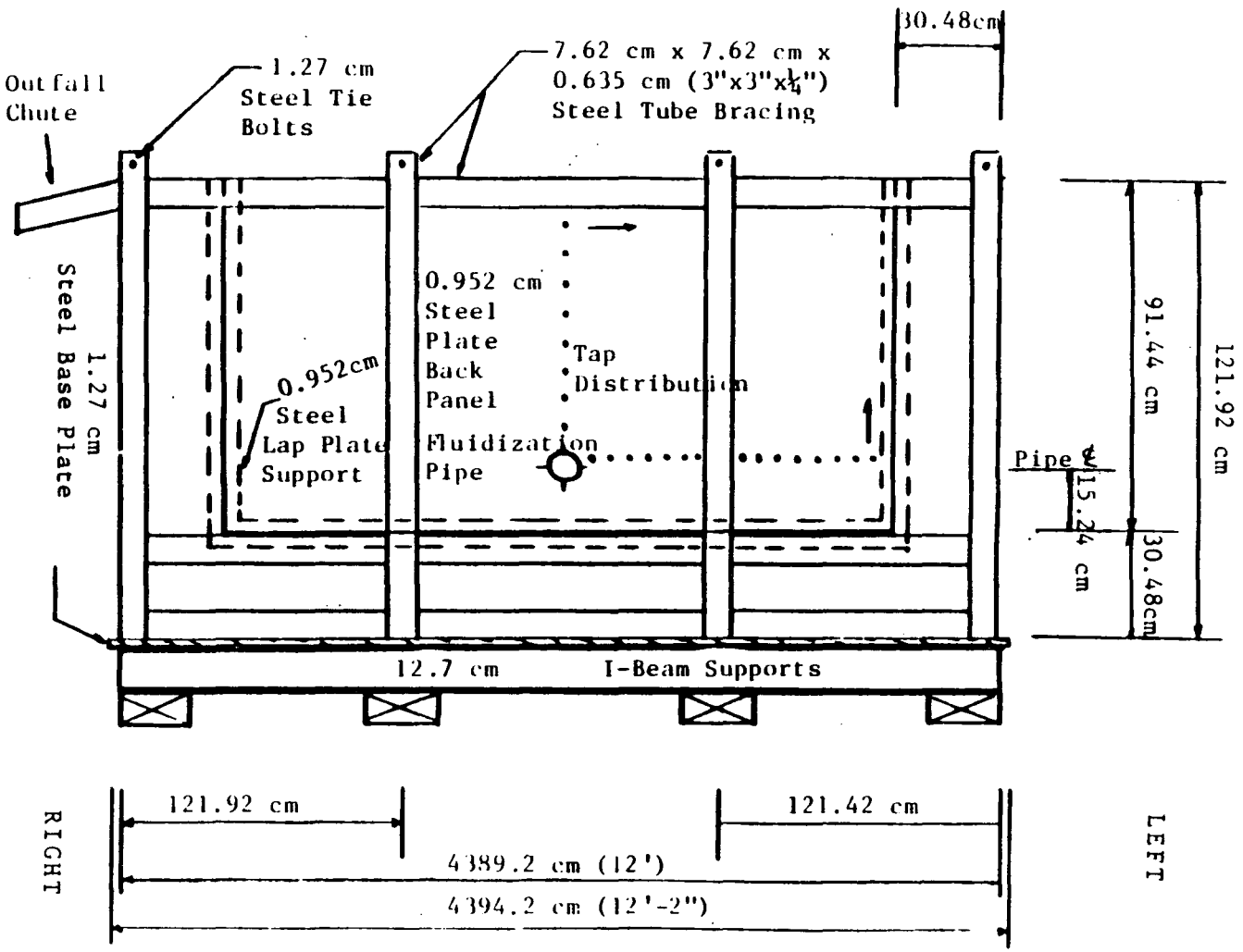


**Figure A2:** Back Profile Structural Detail of Two-Dimensional Fluidization Tank (Not to Scale)

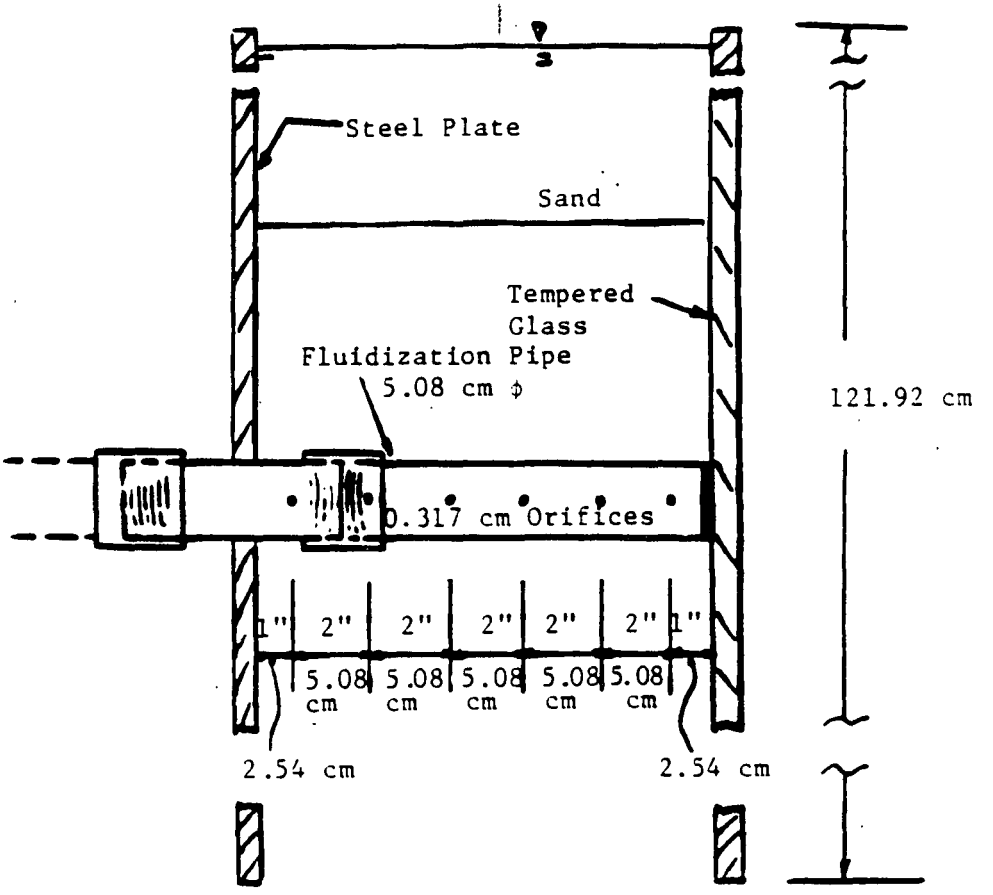


**Figure A3:** Profile Detail of the Fluidization Pipe
(Not to Scale)

# APPENDIX B: Data Acquisition System Schematics

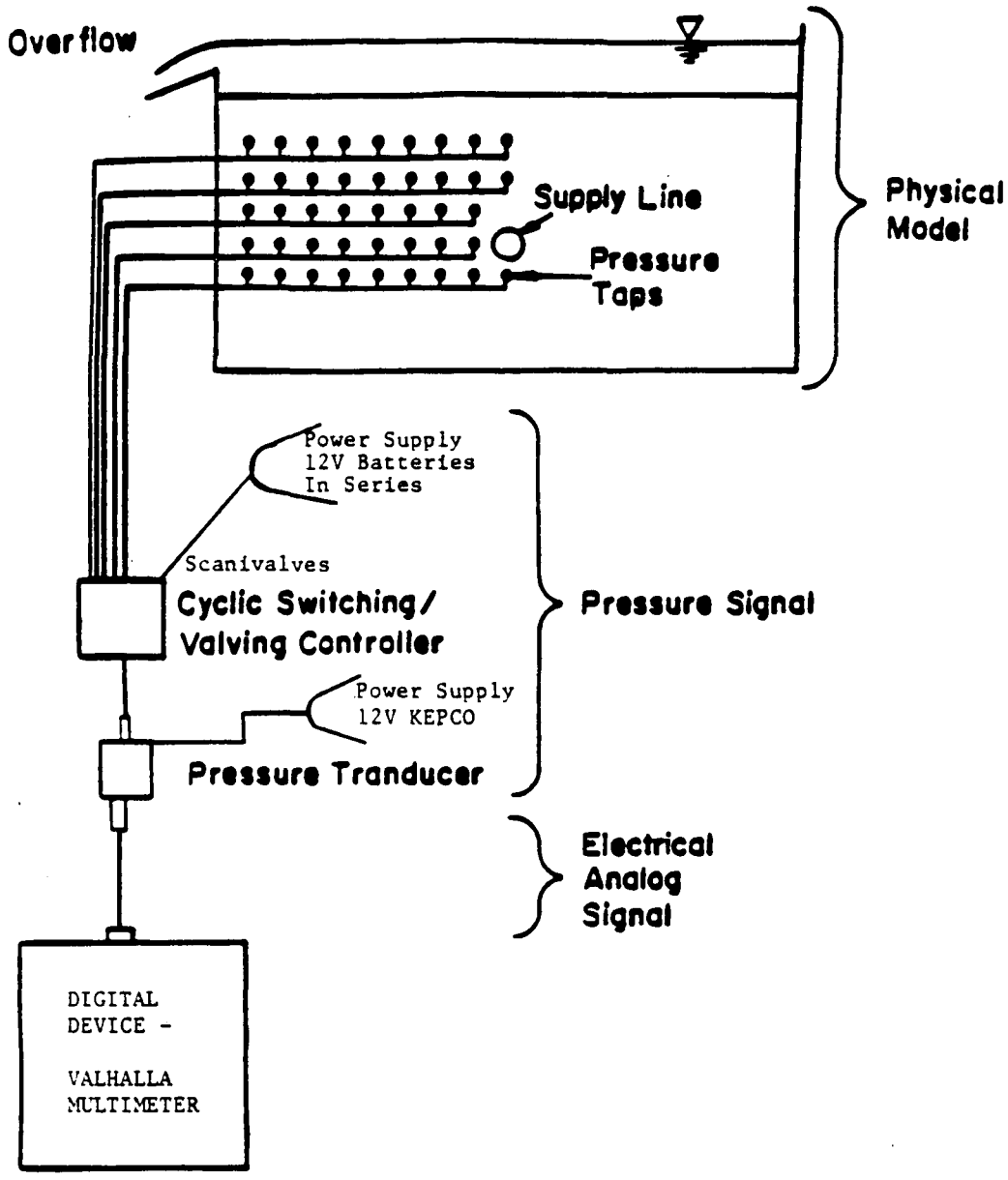


**Figure B1:** Schematic of Existing Data Acquisition System. Figure is taken from Ref. [33]

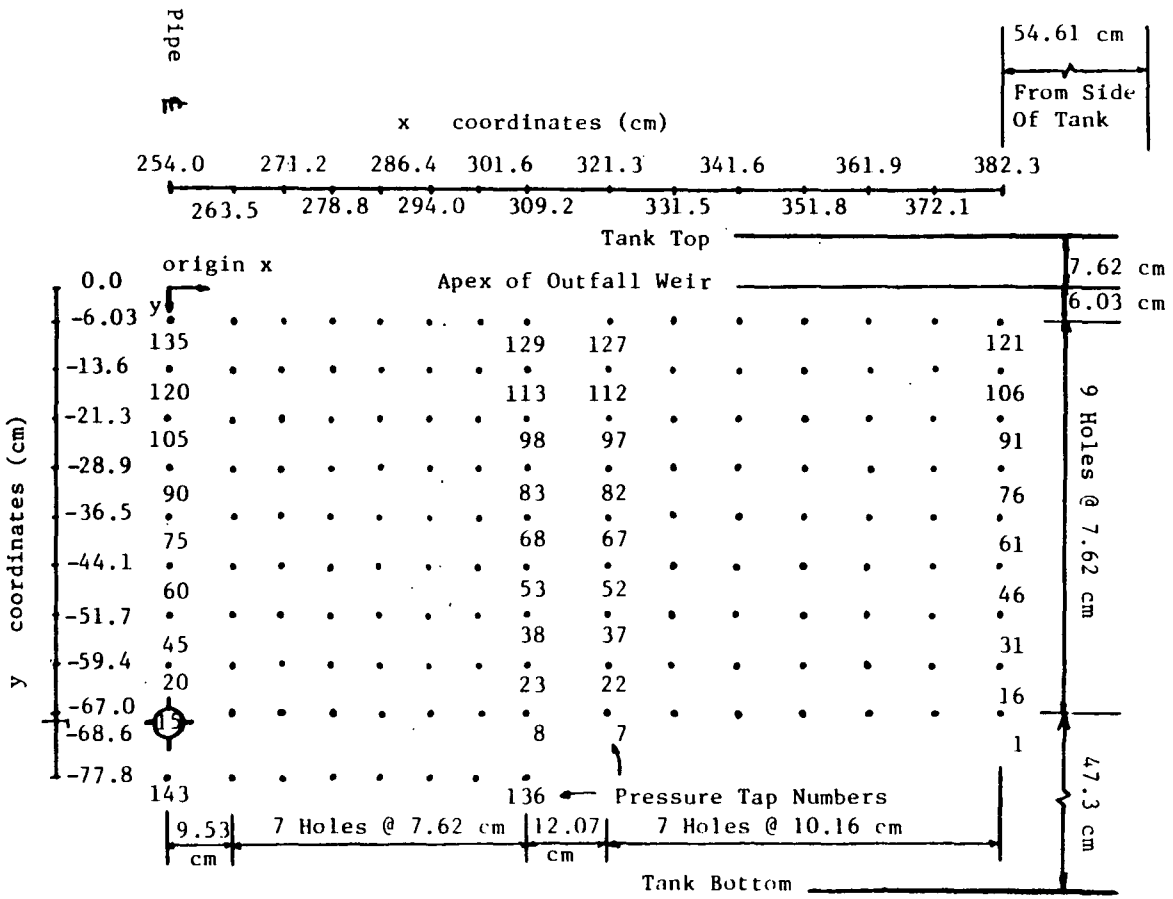


**Figure B2:** Schematic of Coordinate System (Grid) for Pressure Tap Distribution on Back Panel of Fluidization Tank

# APPENDIX C: Sand Characteristics

**Table C1:** Properties of Sand Medium

| SAND PROPERTY | VALUE | TECHNIQUE USED FOR ITS DETERMINATION |
|---|---|---|
| Specific Gravity ($S_s$) | 2.67 | ASTM Test |
| Porosity ($\varepsilon$) | | |
| Compacted | 39% | ASTM Test |
| Undisturbed | 46% | |
| Hydraulic Conductivity | | |
| Average Horizontal ($K_H$) | 0.018 cm/s | Two-Dimensional Flow Model (Dupuit-Forchheimer Theory) $K_H = \frac{Q'2L}{(h_1^2 - h_2^2)}$ |
| Average Vertical ($K_V$) | | |
| Compacted | 0.0083 cm/s | |
| Undisturbed | 0.0114 cm/s | Constant Head Permeameter |

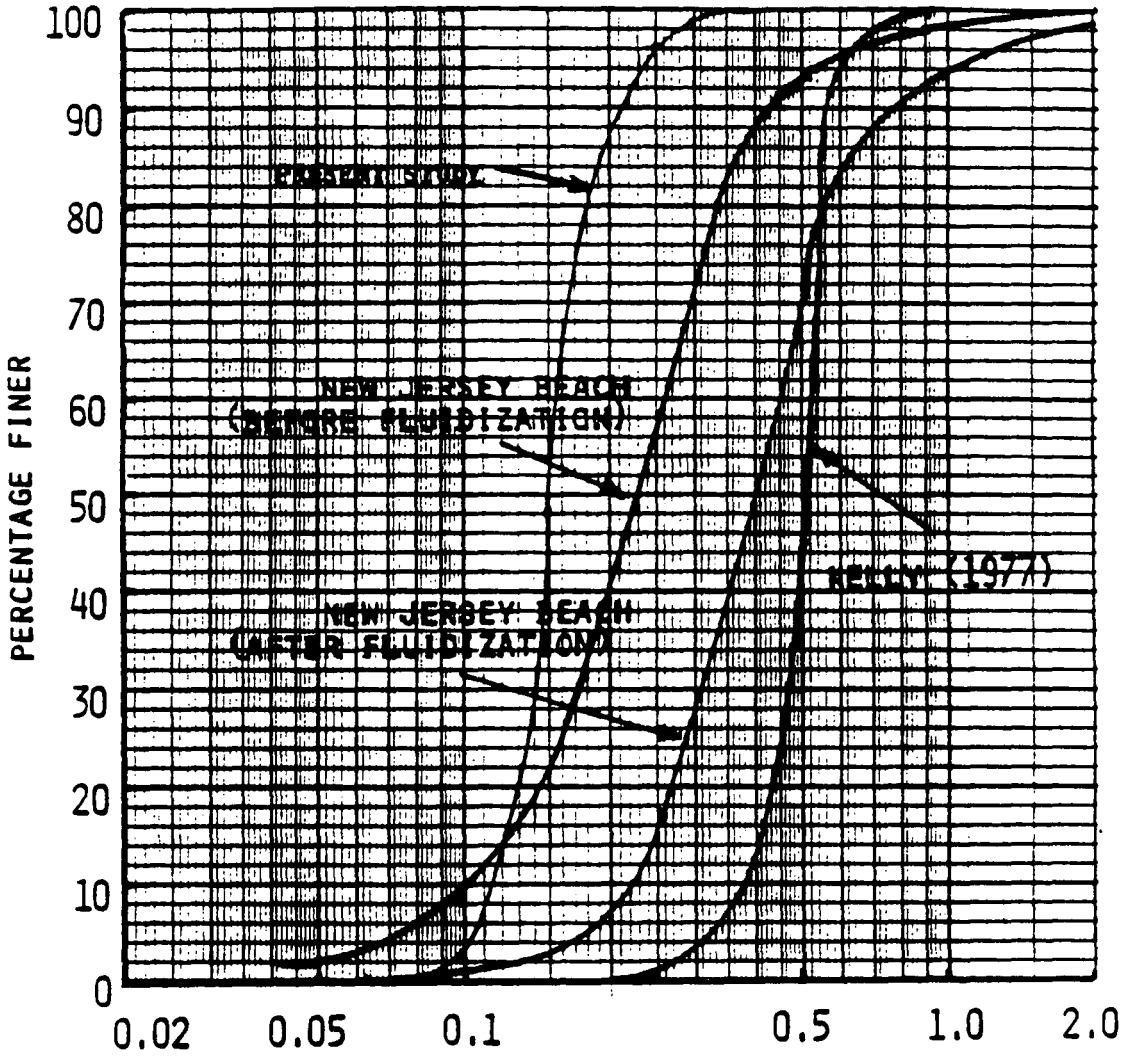


| | | |
|---|---|---|
| SPECIFIC GRAVITY: | Kelley (1977) | 2.52 |
| | Weisman & Collins (1979) (NJ Beach) | 2.42 |
| | Present Study | 2.67 |

**Figure C1:** Sieve Analysis for Sand of the Present Study and for Sands of Weisman and Collins [30] and Kelley [20]. Figure is taken from Ref. [30].

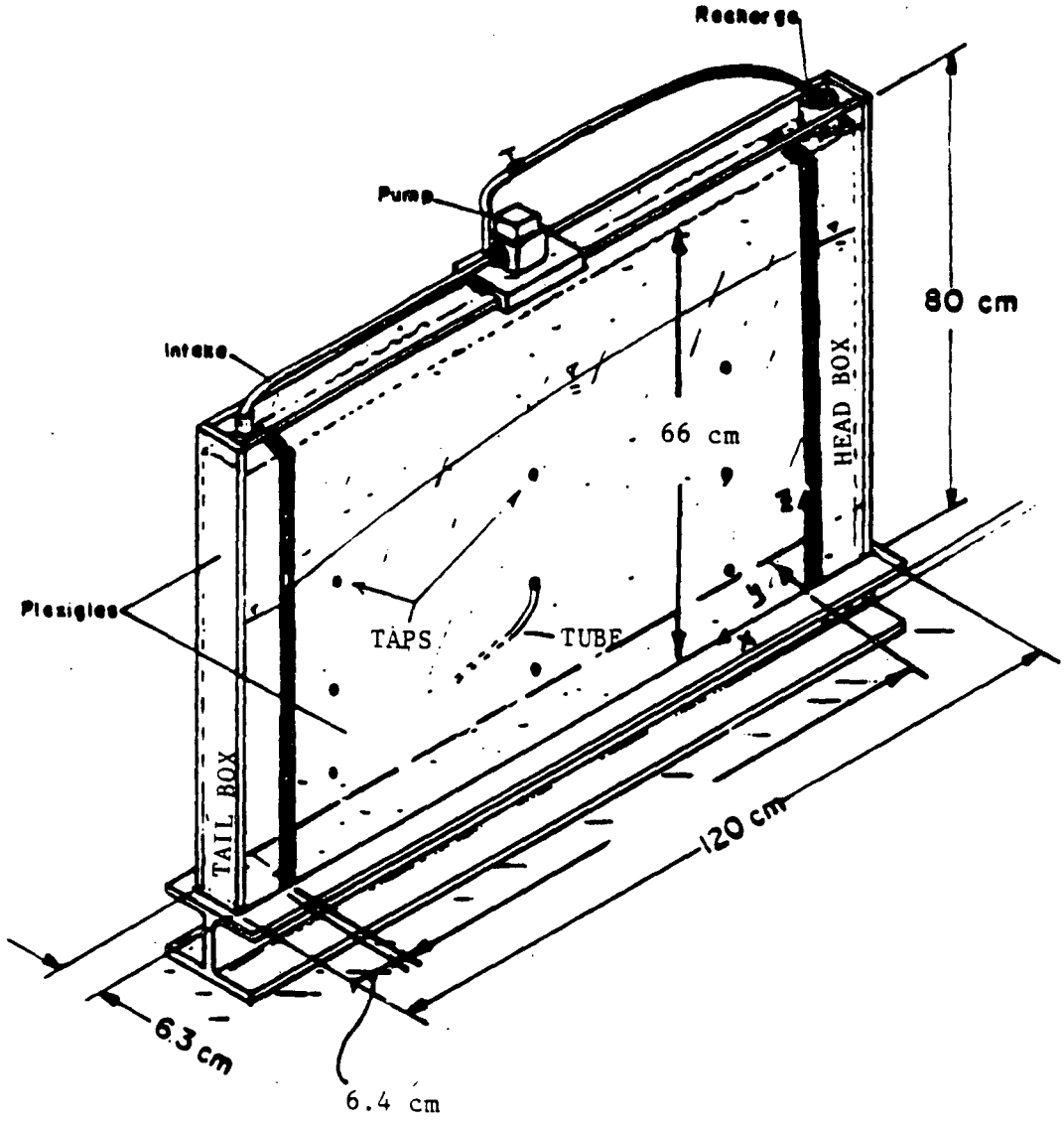


**Figure C2:** Schematic of Two-Dimensional Physical Flow Model (Not to Scale).
Figure is taken from Ref. [36].

# APPENDIX D: Growth of Fluidized Region for Tests 1,3,4,5

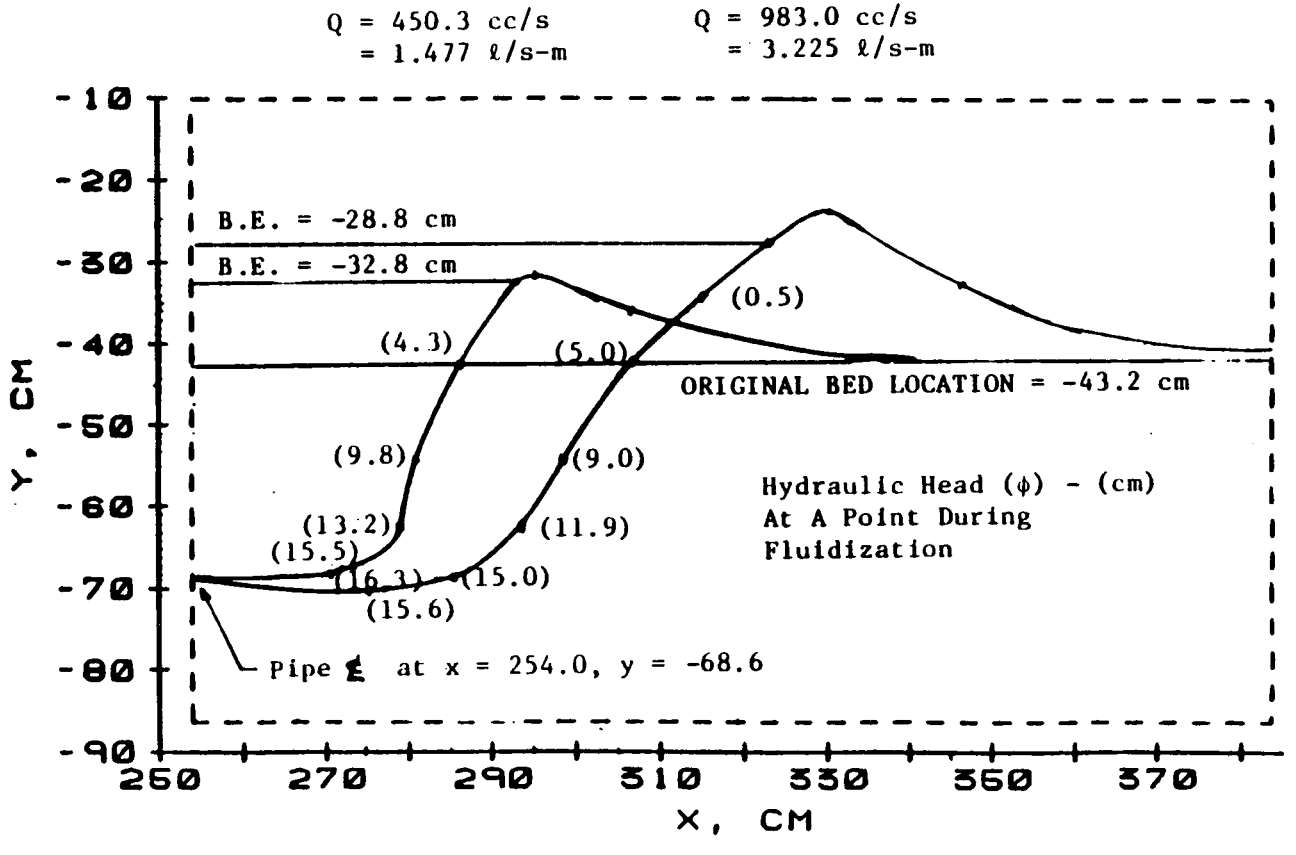


**Figure D1:** Test 1. Growth of Fluidized Region for Various Flow Rates. Original Bed Depth = 25.4 cm, y = -43.2 cm. Original Bed Porosity ($\epsilon_o$) = 39%

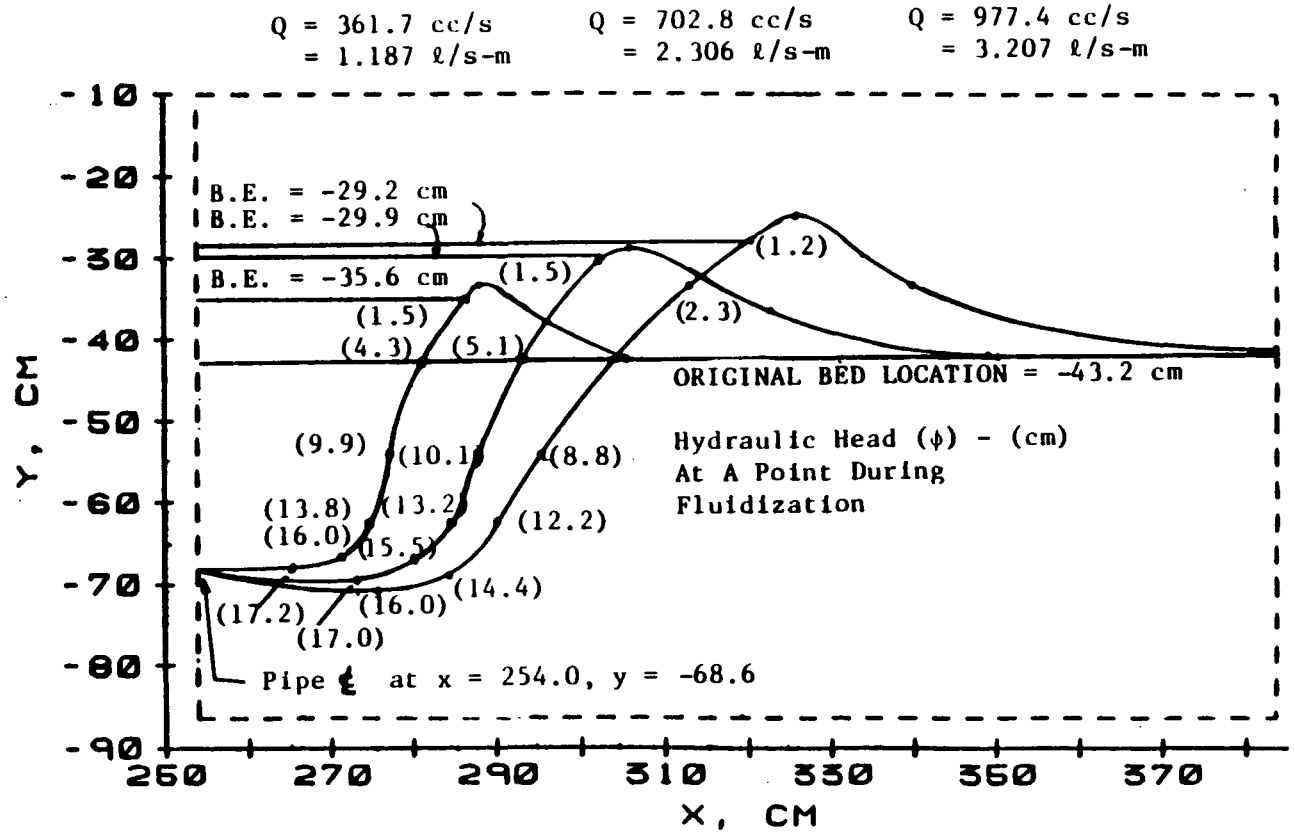


**Figure D2:** Test 3. Growth of Fluidized Region for Various Flow Rates. Original Bed Depth = 25.4 cm, y = -43.2 cm. Original Bed Porosity ($\epsilon_o$) = 39%

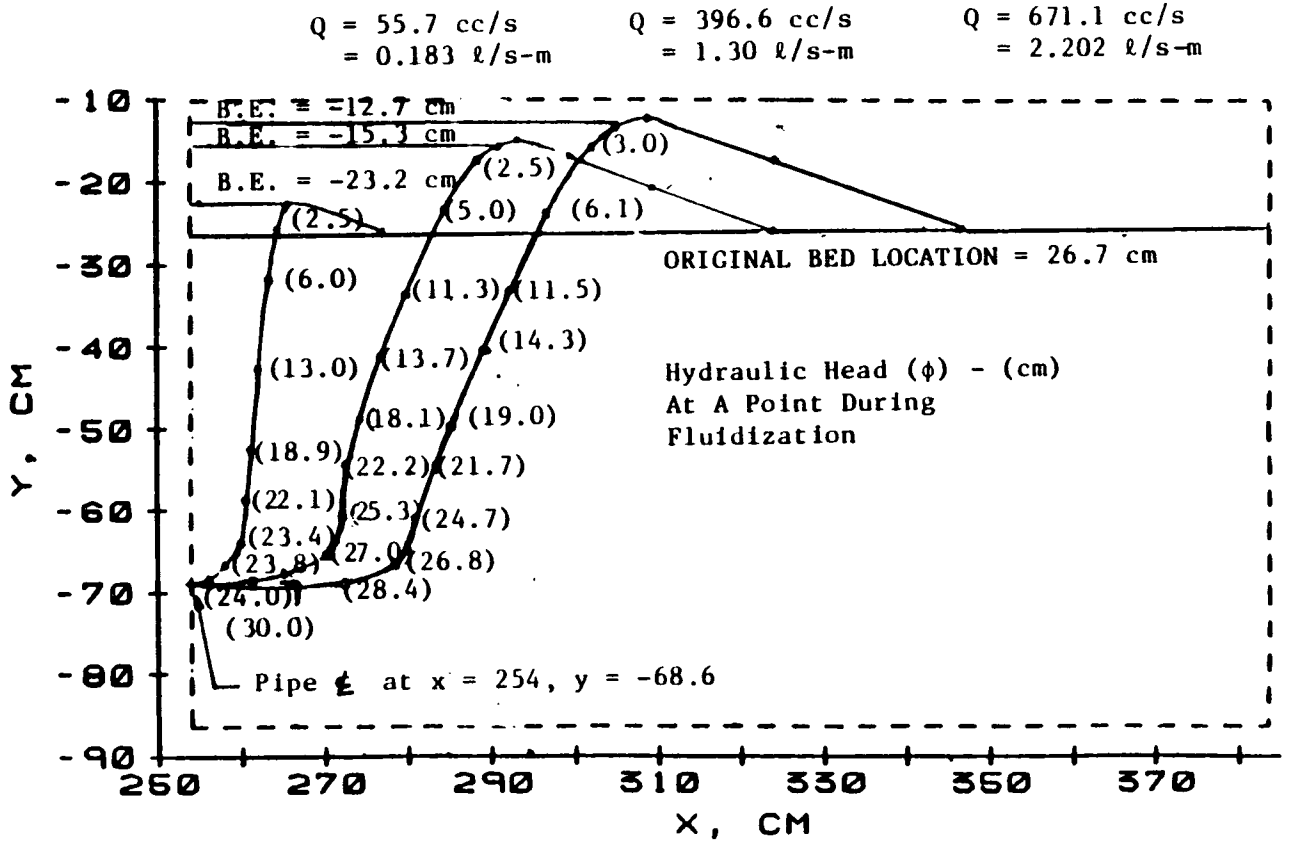


**Figure D3:** Test 4. Growth of Fluidized Region for Various Flow Rates. Original Bed Depth = 42 cm, y = -26.6 cm. Original Bed Porosity ($\epsilon_o$) = 39%

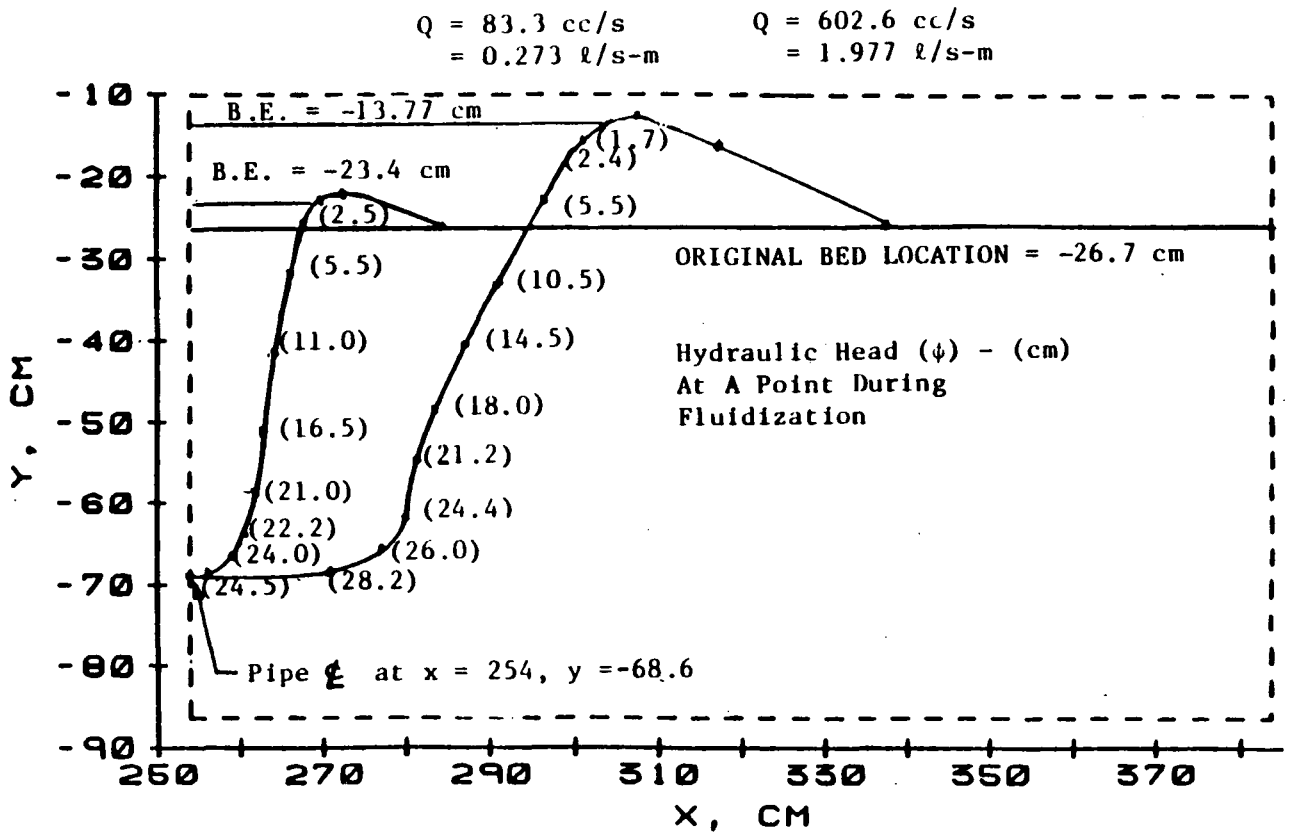


**Figure D4:** Test 5. Growth of Fluidized Region for Various Flow Rates. Original Bed Depth = 42 cm, y = -26.6 cm. Original Bed Porosity ($\epsilon_o$) = 39%

# APPENDIX E: Hydraulic Head Distributions for Tests 1,3,4,5,6

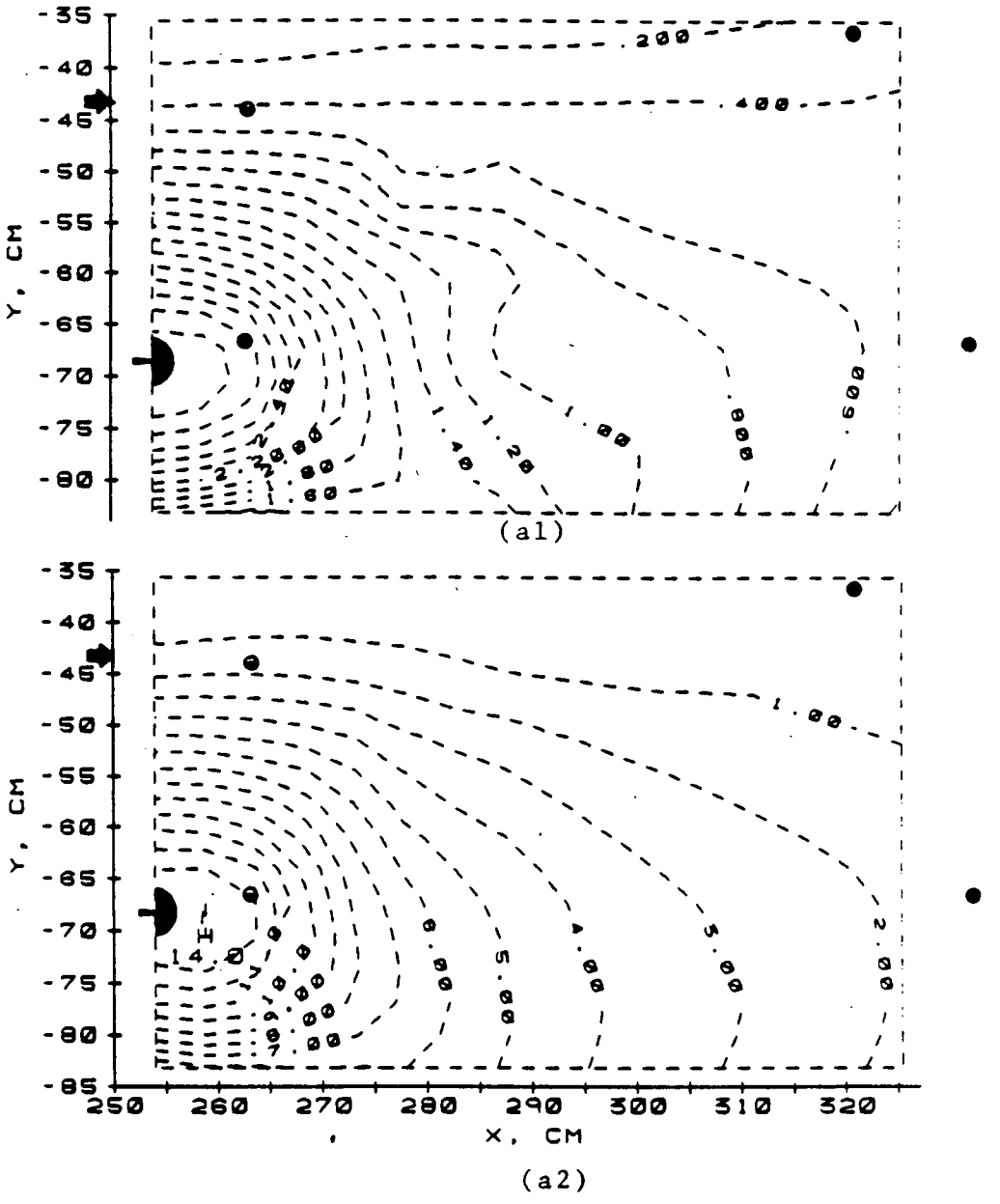


**Figure E1a:** Test 1. Hydraulic Head Distribution ($\phi$) in Two-Dimensional Unbounded Domain. Initial Bed Depth = 25.4 cm, y = -43.2 cm. Initial Bed Porosity ($\epsilon_o$) = 39% Flow Rate (l/s-m): (a1) Q = 0.012, (a2) Q = 0.053

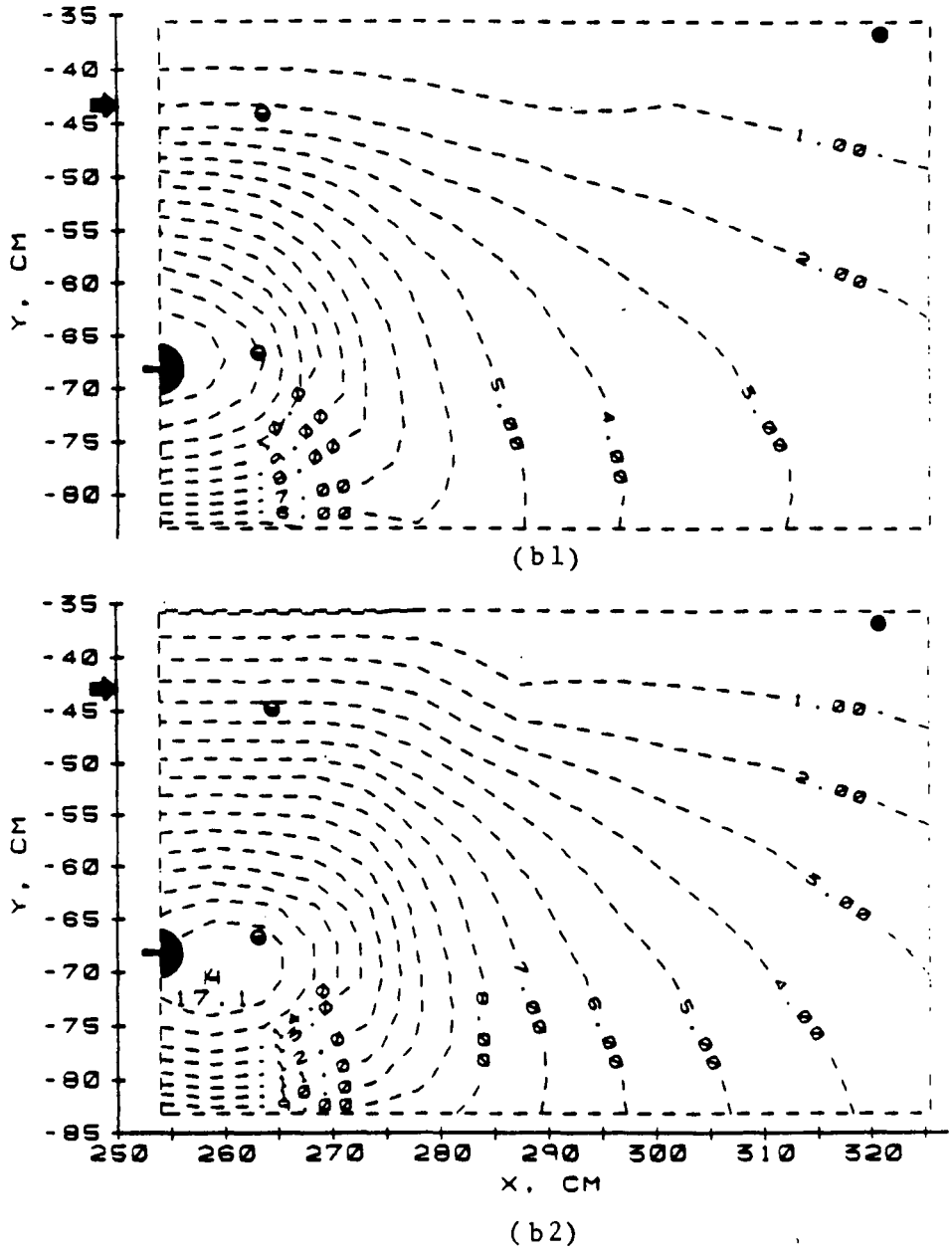


**Figure E1b:** Test 1. Hydraulic Head Distribution ($\phi$) in Two-Dimensional Unbounded Domain. Initial Bed Depth = 25.4 cm, y = -43.2 cm. Initial Bed Porosity ($\epsilon_o$) = 39% Flow Rate (l/s-m): (b1) Q = 0.014, (b2) Q = 0.603

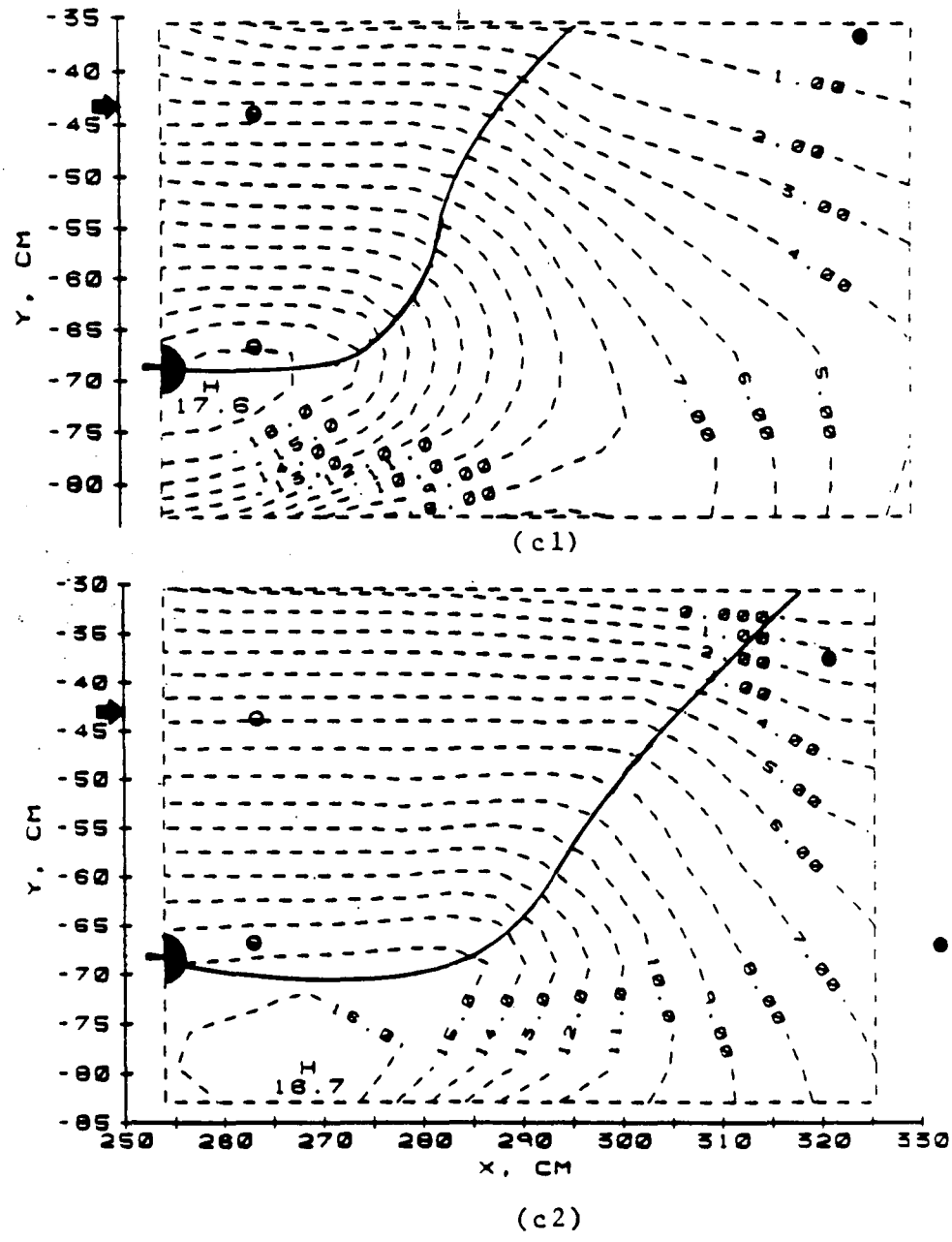


**Figure E1c:** Test 1. Hydraulic Head Distribution ($\phi$) in Two-Dimensional Unbounded Domain. Initial Bed Depth = 25.4 cm, y = -43.2 cm. Initial Bed Porosity ($\epsilon_o$) = 39% Flow Rate (l/s-m): (c1) Q = 1.477, (c2) Q = 3.225

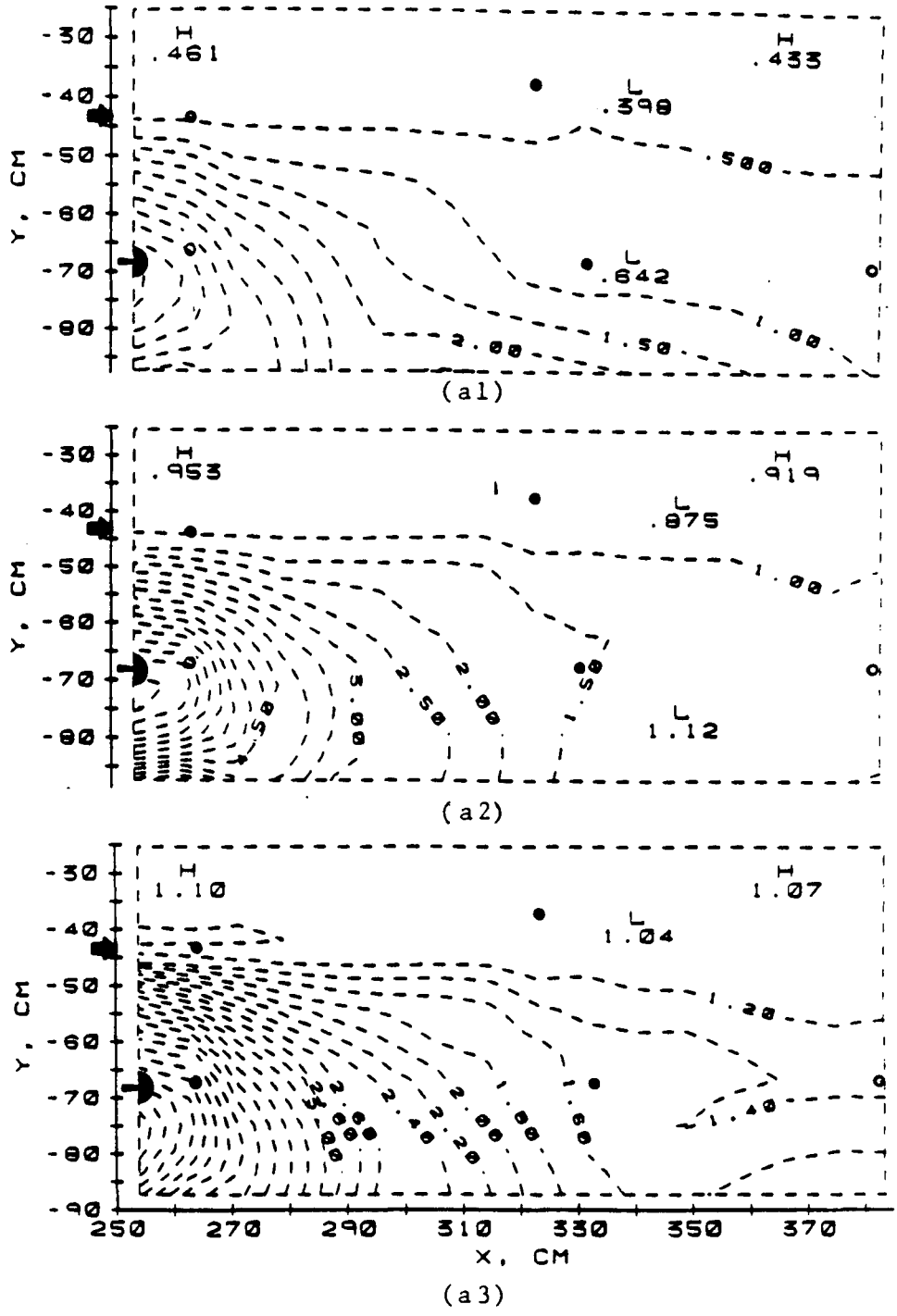


**Figure E2a:** Test 3. Hydraulic Head Distribution ($\phi$) in Two-Dimensional Unbounded Domain. Initial Bed Depth = 25.4 cm, y = -43.2 cm. Initial Bed Porosity ($\epsilon_o$) = 39% Flow Rate (l/s-m): (a1) Q = 0.025, (a2) Q = 0.029, (a3) Q = 0.084

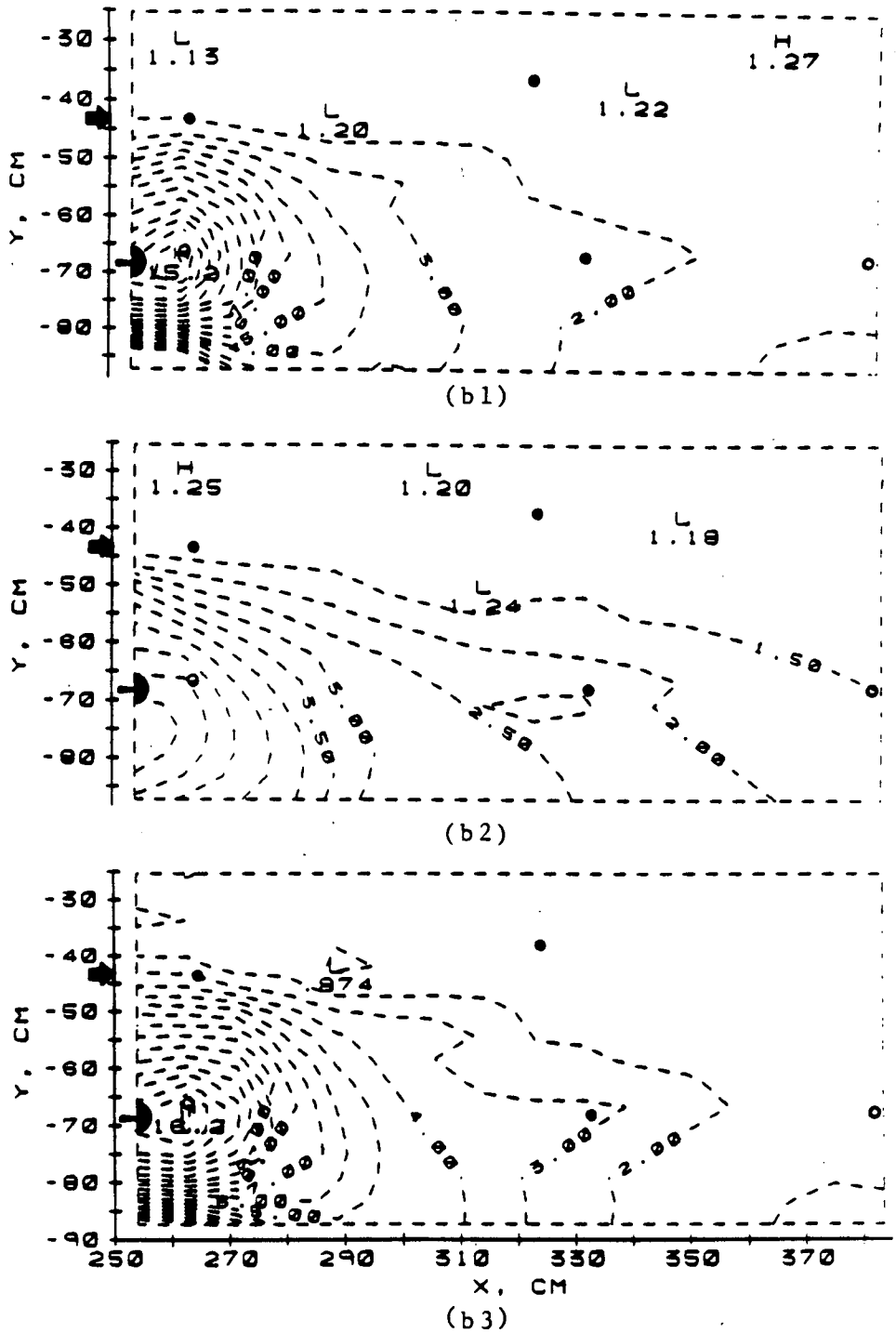


**Figure E2b:** Test 3. Hydraulic Head Distribution ($\phi$) in Two-Dimensional Unbounded Domain. Initial Bed Depth = 25.4 cm, y = -43.2 cm Initial Bed Porosity ($\epsilon_o$) = 39% Flow Rate (l/s-m): (b1) Q = 0.115, (b2) Q = 0.225, (b3) Q = 0.234

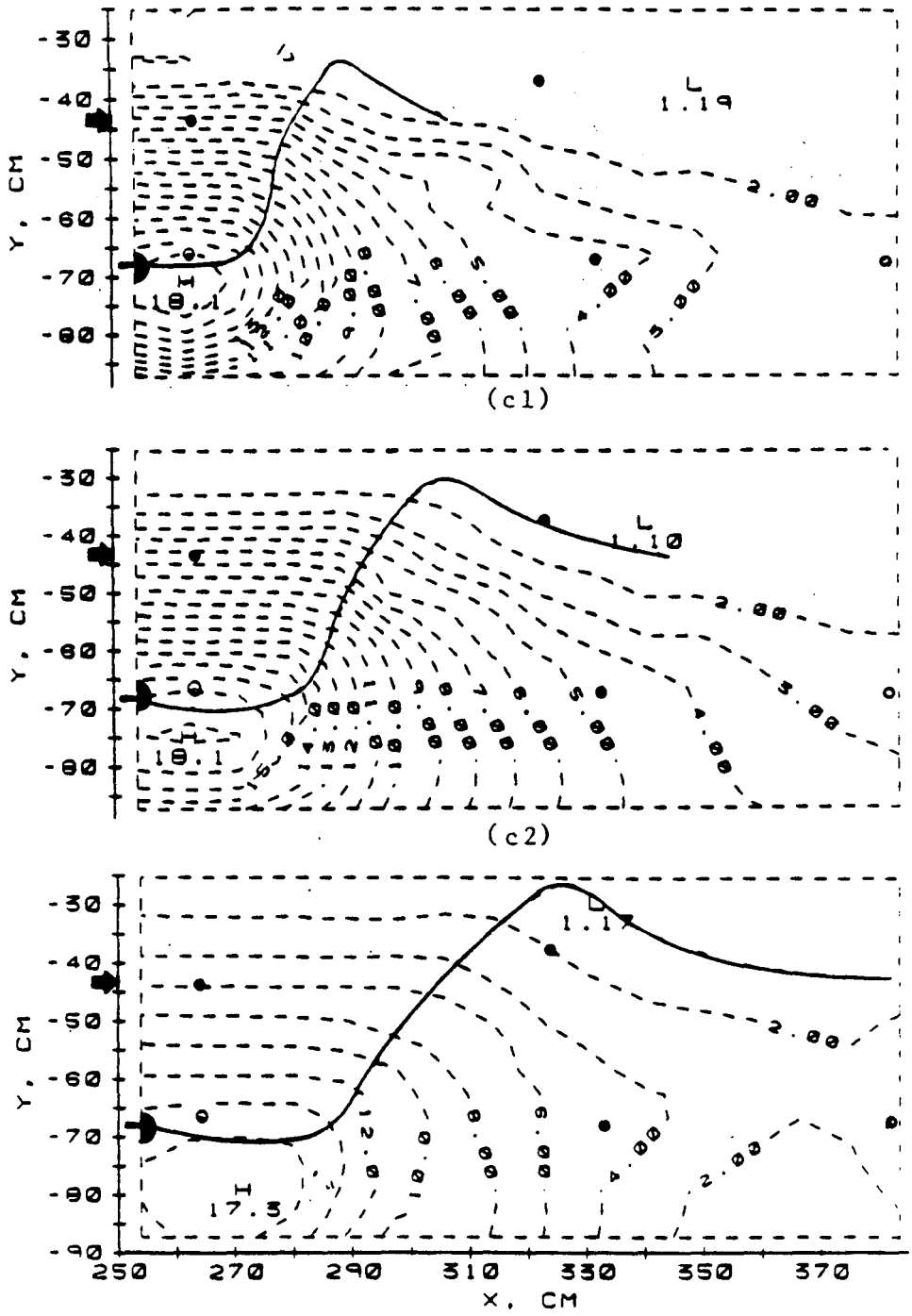


**Figure E2c:** Test 3. Hydraulic Head Distribution ($\phi$) in Two-Dimensional Unbounded Domain. Initial Bed Depth = 25.4 cm, y = -43.2 cm. Initial Bed Porosity ($\epsilon_o$) = 39% Flow Rate (l/s-m): (c1) Q = 1.187, (c2) Q = 2.306, (c3) Q = 3.207

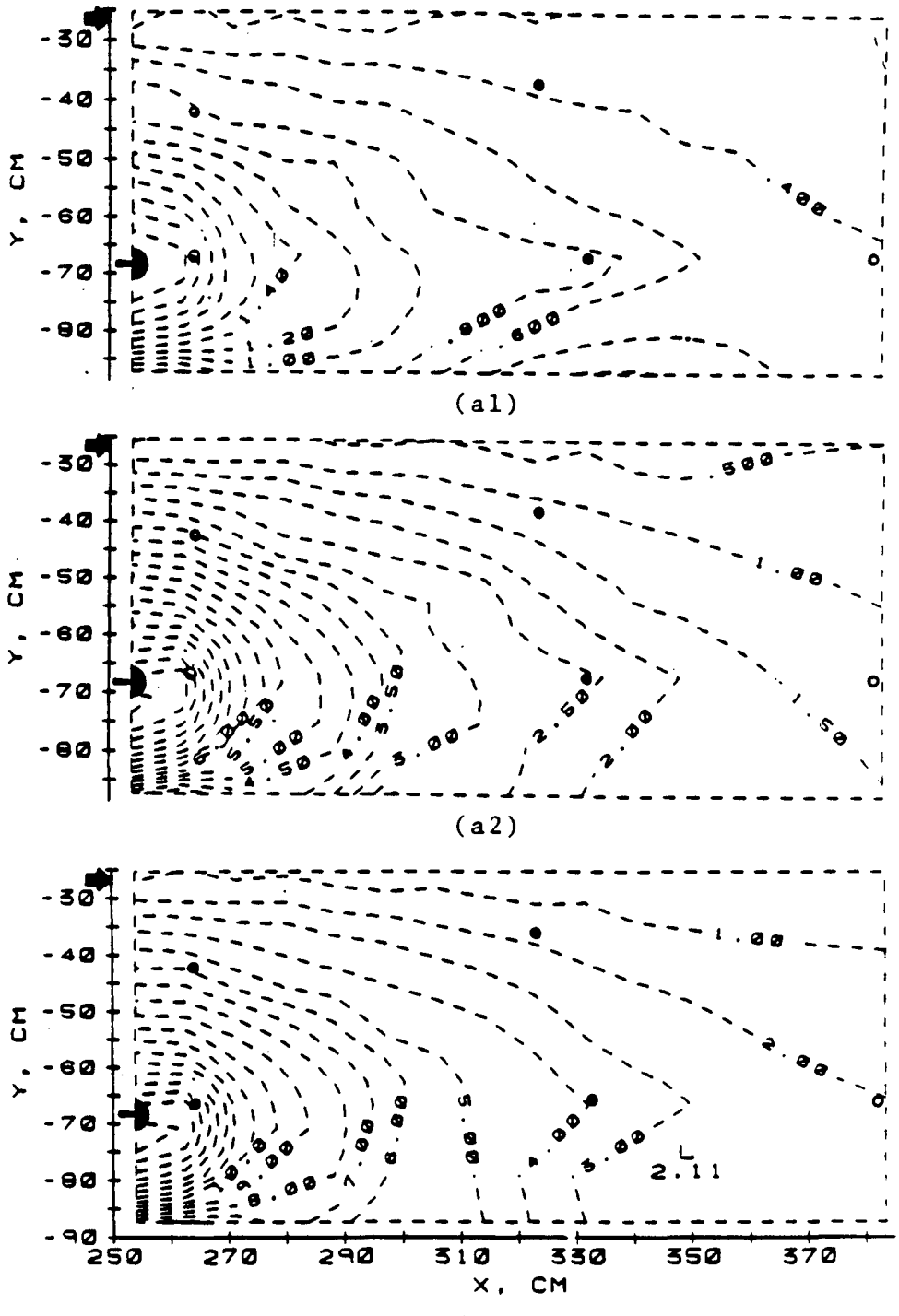


**Figure E3a:** Test 4. Hydraulic Head Distribution ($\phi$) in Two-Dimensional Unbounded Domain. Initial Bed Depth = 42 cm, y = -26.6 cm Initial Bed Porosity ($\epsilon_o$) = 39% Flow Rate (l/s-m): (a1) Q = 0.007, (a2) Q = 0.029, (a3) Q = 0.053

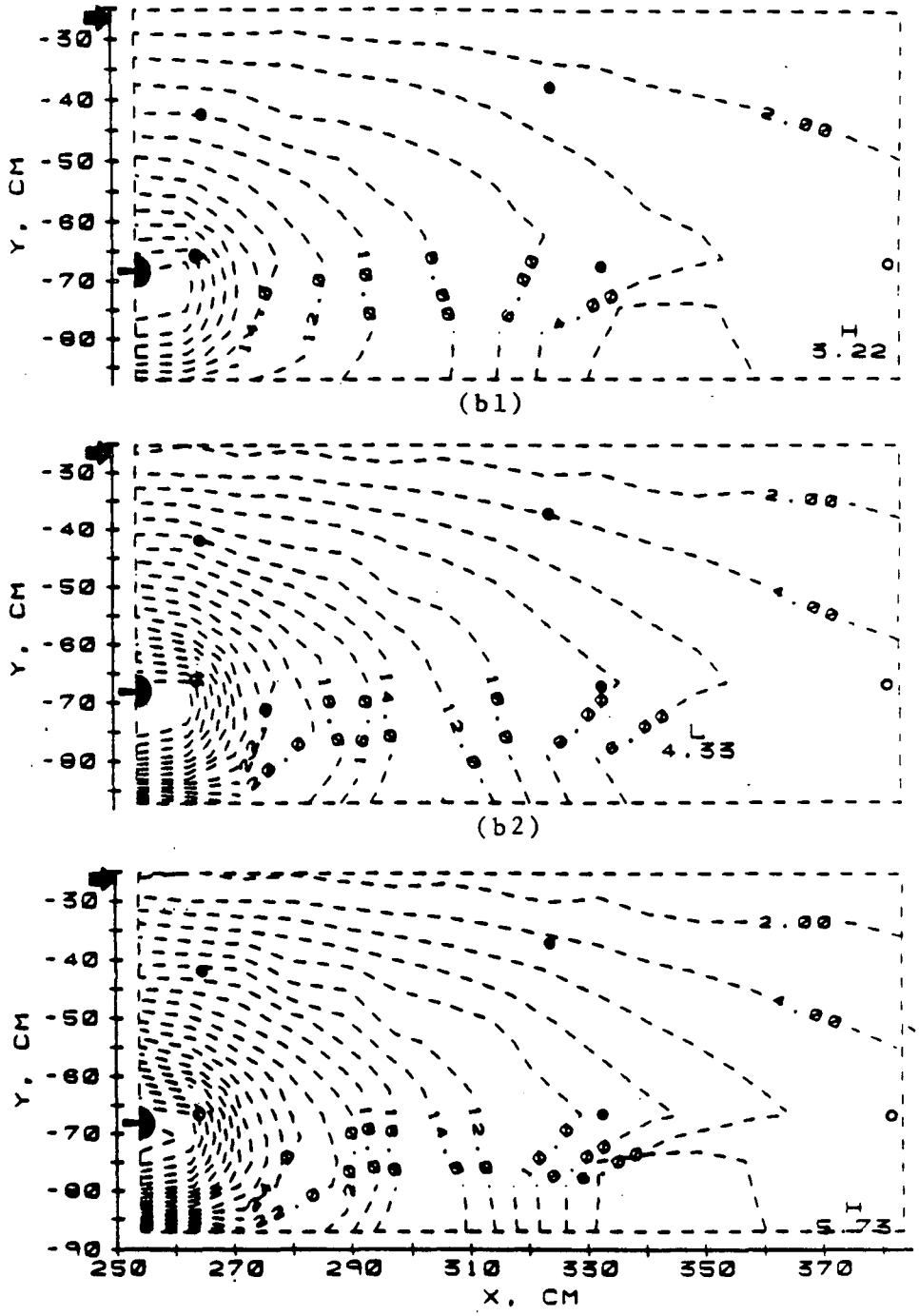


**Figure E3b:** Test 4. Hydraulic Head Distribution ($\phi$) in Two-Dimensional Unbounded Domain. Initial Bed Depth = 42 cm, y = -26.6 cm. Initial Bed Porosity ($\epsilon_o$) = 39% Flow Rate (l/s-m): (b1) Q = 0.081, (b2) Q = 0.126, (b3) Q = 0.149

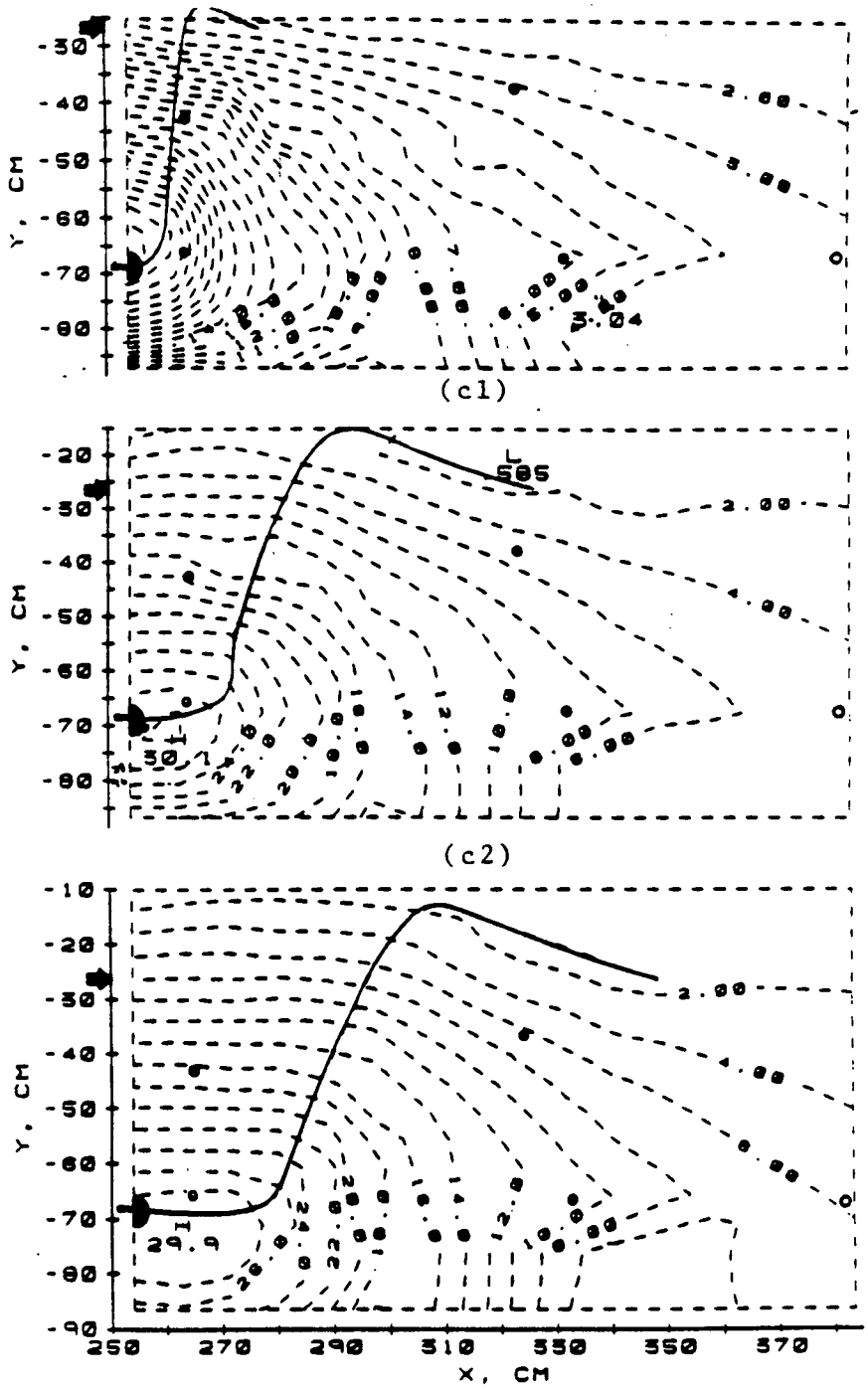


**Figure E3c:** Test 4. Hydraulic Head Distribution ($\phi$) in Two-Dimensional Unbounded Domain. Initial Bed Depth = 42 cm, y = -26.6 cm. Initial Bed Porosity ($\epsilon_o$) = 39% Flow Rate (l/s-m): (c1) Q = 0.183, (c2) Q = 1.3, (c3) Q = 2.202

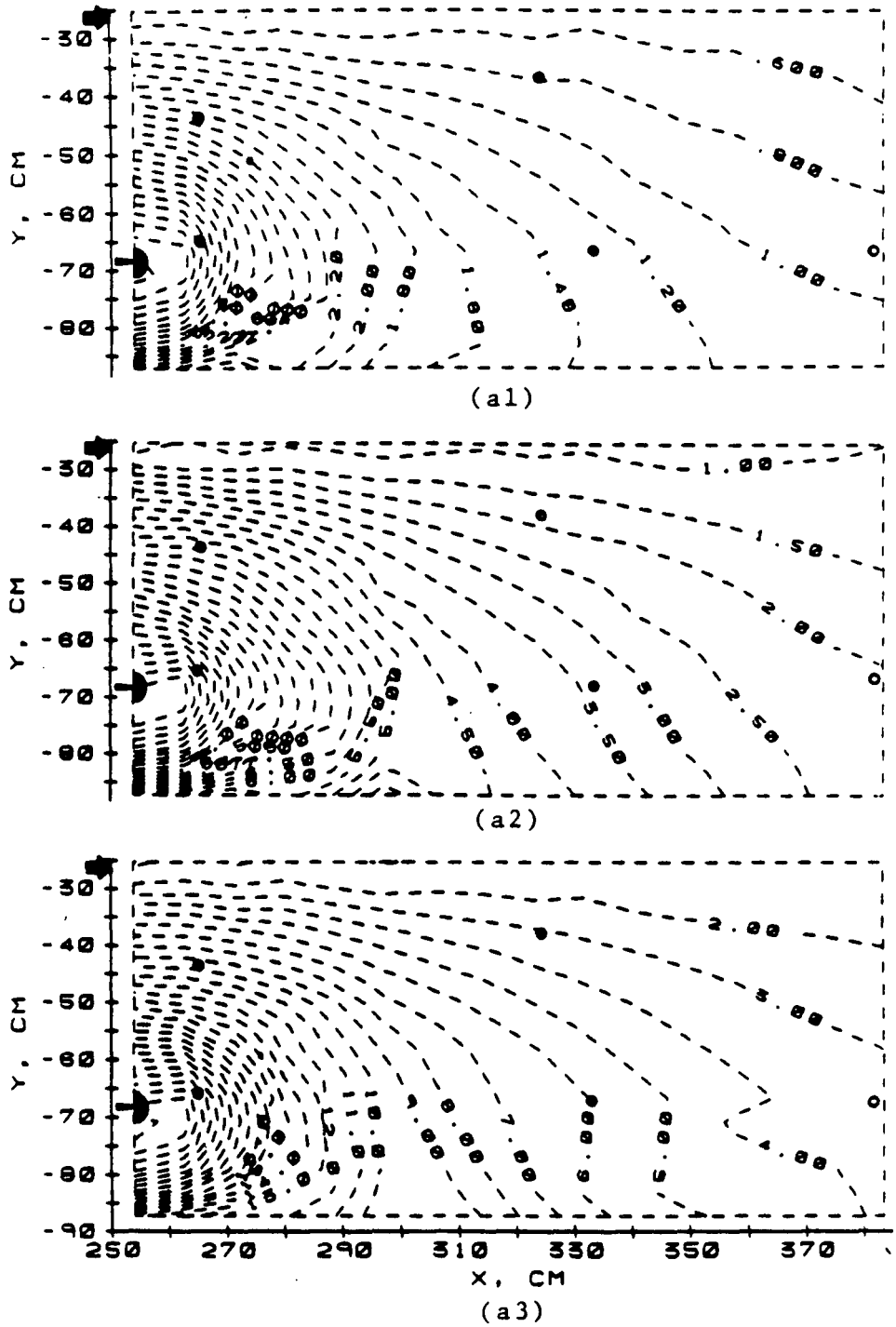


**Figure E4a:** Test 5. Hydraulic Head Distribution ($\phi$) in Two-Dimensional Unbounded Domain. Initial Bed Depth = 42 cm, y = -26.6 cm. Initial Bed Porosity ($\epsilon_o$) = 39%
Flow Rate (l/s-m): (a1) Q = 0.012, (a2) Q = 0.041, (a3) Q = 0.082

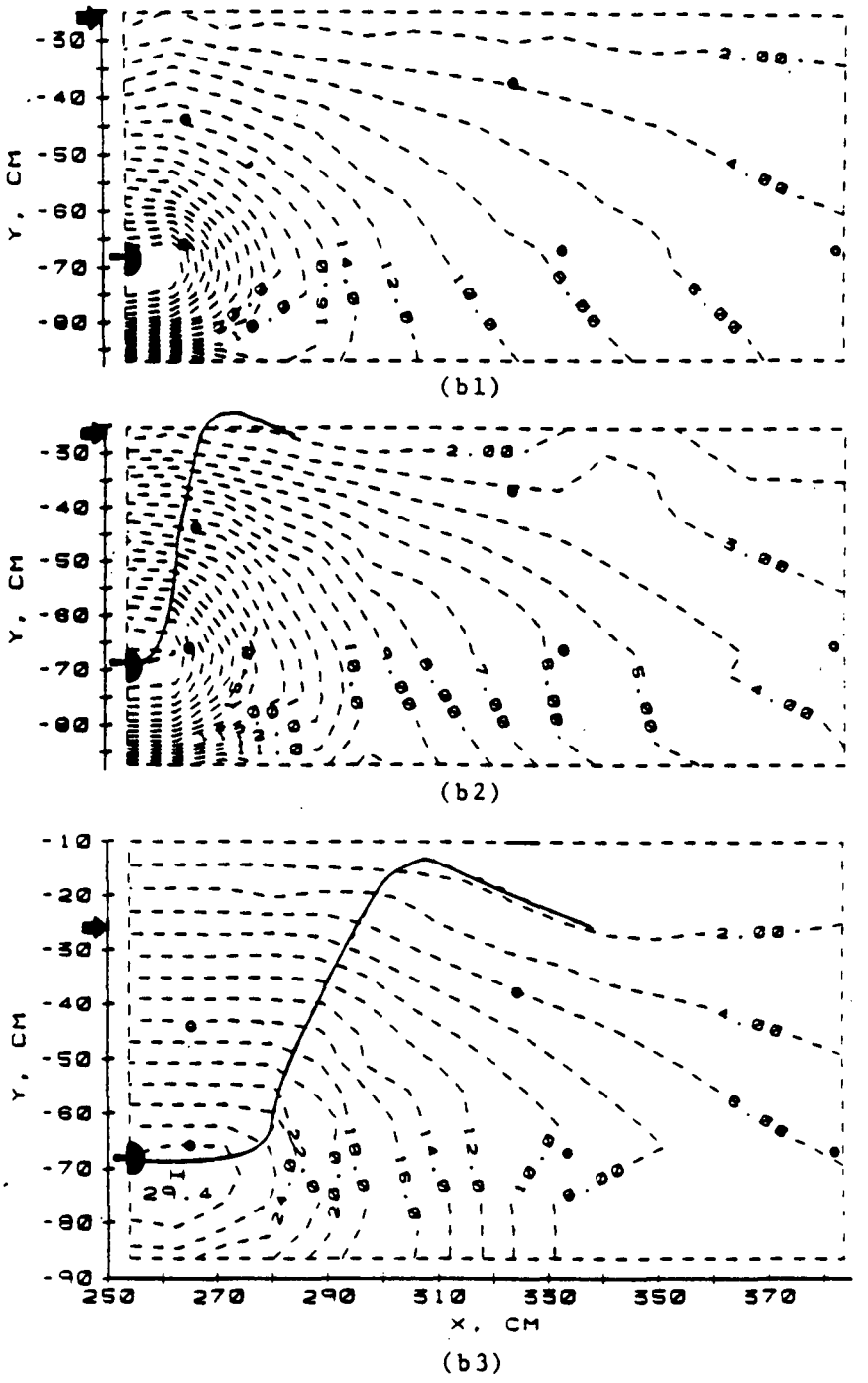


**Figure E4b:** Test 5. Hydraulic Head Distribution ($\phi$) in Two-Dimensional Unbounded Domain. Initial Bed Depth = 42 cm, y = -26.6 cm. Initial Bed Porosity ($\epsilon_o$) = 39% Flow Rate (l/s-m): (b1) Q = 0.106, (b2) Q = 0.273, (b3) Q = 1.977

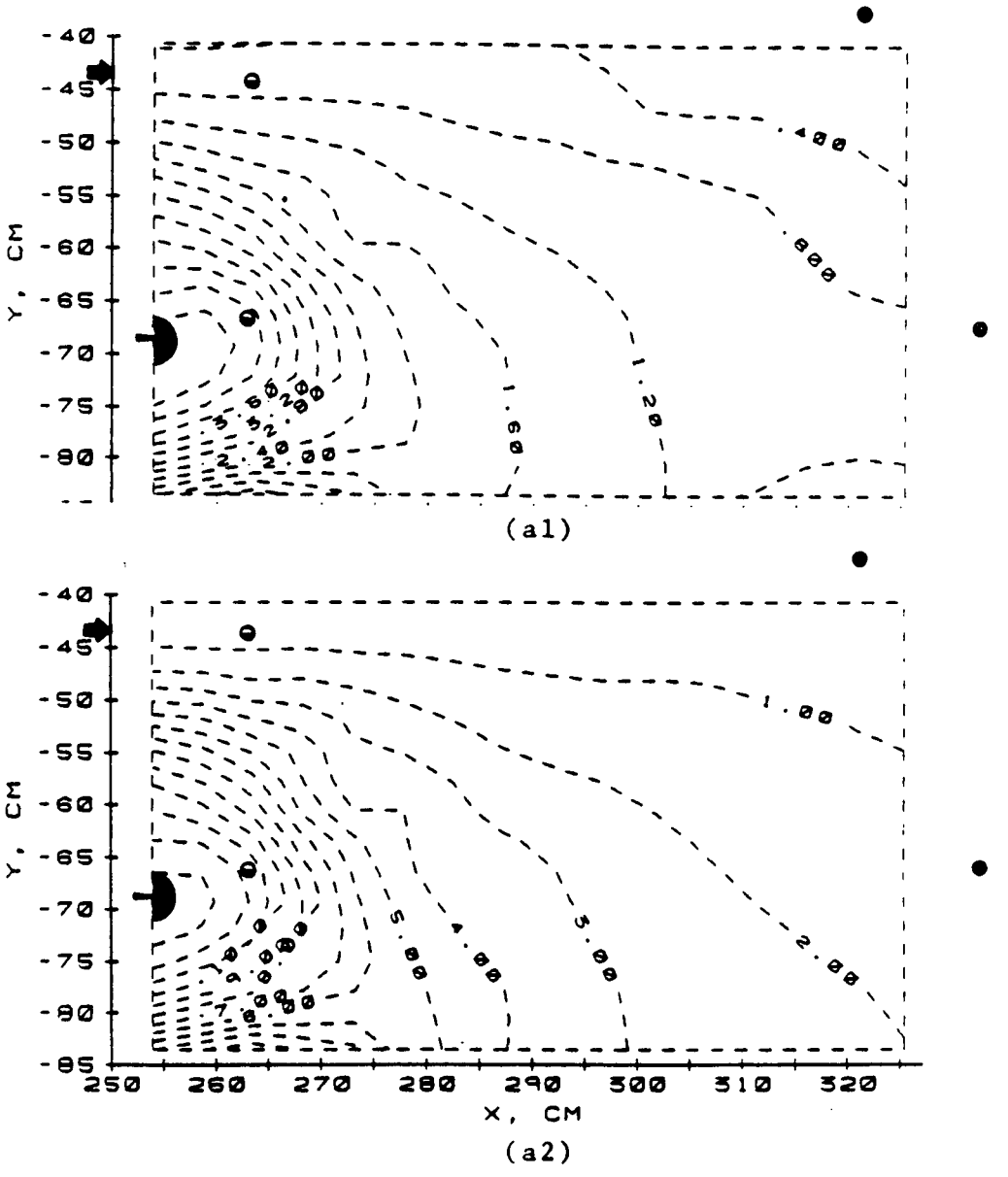


**Figure E5a:** Test 6. Hydraulic Head Distribution ($\phi$) in Two-Dimensional Unbounded Domain. Initial Bed Depth = 25.4 cm, y = -43.2 cm. Initial Bed Porosity ($\epsilon_o$) = 39% Flow Rate (l/s-m): (a1) Q = 0.014, (a2) Q = 0.041

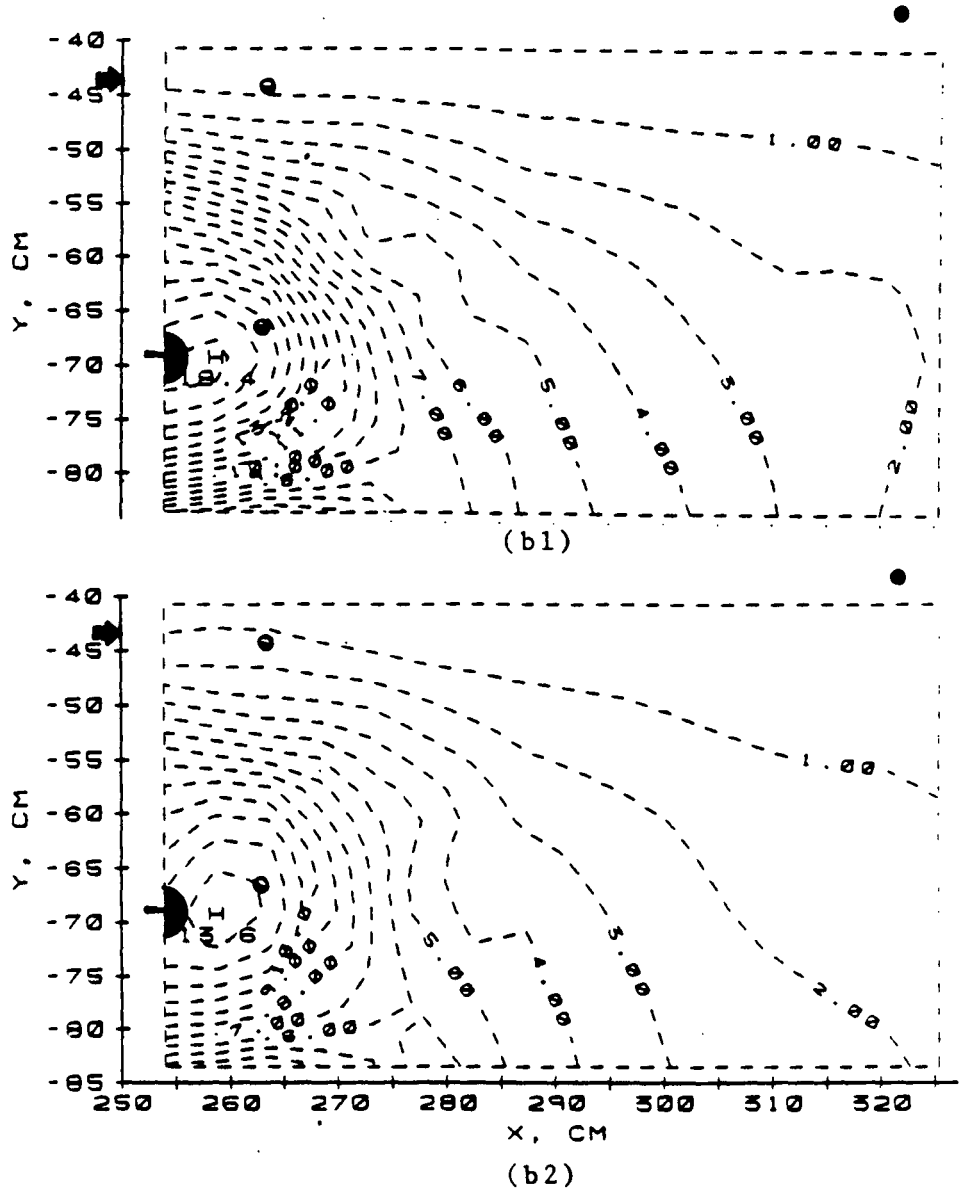


**Figure E5b:** Test 6. Hydraulic Head Distribution ($\phi$) in Two-Dimensional Unbounded Domain. Initial Bed Depth = 25.4 cm, y = -43.2 cm. Initial Bed Porosity ($\epsilon_o$) = 39% Flow Rate (l/s-m): (b1) Q = 0.057, (b2) Q = 0.093

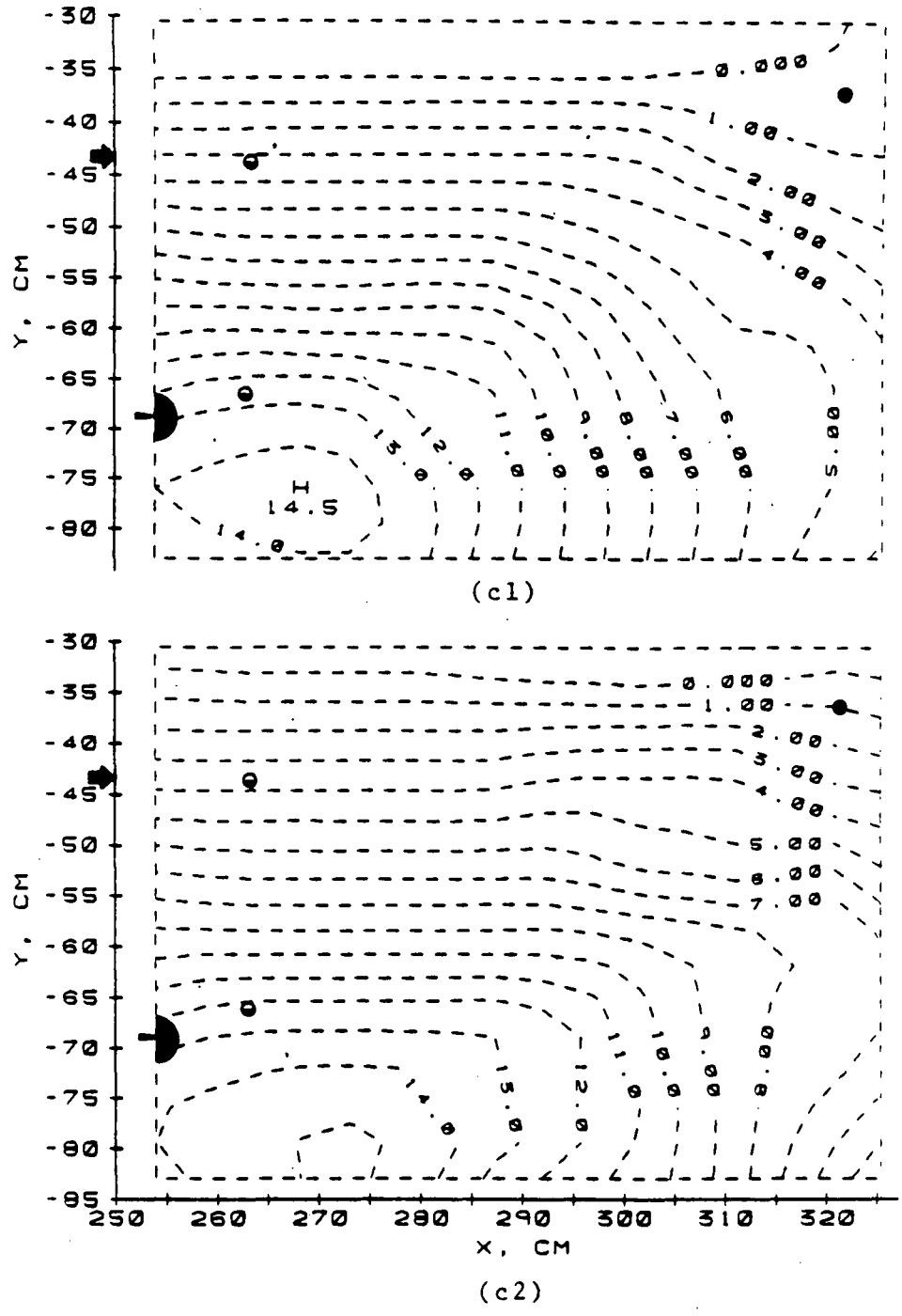


**Figure E5c:** Test 6. Hydraulic Head Distribution ($\phi$) in Two-Dimensional Unbounded Domain. Initial Bed Depth = 25.4 cm, y = -43.2 cm Initial Bed Porosity ($\epsilon_o$) = 39% Flow Rate (l/s-m): (c1) Q = 2.798, (c2) Q = 3.773

# ACKNOWLEDGEMENTS

The authors wish to thank Mr. Herbert R. Imbt for his generous donation of funds which made possible the construction of the experimental apparatus and to the Ingersoll Rand Corporation for the donation of the pump used in this study.

Messrs. Elias Dittbrenner and Dan Pense helped with the construction of the experimental apparatus and Dr. Ben L. Du assisted in preparing the contour plot computer program.

OCLC
176629796

No Fritz Lab Report
number on publication
Ⓑ Thesis Reel #247